POLITECNICO DI TORINO

Corso di Laurea Magistrale

in Ingegneria Energetica e Nucleare

Tesi di Laurea Magistrale

Numerical Analysis of the Flow Field in a Packed Bed Thermal Energy Storage and its Improvement

Relatori

Massimo Santarelli

Wujun Wang

Co-relatore

Silvia Trevisan

Candidato

Luca Pintaudi

Anno Accademico 2019/2020

Acknowledgment

First of all, I would like to show my gratitude to the CSP group of KTH which allowed me to realize this thesis and welcomed me as part of the team during these months. In particular my supervisor Silvia Trevisan, who assisted me with competence and friendliness, also giving me precious advices for my future career

Special thanks to my group in Politecnico di Torino, "ICHTus", for all the crazy and funny moments spent together. During these two years we shared days, projects and dreams, and you became a sort of family to me. Hope to have the occasion to meet you again as friends and colleagues.

Last but not least, I would like to thank my family and friends for giving me their support when I needed it and having the patience of listening to my complaints and problems when something was not working. I owe you all, without you I would not be the person I am now.

Abstract

The integration of thermal energy storage (TES) systems is key for the commercial viability of concentrating solar power (CSP) plants. Furthermore, TES units can be integrated in different power cycles as a source of flexibility and stability for the grid, particularly in locations with high renewable penetration, and can be employed in industrial processes, to reduce the requirement and waste of thermal energy.

A packed bed TES consists of storage material elements in various shapes and sizes and the use of an HTF that flows between these elements. The TES unit exploits the heat capacity of the particulate material in order to store energy. Inside a packed structure, the heat transfer area between solid and HTF is maximized, improving the heat transfer and minimizing the heat transport within the TES media (particularly when low conductivity materials, such as rocks, are used).

The work presented in this thesis concerns the CFD modeling of a lab-scale pilot Thermal Energy Storage (TES) built by the members of the Energy Department of KTH – Royal Institute of Technology. The simulation software Comsol Multiphysics has been used to create a suitable model which permits to assess its performance in different conditions. The assessment consists in a first start of the TES, with a complete charge and discharge starting from uniform temperature distribution. A cycle stability analysis has been done, to evaluate the behavior of the storage and the thermocline spread during reasonable working conditions. The effect of thermal insulation and thermal dispersion during charge, discharge and stand-by has been evaluated.

Once the model is verified, a series of measures have been proposed and analyzed, in order to improve its performances. The improvements influence both the fluid flow and the thermal behavior, therefore appropriate performance indicators have been chosen. The study ends with some recommendations about further possible investigations and future directions.

Index

List of symbols

A	Area
c_p	Specific heat
E	Energy
F	Body forces
h	Heat transfer coefficient
k	Thermal conductivity
L	Characteristic length
$\dot{m}$	Mass flow rate
N	Number of elements
p	Pressure
P	Power
q	Volumetric heat flux
Re	Reynolds number
t	Time
T	Temperature
u	Velocity
V	Volume
x	Average cell dimension
ε	Porosity
η	Efficiency
θ_p	Volume fraction
κ	Permeability
μ	Dynamic viscosity
ρ	Density
Ψ	Emissivity

List of abbreviations

Compressed Air Energy Storage	CAES
Computational Fluid Dynamics	CFD
Concentrated Solar Power	CSP
Energy Storage	ES
Heat Transfer Fluid	HTF
Key Performance Indicator	KPI
Latent Heat Storage	LHS
Levelized Cost Of Energy	LCOE
Organic Rankine Cycle	ORC
Phase Change Material	PCM
Photovoltaics	PV
Pumped Hydro Storage	PHS
Reynolds Averaged Navier-Stokes	RANS
Renewable Energy	RE
Sensible Heat Storage	SHS
Superconductive Magnetic Energy Storage	SMES
Thermal Energy Storage	TES

Objective and methodology

The scope of this work is to explore an alternative solution to store thermal energy and use it subsequently. To overcome many operative limitations of the current state-of-art technology in terms of thermal energy storage (TES), a novel storage concept has been proposed, in collaboration with KTH – Royal Institute of Technology. This study is part of a larger project, funded by Swedish Energy Agency and Azelio AB, whose scope is to develop, test and verify Thermal Energy Storage (TES) systems for Stirling engine and supercritical CO_2 based power generation, fueled by concentrated solar irradiation. The new concept design consists in a radial packed bed TES, potentially able to combine the advantages of packed bed structures with the reduced requirements of insulation due to its radial configuration. A first assessment of radial packed bed structures and TES is available in literature, but none of previous studies gives an accurate reproduction of fluid flow and heat transfer mechanisms for this storage concept, furnishing only general and oversimplified methods based on simple mathematical equations. Those simple equations are useful for a very general and first assessment, but neglect a great part of the mechanisms involved inside the storage, such as multiple heat exchange phenomena and multi-directional irregular fluid pattern. Therefore, this thesis proposes a different methodology, partly employed to evaluate the behavior of axial packed bed TES, in order to fill an empty space in literature and permit to accurately evaluate similar technologies.

Therefore, a structured procedure, consisting in numerical models combined with experimental evaluations, is necessary. Analyzing more in detail the procedure used in the thesis, it is divided in different steps and includes the following research topics:

- Concept analysis and introduction to energy storage technology and TES;
- Literature study on packed bed TES, including relevant parameters and challenges;
- Design concept and presentation of the lab-scale storage;
- Literature study on modeling of a packed bed TES system to predict the fluid flow and heat transfer mechanism;
- CFD modeling of the built TES in different operative conditions using the commercial software Comsol Multiphysics;
- Variation of some parameters or addiction of components to improve the performance of the storage, evaluated through apposite Key Performance Indicators (KPI).

The literature research on TES is initially focused on general aspects of the technology, in order to understand exactly which is the state-of-art and detect possibilities of improvements. Once the basic knowledge has been built and the topic is clear, the research moves deeper in the packed bed technology, to understand the principal advantages and challenges to overcome for its application on a larger scale. A key point in the first literature research is to individuate the principal parameters which influence the performances of packed bed TES, for the improvement phase. A description of the most innovative design concepts in this field is mandatory, as the TES modeled in this thesis is one of them.

Known the features of the technology, the lab-scale storage is described in terms of working principle, geometry and materials. Some requirements related to its working conditions are pointed out, especially in terms of material resistance. Other considerations are done on the size of the TES, as all the following steps of the thesis and also some of the results are strongly influenced by that, as industrial-scale TES are less sensitive to some aspects, such as thermal dispersions through the ambient.

After that, in the theoretical background and literature study on modeling of packed bed TES, a review of the heat transfer phenomena and fluid flow inside a packed bed is provided, to give an insight on the equations that can be used for the modeling steps. Moreover, all the possible ways to model a packed bed TES or similar technologies have been investigated, in order to have a complete scenario and find the best compromise for the study.

Once the preliminary study is completed, it is possible to start with the modeling section. The approach consists in a combined CFD and porous media approach, as in the packed region the turbulence is partially suppressed and simpler mathematical laws can substitute a complete modeling of the particles. This section is divided into many steps, each one with a precise aim:

- Preliminary analysis: it consists in a first assessment of the behavior of the storage, and includes a comparison of different turbulent models based on velocity patterns in specific zones of the inner channel. This comparison evaluates both the potential accuracy of the turbulent model adopted and the computational cost, as the best compromise between the two is the chosen model.
- Simple charge and discharge: consist in a simulation with uniform initial temperature, and represents the initial functioning of the storage, giving the first impression of its performance and on the development of the thermocline.
- Cycle stability analysis: continuous charge and discharge cycles under prescribed stopping conditions, until stabilization of the TES behavior, in terms of thermal evolution in time and space and therefore in terms of thermocline spread. After this analysis, the resulting cycle represents the predicted temperature and fluid pattern during regular operation of the TES.
- Charge, discharge and stand-by with insulation layer: here the tank is no more adiabatic, but it is insulated externally. This procedure helps to understand the behavior of the storage during

operations and during significantly long stand-by periods if thermal dispersions through the ambient are accounted for. The results are greatly influenced by the size of the TES.

All the models are verified and mesh independent.

Once the models are verified and verified, the improvement procedure can be implemented, to understand where is possible to intervene to improve the performance of the TES. The procedure is divided in any steps:

- Identification of suitable KPI to identify the general behavior of the storage. Among all the possibilities, thermal and hydrodynamic efficiencies, pressure drop and thermocline thickness have been shown to be the most interesting;
- Identification of possible parameters to vary in order to improve the performance of the storage. More in detail, the latter are divided into operative and design parameters. Furthermore, another classification can be done to distinguish measures which influences mainly the fluid flow or the thermal characteristics, even if the two are strictly connected.
- Analysis of the results: the results have the aim to show which measures allow to improve the performance of the TES and to validate the KPI adopted, if they do not generate contradictions with the general expectations.

The work is concluded by a series of observations on what is missing to complete the investigation and allow to proceed with further technical and economic studies. In case of positive outcomes, the TES is ready to be developed at a commercial scale.

1 Introduction

1.1 Energy storage

The ever-growing demand for electricity in the world, resulting partly as a cause of the demographic increase and in part from an improvement in welfare, requires a parallel increase in energy production and transmission. However, the progressive depletion of fossil fuel reserves and the inevitable production of greenhouse gases deriving from the combustion of this type of resources opens the way for a massive use of energy produced by renewable sources.

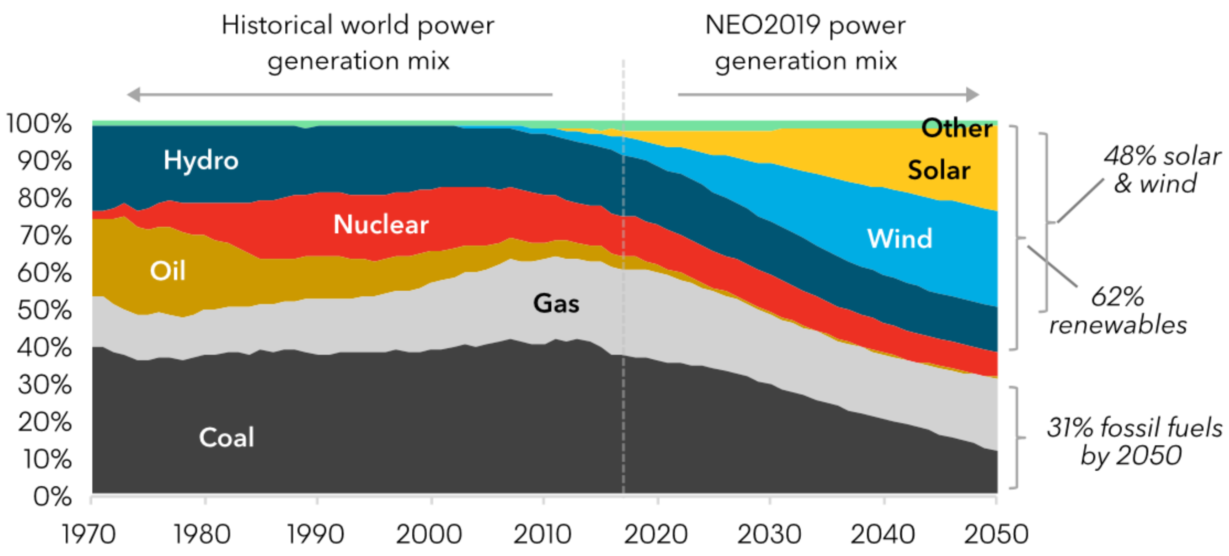

Figure 1 Prediction of energy sources by BloombergNEF [1].

Globally, according to the 2019 Energy Outlook published by BloombergNEF [1], it was estimated that currently the electricity production is based on fossil fuels, with a share of more than 60%. However, as can be observed, today more than 30% of the total electricity production comes from renewable sources. Major renewable energy (RE) contributor is represented by hydropower, followed by wind and solar. Looking more in detail to the previsions furnished by BloombergNEF, a progressive and exponential increase in the share of wind and solar technologies in the energy mix is predicted, with a total contribute up to 48%. Moreover, the total amount of electricity produced by RE is expected to reach up to 62% of the total production. Less relevant is the contribution of biomasses and biofuels, which are more employed in other sectors, such as heat generation and transportation.

Nonetheless, there are still some issues to the development of RE. Firstly, these technologies tend to require higher investment capitals if compared to the traditional ones and not always they are competitive in the market without incentives. Secondly, RE are mostly related to the environment and natural sources: due to that, there is a limit in the possibility of their exploitation for energy production. Moreover, the increase of the renewable fraction in the electricity mix could lead to problems related to the grid, connected to the unpredictability and non-regularity of some sources, such as wind and solar. In particular, the exponential growth of the two mentioned technologies would inevitably lead to high investments related to the empowering of the electrical grid. Furthermore, a huge amount of reserve capacity is also needed to meet the demand when the RE sources are not available.

To overcome the latter issues and meanwhile reduce the LCOE associated to the unpredictable renewable technologies, energy storage could be the key solution. Indeed, storing large quantities of solar and wind generated electricity may become as important as renewable power itself. In most of the cases, the combination of renewable power generation and energy storage can overcome the variability of renewable power generation and create the conditions to provide base-load electricity, increasing also the capacity factor of power plants and reducing the reserve power from traditional plants.

There are multiple beneficial outcomes related to ES, in both the cases of system implementation and/or grid connection, which can be synthetized in the following points [2]:

- Renewable energy integration: ES helps in flattening intermittent renewable generation output. It also reduces the need for grid regulation services, allowing a better use of grid infrastructure;
- Frequency regulation: ES could provide ancillary service, by charging the storage when grid frequency increases and discharging it in the opposite case. Moreover, it is useful for the correction of power factor;
- Peak shifting: by charging during off-peak hours and discharging during peak hours, ES offers a valid alternative to conventional grid strengthening; in energy systems, it permits the reduction of peak generation, leading to smaller size of the systems;
- Spinning reserve: ES supplies power to maintain network continuity while the back-up generator is started and brought on line. This enables generators to work at optimum power output, without the need to keep idle capacity for spinning reserves;
- Capacity Market: the aim of the Capacity Market is to achieve long-term security to supply and ES can be helpful to allow higher availability, in order to provide backup power during outages;
- Arbitrage: ES permits to purchase and store energy when it is cheap and sell it when the cost of energy increases. This allows to obtain consistent economical revenues.

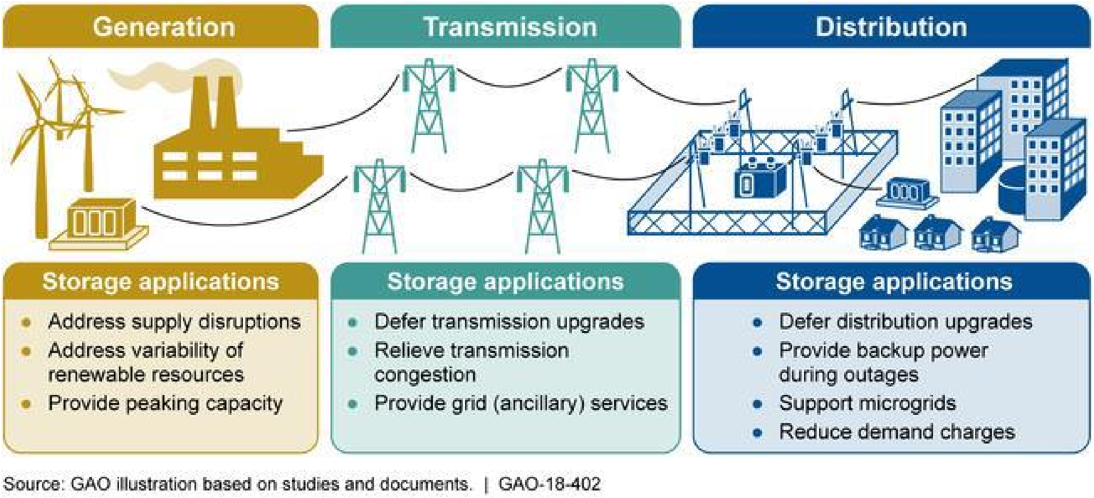

Figure 2 Beneficial outcomes of energy storage at a generation, transmission and distribution level [2].

Energy storage typically converts electricity into another form of energy, which is easier to storage. Depending on the form in which energy is stored, it is possible to distinguish them with a summarizing classification [3]:

- Electrochemical or Chemical: batteries, reversible fuel cells, supercapacitors, hydrogen produced by electrolysis;
- Electromagnetic: superconducting magnetic energy storage (SMES);
- Electro-mechanical: compressed air energy storage (CAES), pumped hydro storage (PHS), Flywheels;
- Thermal: thermal energy storage (TES).

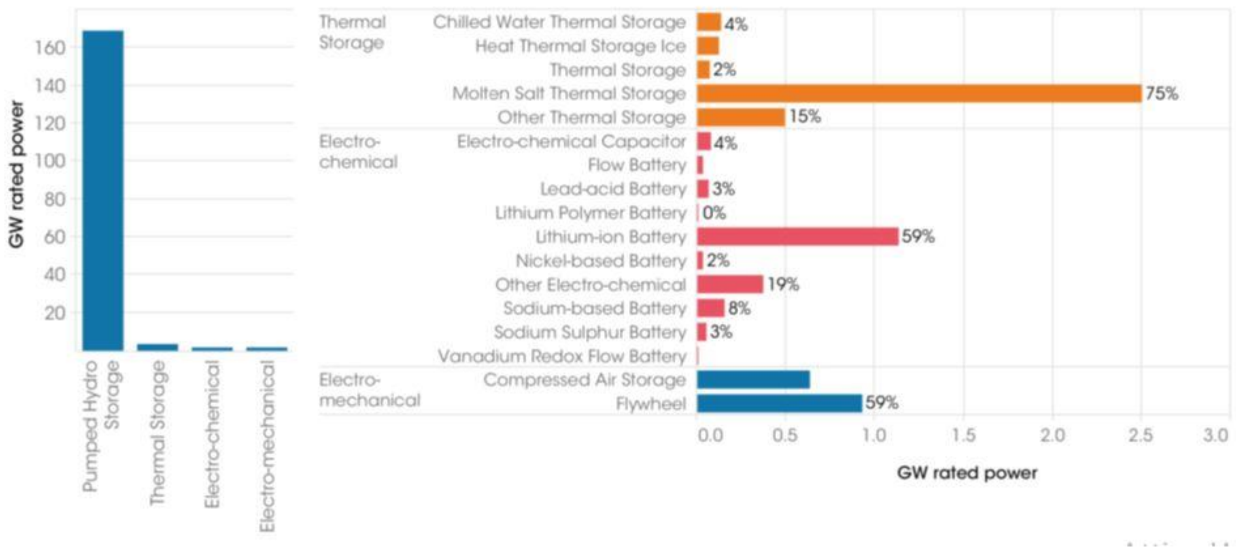

Figure 3 Global operational electricity storage power capacity by technology, mid-2017 [4].

The current national trends about the installation of energy storage is currently based on the concept of diversification, as different technologies are often suitable for different applications. Indeed, the choice of a solution may involve many considerations based on application and involves different characteristics, such as cost-effectiveness, storage capacity, power rating, lifetime and efficiency. Therefore, not all the technologies are in competition, being suitable to satisfy different requirements and covering different sector of the market [2], as shown in Figure 4.

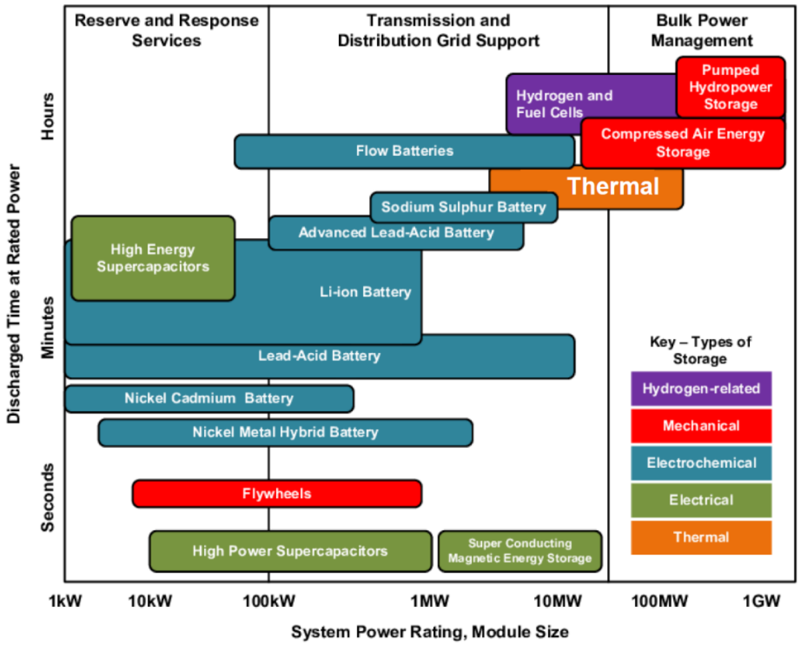

Figure 4 Energy storage technologies classified by size and time of discharge.

Among them, Thermal Energy Storage could represent a cheap, simple and reliable way to storage energy at a utility scale level. For this reason, many companies are exploring the possibility to use it for electricity storage, associating it to a power block able to produce again electricity as done in traditional power plants. Furthermore, due to its versatility, this system can be exploited also in residential applications, for heating and cooling demand, or industrial processes.

Although TES is not a new concept, it has seen an important development in the last decades for its application in combination with Concentrated Solar Power (CSP) systems, whereby solar heat can be stored in order to produce electricity when sunlight is not available. Thanks to that, CSP can be competitive in the market and used for base load electricity production.

1.2 Thermal Energy Storage

1.2.1 TES definition

Thermal Energy Storage systems store heat (or cold) to be used later under different conditions such as temperature, place or power released. With this technology, energy is stored in form of material internal energy, including sensible and latent heat. The principal scope of TES consists in overcoming the mismatch between energy generation (or availability) and energy use.

The benefits obtainable by implementing a TES in an energy system are principally related to:

- Better economics: it could reduce the investment and operational costs concerning the system;
- Higher efficiency: a more efficient use of energy can be achieved, reducing the wastes;
- Reduce pollution: maximizing the efficiency of power plants or industrial processes, the amount of CO_2 emitted is reduced;
- Better system performance and reliability;
- Energy arbitrage.

During operation, the working mechanism of the storage involves generally three steps: charge, storage and discharge.

The main requirements for TES systems can be summarized in:

- High energy density in the storage material, good heat transfer between the HTF and the storage material;
- Compatibility between HTF and storage material;
- Mechanical, thermal and chemical stability of all the components and materials;
- Compete reversibility over a large number of cycles;
- Minimum thermal losses and maximum roundtrip efficiency.

Analysing the basic design concept, TES can be classified in active or passive systems. The first is characterized by forced convection of the storage material. The latter circulates through a heat exchanger, which could be for example a solar receiver or a steam generator. Active storage systems can be under-classified in direct, if the heat transfer fluid (HTF) is employed also as a storage medium, or indirect, in which a second medium is used for storing heat. Passive systems are generally dual-medium, with the HTF crossing the storage material to charge/discharge a solid or phase change material.

In terms of quality of the thermal energy stored, TES can be classified in high, medium or low temperature storage. Usually, low and medium temperature TES are employed for heat generation for residential and industrial sector, or for district heating and cooling; instead, an high temperature storage is required for power generation and other particular industrial processes. When coupled with power blocks, higher temperatures result in higher efficiency of conversion from heat to electricity, leading to better performance of the system, as can be observed in Figure 5.

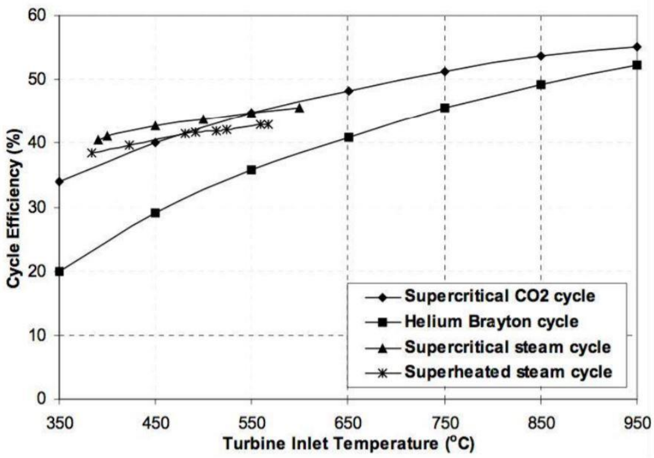

Figure 5 Efficiency of different power blocks depending on turbine inlet temperature [5].

Basing on the physics phenomena involved while storing heat, TES are usually distinguished into three general categories:

- Sensible TES;
- Latent TES;
- Thermochemical TES.

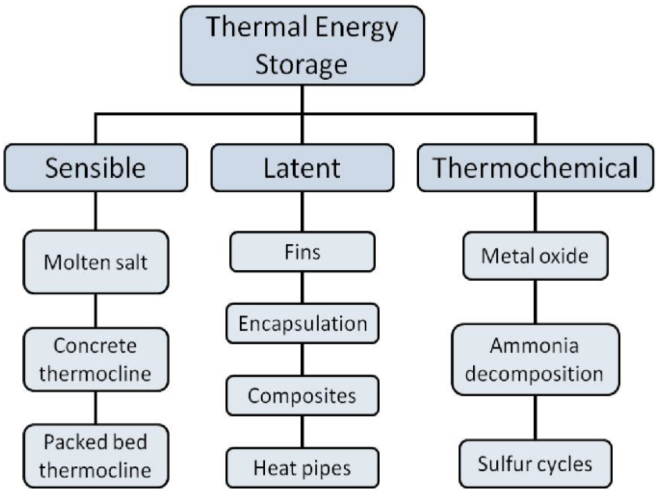

Figure 6 TES for CSP plants, classified by technology [6].

Although the basic concept is almost the same, these three categories present some relevant differences in terms of technology and challenges. These differences influence both the cost of the storage and its possible applications.

1.2.2 Sensible Thermal Energy Storage

Sensible heat storage is the simplest method to store energy by heating or cooling a medium [7]. Water is the cheapest option, being also the most used medium in residential and industrial applications. Other options are employed for large scale and high temperature applications. The main advantage related to this concept is the low cost. SHS system exploits the heat capacity and the change in temperature of the storage medium during the process of charging and discharging. The amount of heat stored depends on the thermal capacity of the medium, the temperature change, and the amount of storage material.

The medium is contained in a tank, often insulated in order to ensure hours of storage and reduce at the minimum the thermal losses through the external environment. For thermodynamic reasons, it is desirable to have a temperature gradient across the storage. Sensible heat storage can be made by solid or liquid media. Solid media are used in packed beds, requiring a fluid to exchange heat. If the fluid is liquid, heat capacity of the latter in the packed bed is not negligible, and the system is called dual storage system. Solid materials have the advantages to be relatively cheap and give the possibility to reach high temperatures. Liquid media (mainly molten salts, mineral and synthetic oils) maintain natural thermal stratification due to density differences linked to the temperature variations. Even with fluids, a thermal stratification across the storage is desirable. In order to reach that condition, it is important that the hot fluid is supplied to the upper part of the storage during charge and the cold fluid enters from the bottom during discharge. This procedure avoids induced fluid mixing; in some cases, stratification devices are employed [8].

1.2.3 Latent Thermal Energy Storage

In latent storages, thermal energy can be stored nearly isothermally, or in a limited range of temperature variation. This possibility is mainly related to the exploitation of the change of phase in the medium, so that the heat of fusion (solid-liquid) or vaporization (liquid-vapour) can be used.

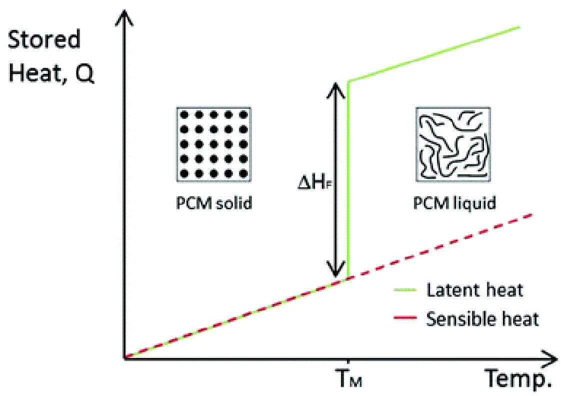

Figure 7 Comparison between SHS and LHS, ΔH_F is the latent heat of fusion during melting. T_M is the melting temperature [9].

Having both latent and sensible enthalpies contributing to the energy stored, this technology presents a higher energy density, allowing a reduction of the storage size and promising consequently to lower the costs.

Currently, almost all the substances adopted, generally called phase change materials (PCM), are employed in their solid-liquid transition. The principal drawbacks are linked to the low thermal conductivity of the solid phase, resulting in reduced heat transfer during the last part of the discharge and the initial one of charge. This limitation causes low power density of the device and the need of some improvements. Moreover, design and media selection are more complex, and the material often tends to degrade after a moderate number of cycles which include a change of phase. For all these reasons, the state-of-art material for latent TES has not been developed yet and this technology is not at a commercial state.

Eventually, as mentioned before, latent storage could represent the most suitable technology to reduce the cost of TES.

1.2.4 Thermochemical Energy Storage

Thermochemical energy storage is generally referred to a mechanism which involves one or more reversible chemical reactions able to release or absorb high amounts of energy. The products of the reaction should be able to be stored in a stable substance and the heat stored separately during the reaction should be able to be retrieved when the reverse reaction occurs [10]. The main reactions studied for use in storage media reactions are carbonation, ammonia decomposition, metal oxidation and sulfur cycles.

The most important advantages of Thermochemical ES are related to the high energy density and infinitely long storage durations at near ambient conditions; however, this technology is still at a prototype or early concept stage and presents many issues in terms of efficiency, feasibility and stability of the reactants.

During the charge phase, the storage is using thermal energy to drive a reversible endothermic chemical reaction, whereas the opposite takes place during the discharge phase.

$$AB + Heat \; <=> A + B$$

Thermochemical energy storage is an interesting technology to reduce the overall cost of TES. The endothermic chemical can operate at higher temperature than the current state-of-the-art, molten salts storage, and enables the use of high-efficient power cycles. In addition, it has higher energy density if compared to both LHS and SHS, leading to a reduction of the cost of solar-derived power [11]. However, the technology is still not fully commercial and presents serious problems of instability and low storing efficiency, needing ulterior development before reaching the commercial state.

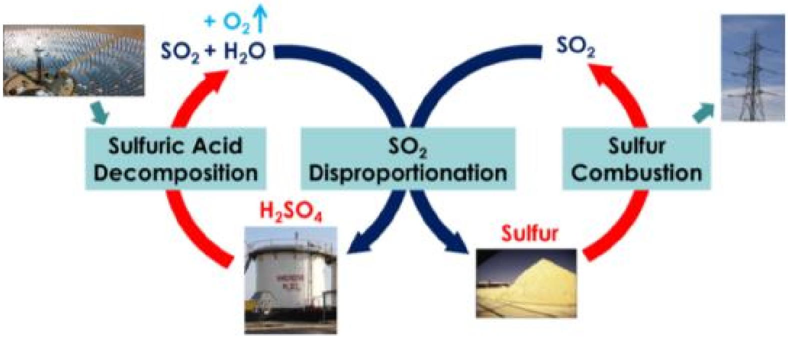

Figure 8 The sulfur based thermochemical cycle for thermal energy storage in a CSP power plant [12].

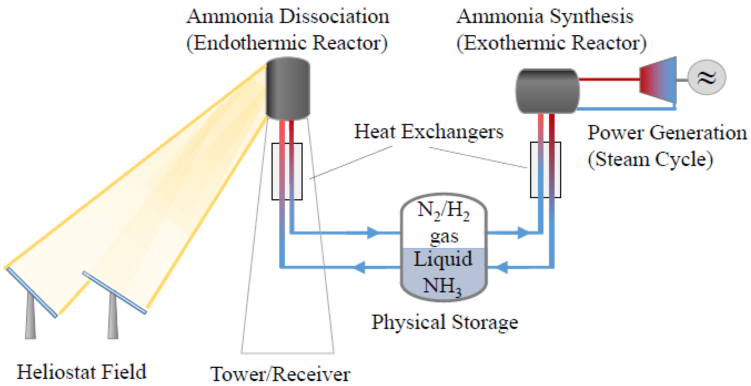

Figure 9 Schematic of ammonia-based thermochemical energy storage system [13].

1.2.5 TES in Concentrated Solar Power

CSP technologies generate electricity or heat by converting concentrated solar irradiation into energy. The solar radiation is concentrated onto a small area and then converted to usable thermal energy by heating a heat transfer fluid (HTF). Once available as thermal energy, solar radiation can be converted into electricity using a power cycle. CSP can be classified into parabolic trough, tower, linear Fresnel, and parabolic dish. They can be further classified into two families, depending on how the sunrays are focused [14]:

- Linear concentrators, such as linear Fresnel and parabolic trough;
- Central receiver plants, such as tower and parabolic dish system.

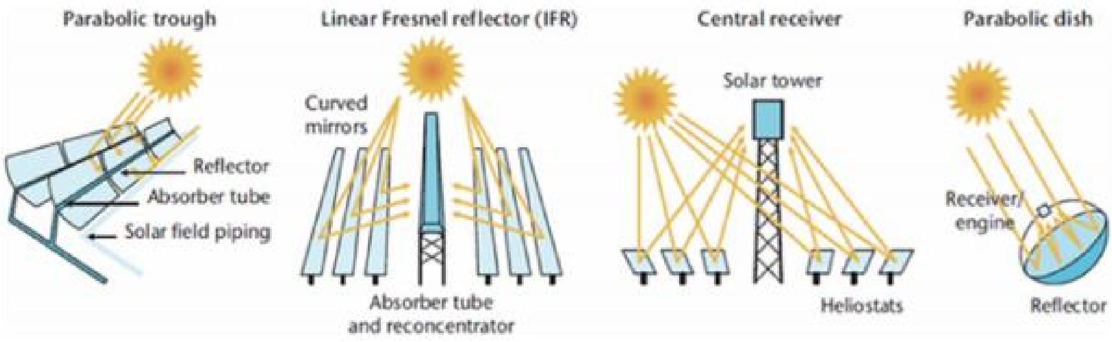

Figure 10 Main CSP technologies [14].

Thermal energy storage has been often coupled with thermal solar plant, with the aim to store medium/high temperature heat to use it in a power block or for direct heat production. The implementation of a TES permits the production of consistent power generation irrespective of weather conditions or solar availability. In this way, CSP plants is able to provide baseload power by using more energy from the solar field, by allowing the plant to accommodate a larger solar field and by shifting CSP generation to hours with higher energy prices. As reported by IRENA [15], higher levels of storage increase the capacity factor and improve the overall utilization of the power block and associated investment. Furthermore, CSP plants can lower their LCOE and be competitive in the market by including storage, even if resulting in higher initial investment costs.

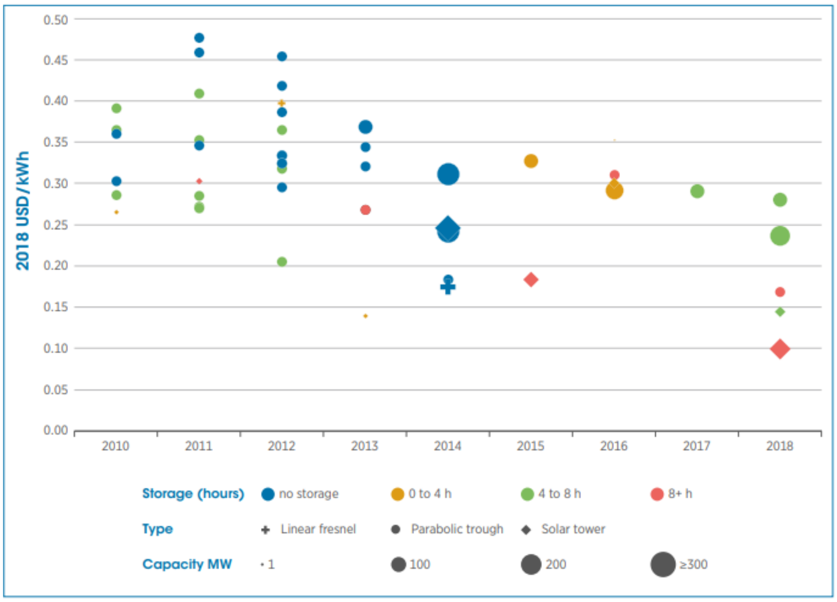

Figure 11 LCOE for CSP projects by year of commissioning and storage normalized capacity, 2010–2018 [15].

1.2.6 TES for Electric Energy Storage

Although TES is often used in solar thermal plants, it also has a potential in storing electrical energy. In this case, the electricity in excess is converted into thermal energy, which can be used for district heating, industrial processes or to convert it again into electricity when needed. Considering that electricity can be converted 100% into thermal energy, the roundtrip efficiency is principal dominated by the re-conversion operated by the power block. As mentioned in the introduction to TES, the efficiency of the power block depends extensively from the temperature and pressure parameters. Advanced thermal power-cycle plant can achieve close to 60% conversion efficiency in a combined-cycle mode, while conventional Rankine cycles will not overcome a 40%-50% efficiency. Nonetheless the low efficiency, even in this case thermal storage offers grid flexibility and the opportunity to reduce costs and CO_2 emissions. As stated by [16], TES could be very convenient in storing electricity in combined CSP-PV and CSP-wind power plants.

1.2.7 TES for industrial waste heat

Another possible application for TES is the industrial sector [17]. Indeed, in most of the cases the integration of this technology could allow to reduce considerably the energy consumption. The strength of TES consists basically in the possibility of solving the mismatch between the industrial waste heat supply and the heat demand, achieving a better capacity factor and allowing the reduction in size of the process components during the design. As a result, the investment cost related to cost intensive components (such as refrigerators or ORC engines) is reduced and the introduction of TES results profitable in many cases.

The principal field of application is the manufacturing industry, which includes metallic and non-metallic industries, chemical industry, paper industry and food processing industry. Low thermal TES could also represent a valid alternative for commercial and residential sector.

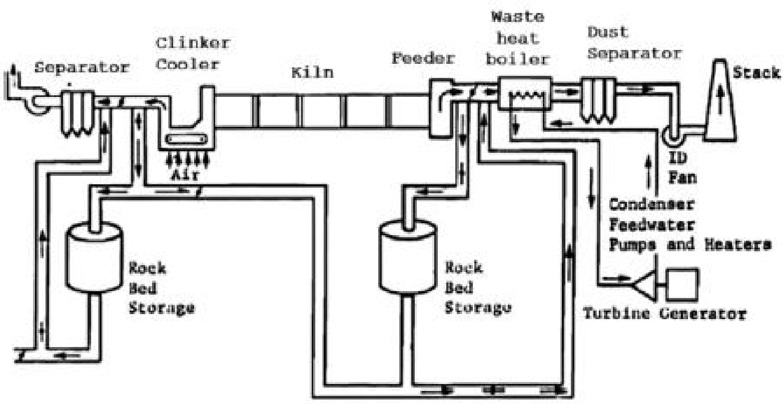

Figure 12 TES system proposed in a cement plant [17].

1.2.8 TES state-of-art

The current state-of-art in TES is represented by molten salt double tank technology, used principally in Concentrated Solar Power applications [18]. It basically consists in the exploitation of two separated tanks maintained at different temperatures: a hot tank at a temperature of 565 °C and a cold one at 290 °C. During operations, the salts are pumped from the hot tank to the cold one during discharge, and in the opposite direction during charging phase. The two tanks are maintained separated and at constant prescribed temperatures, in order to release heat more efficiently. The greater advantage of molten salts TES is the very high efficiency, estimated around 95% or even superior. Moreover, this material presents high thermal capacity and density. However, the use of molten salts poses technological problems due to the fact that these mixtures solidify at a relatively high temperature (from 142 to 238 °C depending on the components). For this reason, it is necessary to keep them always liquid with appropriate technological devices, especially in the "first start-up" phases of the plant, ensuring a continuous circulation of salts in the pipes even at night. Given the lower and upper temperature limits, molten salts require inside the circuit a heating system, often electrical, of the pipes that allows to maintain these high temperatures, with consequent energy consumption. Another last concern related to the use of these salts is corrosive, both as regards valves and pumps and as regards tanks and exchanger. Moreover, the salts are subject to instability at temperatures superior than 600 °C; furthermore, the system is relatively expensive, limiting the applicability for many industrial processes and power cycles.

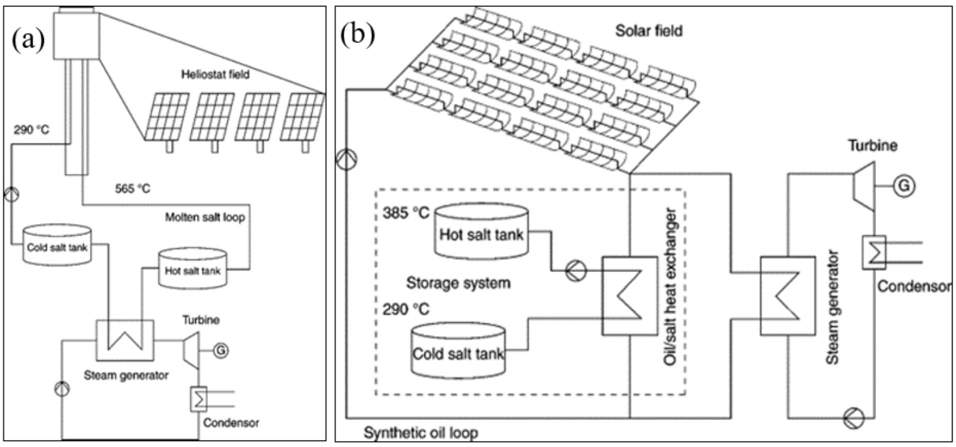

Figure 13 Simplified schemes of a CSP system with a two-tank molten salts storage concept, central tower (a) and parabolic trough (b) dispositions [19].

Many studies have been performed to overcome these limitations or to find alternatives to molten salts technology. Recent developments have been done in solid storage systems, with the introduction of packed bed thermocline configuration, which is discussed in the following section. This design allow the possibility to employ low cost materials, such as concrete or rocks, and to achieve wider ranges of temperature, which constitute one of the most relevant limitation for molten salts.

1.3 Thermocline packed bed TES

In order to increase the temperature range in TES and reduce the costs, a packed bed thermocline configuration could represent a valid solution. Packed beds have been used extensively in many engineering processes, especially in the chemical and industrial sector for heat and mass storage, industrial stripping and catalysis.

1.3.1 General description

Packed bed thermal energy storage systems have been investigated in the last years as one of the most promising sensible TES in terms of thermal efficiency and economic feasibility; however, their full potential for implementation at commercial scale is still unclear [20] [21].

A packed bed TES consists of storage material elements in various shapes and sizes crossed by an HTF. In particular, a tank filled with solid particles (named filler) or a mixture of liquid and solid material is used in most of the cases. In the second case, the liquid substance is encapsulated with the solid filler that goes under the name of "dual phase" storage. The TES unit exploits the heat capacity of the particulate material in order to store energy. Although it has been classified as a sensible storage technology, this system can be sensible, latent or thermochemical, depending on the materials, or combination of them, employed for the scope: if it is an encapsulated PCM, the heat transfer is not only related with temperature variations and thus it cannot be considered sensible. Moreover, packed bed configuration is particularly suitable for chemical reactions in presence of a catalyst, enhancing the contact area and the efficiency of the catalytic reaction.

TES charge and discharge consists in shifting hot and cold regions in the tank by circulating heat transfer fluid through the filler material [22]. Worth highlighting that in such a concept heat cannot be added and subtracted simultaneously. In general, in operation the HTF flows in one direction, during the addiction of heat (charge phase), and in the opposite one during the subtraction of heat (discharge phase). In the case of axial design, the HTF goes from the top to the bottom of the tank during charging and the flux is reversed during discharging: this is made in order to follow the buoyancy driven forces and reduce the energy needed to move the fluid.

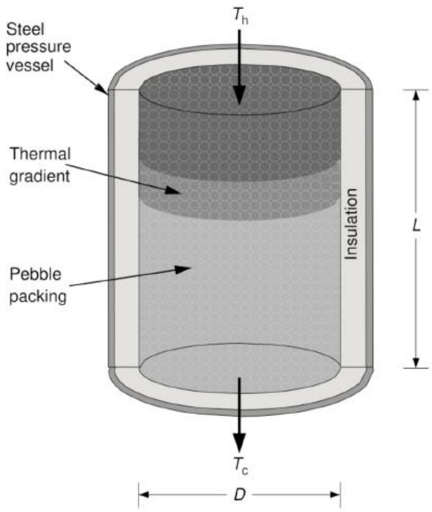

Figure 14 Simple concept description of a packed bed TES [23].

One of the most important issues related to this storage, and more in general to all one tank configuration, is the thermocline (or thermal front). Thermocline basically consists in an intermediate region between the hot and the cold ones; this region is characterized by a high thermal gradient, which is one of the main causes of irreversibility in single tank thermal energy storage. For this reason, an effective heat transfer and suitable stratification have been shown as a key aspect in the design concept. A perfect stratification consists in an infinitesimal thermocline thickness, with two defined different temperature zones inside the storage, perfectly separated.

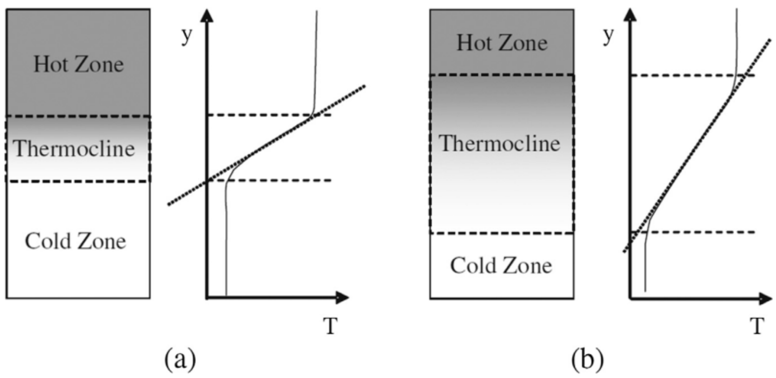

Figure 15 Differing degrees of stratification within a storage tank with the same amount of stored heat (a) left, highly stratified, (b) right, moderately stratified [24].

In case of porous structure, the contact surface between the HTF and the filler is maximized, in order to improve heat transfer and minimize heat transport within the TES media. This becomes relevant when materials with low thermal conductivity, such as ceramics or rocks, are employed. Another difficulty is then maintaining thermal stratification during transients to improve the exergy efficiency of the system, i.e. maximizing the energy extractable from the TES. Indeed, it has been extensively

proven that the exergy efficiency of a perfectly stratified storage is sensibly higher than the one of the same storage, but in a completely mixed conditions. Moreover, stratification influences also the outflow temperature, being higher in the first case mentioned.
The relative simplicity of packed bed, in terms of storage concept, opens important opportunities of implementation in many environments, from the renewable solar-thermal sector to the industrial waste heat recovery. Moreover, its flexibility allows the use of a wide variety of solid materials and heat transfer fluids, depending on the quality requested by the specific application.
However, the full implementation of the packed bed storage concept is still incomplete, since no industrial scale units are under operation. This is principally related to the lack of knowledge in terms of optimization of material selection, design and thermal management, which does not permit to attain high thermal efficiency value (comparable to the state-of-the-art) with improved thermo-economic performance. In order to develop this technology at the industrial scale, more efforts are requested, in terms of optimization, design and material selection.

1.3.2 Advantages, disadvantages and challenges

As mentioned briefly before, packed bed thermal storage is particularly interesting for high temperature applications, such as CSP [25] [22]. The principal advantages, related in general to this technology of storage and more in detail to the scope of this study, have been presented below:

- More compact: with respect to the state-of-art, the system consists in a single stank instead of a double tank configuration. This results in a decrease of the total mass and volume requested for the storage and in a better use of the filler. Moreover, due to this, the initial investment is reduced;
- No additional heat exchangers: the filler have at the same time function of storage and heat exchanger. Considering that the material is solid, there is the possibility to directly exchange heat with the HTF, without any ulterior device. This is possible only if the HTF crossing the storage has properties and thermodynamic conditions which allows its direct use in the power block;
- Variety of materials: the possibility to store energy in solid or dual material matrices opens many possibilities in the configuration adopted. One of the added variables is related to the higher variety of materials which can be suitable depending on the application.
- Higher temperature ranges: the new materials applicable in packed bed storages have allowed much higher temperatures with respect to the current state-of-art, limited at 565 °C due to the problems related with the stability of molten salts. This results in increased efficiencies if coupled with power blocks for electricity production.

- Larger heat transfer surface: as described before, this technology allows to use fillers with lower thermal conductivity, compensating this effect by the increase of heat transfer surface. In general, heat transfer surface can be varied controlling the porosity of the system, by modifying the mesh of the filler during the concept design;
- Simple concept: as briefly explained before, the basic concept related to the operative conditions is very simple, consisting in a simple porous media with hot fluid passing throughout.

However, in order to develop this technology to a large scale diffusion, many issues must be overcome and a more detailed knowledge in terms of design optimization is required [26] [23]. The main challenges and issues have been highlighted below:

- Thermocline (or thermal front) effect: as mentioned before, the thermocline is an issue related with the one tank configuration. The gradient of temperature in this region leads to irreversibility, which decrease the total efficiency of the system and reduce the heat available during the discharge phase. A correct thermal design has the aim to make the thermocline as thinner as possible, up to the ideal case of a perfectly stratified storage. In several studies the thermocline has been presented as the main source of losses. During the discharge phase, the outlet temperature is constant as long as the thermal front remains inside the tank. However, if it is not at least partially extracted, a not negligible part of the energy stored is not exploited, reducing in this way the actual capacity. Therefore, particular attention has to be paid in the long term and cyclic TES management;
- Low thermal conductivity: when materials with low conductivity, such as ceramics or some PCMs, are used, in general the equivalent conductivity of the bed is quite low, nonetheless the large exchange surface area. Therefore, a thermal enhancement process, in order to increase the charge/discharge efficiency, is necessary. For the aim, different solutions and designs have been proposed, and the research in this field is very active;
- High thermal stresses: in principle, if high temperatures are reached, the filler tends to expand. Being the structure constrained, the expansion is limited, resulting in non-negligible mechanical stresses, which could compromise the integrity of the structure;
- Thermal ratcheting: this phenomenon is related to the difference in the thermal expansion coefficient for the solid filler particles and the tank walls [22]. In particular, as long as the thermal expansion coefficient of the walls is greater than the one of the filler, during the charging phase a radial gap is created at the outer radius, allowing the cohesionless particles to fill it. During the discharge, when temperature drops, the tank is unable to contract completely, resulting in thermal stresses that could cause plastic deformation [27]. This leads

to a cyclic additional mechanical stress and eventually it might compromise the structural integrity of the tank. If the strain hardening is not sufficient to prevent the same process in the next cycles, the tank wall will be slowly stretched outwards until failure. To elude this problem, some technological solution, such as composite walls and truncated cone shape, have been proposed.

- High pressure drops: another issue with this technology is related to high pressure drops, related to the disposition of the filler in the fixed bed. This parameter depends on many variables, such as the velocity of the HTF, porosity of the filler, flow distribution;
- Complex design and optimization: although the concept is very simple, designing a packed bed storage in a proper way could lead to some difficulties, especially connected to the optimization procedure. Indeed, many factors influence the overall efficiency of the system, requiring an accurate design and multi-objective procedures.

1.3.3 Relevant parameters

When designing a packed bed TES, it is important to know which parameters can influence its performance and how to design them properly.

1.3.3.1 Particle shape and disposition

It has been proven experimentally that the shape of the particles influences considerably the pressure losses and the heat transfer coefficient, having a relevant influence on the flow distribution inside the packed bed. For this reason, some consideration about the shape of the filler elements must be explained, focusing also on technological factors, such as manufactory and stability.

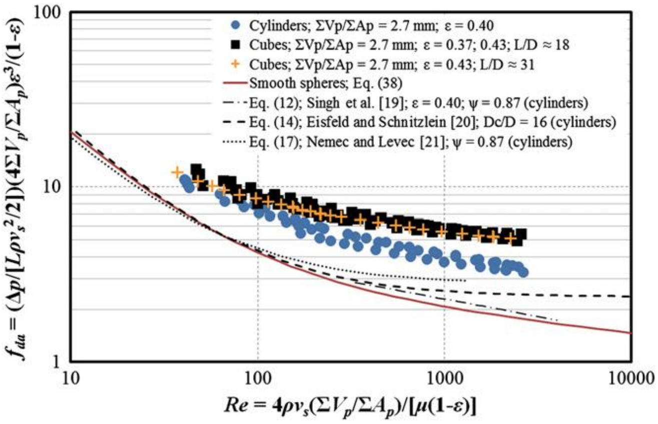

Figure 16 Different shapes and pressure drops with different geometries according to [28].

For equal volumes, literature data and experimental evaluations show that spheres present the best behavior both in terms of heat transfer, due to larger exchange surface, and pressure drop [28]. Furthermore, spheres are easier to manufacture than cubes or cylinders. Other geometries, such as cylinders or cubes, have been investigated too and could be interesting in case of materials with particular anisotropic properties.

Another influencing parameter is the disposition of the particles, which influences the same parameters and the porosity of the bed.

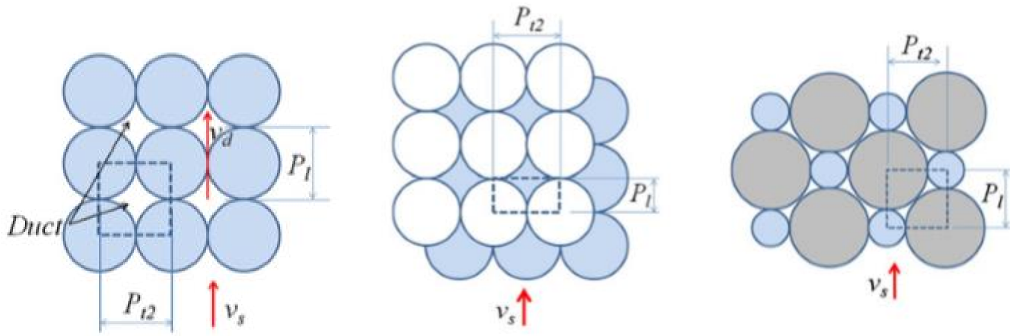

Figure 17 Different particle dispositions for packed beds of spheres [28].

The simple cubic packing is unstable and tends to shift very easily for high Reynolds, while a shifted configuration is more reliable. The disposition with different sizes of particles increases the heat exchange area, but reduced considerably the porosity and increases the pressure drops.

1.3.3.2 Particle size

The size of particles adopted has a great influence on heat transfer, pressure drops, thermocline zone and time of discharge [25], [29]. Increasing the diameter of the spheres, pressure drop decreases and less energy is required to move the HTF; however, the thermal performances of the storage have the opposite trend. Indeed, the heat transfer processes between the HTF and the filler surface and within the solid particle depend highly on the particle size. In particular, with the increase in the particle diameter, the maximum temperature difference between particle center and surface, as well as that between particle surface and the HTF, increases: due to this, heat transfer inside the storage gets worse. As a result, the thermocline region expands faster during the transients, leading to a shorter discharging time and a decreased efficiency. The effect of particle size is less relevant or negligible in case of small Biot number.

1.3.3.3 Aspect ratio

For TES units with a cylindrical shape or similar, it is often unclear which aspect ratio (or height-to-diameter ratio) is optimal for the scope, therefore some investigations have been presented. All the

considerations presented in this section are done with constant volume. The H/D ratio has effect principally on pressure drop and thermal losses, which influence the efficiency of the storage.
In an axial configuration, in general, with increasing height-to-diameter ratio, the lateral wall losses increase due to the reduced ratio of storage volume to lateral surface area, while the cover and bottom losses become lower due the smaller top and bottom areas. The total losses increase slightly with decreasing H/D. The pressure losses increase strongly with higher H/D due to reduced cross section area and increased path of the HTF inside the storage. As shown by [25], the overall efficiency tends to increase with higher H/D, also due to a higher convective heat transfer.
Finally, the tank height-to-diameter ratio needs to be chosen as a compromise between heat losses, pressure losses and construction limitations.

1.3.3.4 Porosity

The porosity of a packed bed (or void fraction) is defined as the ratio of the void volume with respect to the total volume of the bed. As well known, this parameter is used in many equations for modeling packed bed structures and is fundamental for their design. According to Klerk [30], bed porosity can be affected by disposition and shape of the particles, ratio between column and particle diameter (D/d_p), particle size distribution and also by the height of the bed [31].

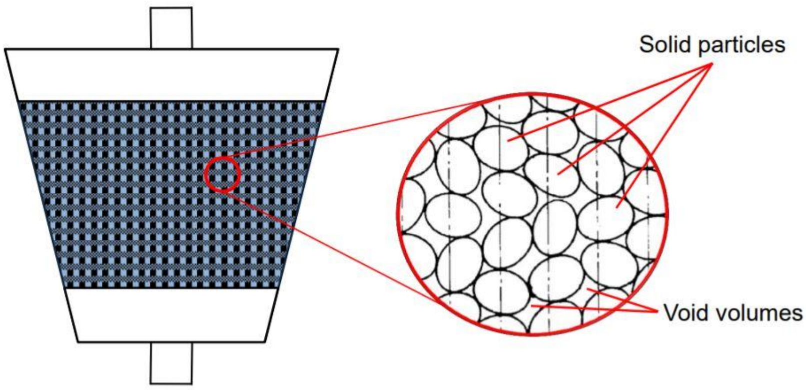

Figure 18 Porosity inside a packed bed of rocks.

For beds of monosized spheres, [32] presents a review concerning the investigations of porosity among the radius, with different models accounting also for the oscillatory porosity near the walls and its variation in dependence of the height of the bed. However, for many applications the knowledge of the mean porosity is sufficient. In the case of randomly packed spherical particles, the reference porosity in the bulk region ranges between 0.36 and 0.43. Those values have been chosen basing on the porosity of a simple cubic disposition, corresponding to the maximum porosity possible for uniform sized spheres, and an offset simple cubic structure.

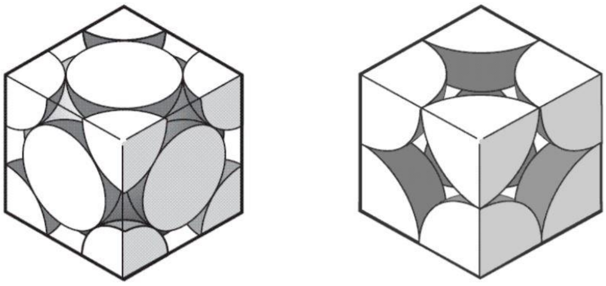

Figure 19 An example of simple cubic disposition (right) and offset simple cubic structure (left) [33].

1.3.4 Different concepts design

1.3.4.1 Cylindrical Tank with Axial HTF Flow

This concept is the most deeply studied, due to its simplicity. Therefore, a large variety of publications are available, so that the thermal behavior of this type of storage during transients has been deeply studied [34] [35]. The filler packed bed is arranged in a cylindrical shape and contained by an insulated tank. HTF moves axially through the storage filler material. As mentioned before, in order to maintain thermal stratification and limit buoyancy effects within the tank, the fluid goes from the top to the bottom during charge, and follows the opposite path during discharge. During charge and discharge, thermocline moves downwards and upwards, respectively, and it tends to spread during the cycles due to thermal diffusion, fluid mixing and finite heat transfer between solid and fluid. Usually, specific distributors are employed in order to have uniform flow distribution inside the bed. Relative low flow velocities could enhance the thermal equilibrium between the HTF and the filler, leading to improved TES efficiency; on the other hand, this could cause mixing, with consequent de-stratification and increase of the importance of heat losses. Regarding the tank design, a cylindrical shape increases the volume-to-surface ratio, reducing thermal losses and flow variation due to corner effects. Moreover, this simple geometry avoids stagnation points and minimize dissipation phenomena connected to the fluid flow. A higher height-to-diameter ratio improves stratification, efficiency and it acts as a flow straightener, improving flow uniformity; however, it also increases pressure losses, because of the longer path of the fluid. The main advantages of this concept have been claimed to be easiness of modelling and thin and straight thermocline that develops during operations [34]. Contrarily, one of the most critical aspects is related to the thermal ratcheting between walls and solid particles.

1.3.4.2 Truncated Cone Tank with Axial HTF Flow

Another concept, proposed in many publications [36] [25], is a truncated conical tank immersed in the ground. Through this configuration, the effect of the surrounding ground is exploited at high loads, reducing the resulting stress on the walls. Furthermore, the normal force on the walls during thermal expansion has been reduced by guiding the particles upwards. The tank can have different wall inclination and the optimum depends on different parameters. This storage concept presents higher volume-to-surface ratio in the top part, resulting in reduced wall losses, but increased thermal dispersions on the top. It has been shown that, in comparison with a cylindrical tank, a smaller volume of filler is required to extract the same energy from the HTF: this is related to the fact that more high temperature energy can be stored in the TES upper part thanks to its larger diameter. The increased volume to surface ratio at high temperature (on the top of the storage), reduced stresses on the walls and reduced risk of thermal ratcheting have been pointed out as the main advantages of this concept. The most severe drawback of this design consists in higher costs, principally due to the insulation requirement on the external surface and the excavation. Moreover, the system performs worse at small scale [25].

1.3.4.3 Self-Insulated Unconstrained Packed Bed

This concept proposed by Allen et al. [37] consists of an unconstrained pile of filler material surrounding a central pipe with a heat and mass exchange end region. During the charge phase, HTF travels through the central duct until reaching the end zone, then it passes to the surrounding filer region and from there it moves across the packed bed towards the outer region [37] [38]. The storage presents approximately a pyramidal shape whose outer slope is determined by the natural disposition of the particles composing the filler (preferably between 34° and 42°). In terms of design, many different solutions can be applied concerning the inner duct, its section and height, shape and aperture of the ending section. The end of the inner pipe is supposed to start between 20% and 50% of the height of the packed bed from the bottom. The aperture area has to ensure a sufficiently uniform flow during charge and discharge. The external surface of the packed bed can be unconstrained and exposed to the environment, in such a way that no insulation is needed; in this way the packed bed is also totally free to expand and shrink while it is heated and cooled. From different CFD studies it has been shown [38] that pressure drops are high in the inner region, close to the duct aperture, where the flow velocity and temperature are higher; then it decreases significantly as the fluid moves towards the outer regions of the bed. The main advantage of this packed bed TES concept consists in the minimal or zero insulation requirements, resulting in a supposed very cheap solution. On the other hand, this concept leads to high operational risk connected to natural convection and thermocline destabilization, being the latter not well defined during the discharge operation. Moreover, also the flow field across the whole pile is largely unpredictable and a significant part of the storage is not crossed by it, reducing the amount of filler exploited and consequently the actual capacity. Finally, a large area is required.

1.3.4.4 Modular Parallel Packed Bed Layers with Horizontal Flow

The concept has been proposed and tested by Enolcon GmbH and STORASOL GmbH [39] as part of the ORCTES HTTES project at the University of Bayreuth. It basically consists in parallel layers filled with a storage media. During operations, a horizontal air flow is used for the charge and discharge phases The packed bed is maintained in the fixed position by several fins, placed on the left and the right side of the storage material. The angled fins also allow to obtain a uniform and horizontal inflow inside the bed, in such a way to enhance the heat transfer between fluid and filler, and to achieve a uniform temperature distribution in the different layers. The main advantage of this concept is the modular design, which allows to use different dispositions in order to increase the power deliverable (parallel disposition) or the capacity (sequential disposition). However, the small scale of each module increases the relative heat losses and introduces challenges in achieving a uniform flow distribution. For these reasons an accurate design is needed.

1.3.4.5 Cylindrical Tank with radial HTF Flow

In this configuration the packed bed has been enclosed between two perforated pipes [22]. The HFT crosses the bed approximately in a radial direction as well as the thermocline. During the charge phase, the hot HFT enters the inner pipe from the top and then crosses outwards the packed bed, reaching the outer side and finally exiting from the bottom of the container. During the discharge, the flow is reverted. Compared to the extended available literature about axial-flow packed bed regenerators, relatively little has been published on radial-flow TES packed bed concepts. McTigue et al. performed a comparison between axial and radial-flow cold thermal storage [23]. It has been showed that pressure losses are smaller in radial-flow storages than those in the classic configuration. This result is principally due to lower gas velocity caused by an increasing cross section. On the other hand, the thermocline slope changes along the radius for radial-flow packed bed: as a consequence, the thermal and conductive losses are higher. However, an accurate CFD modelling, followed by a design optimization, could lead to stable thermocline and decrease the losses.

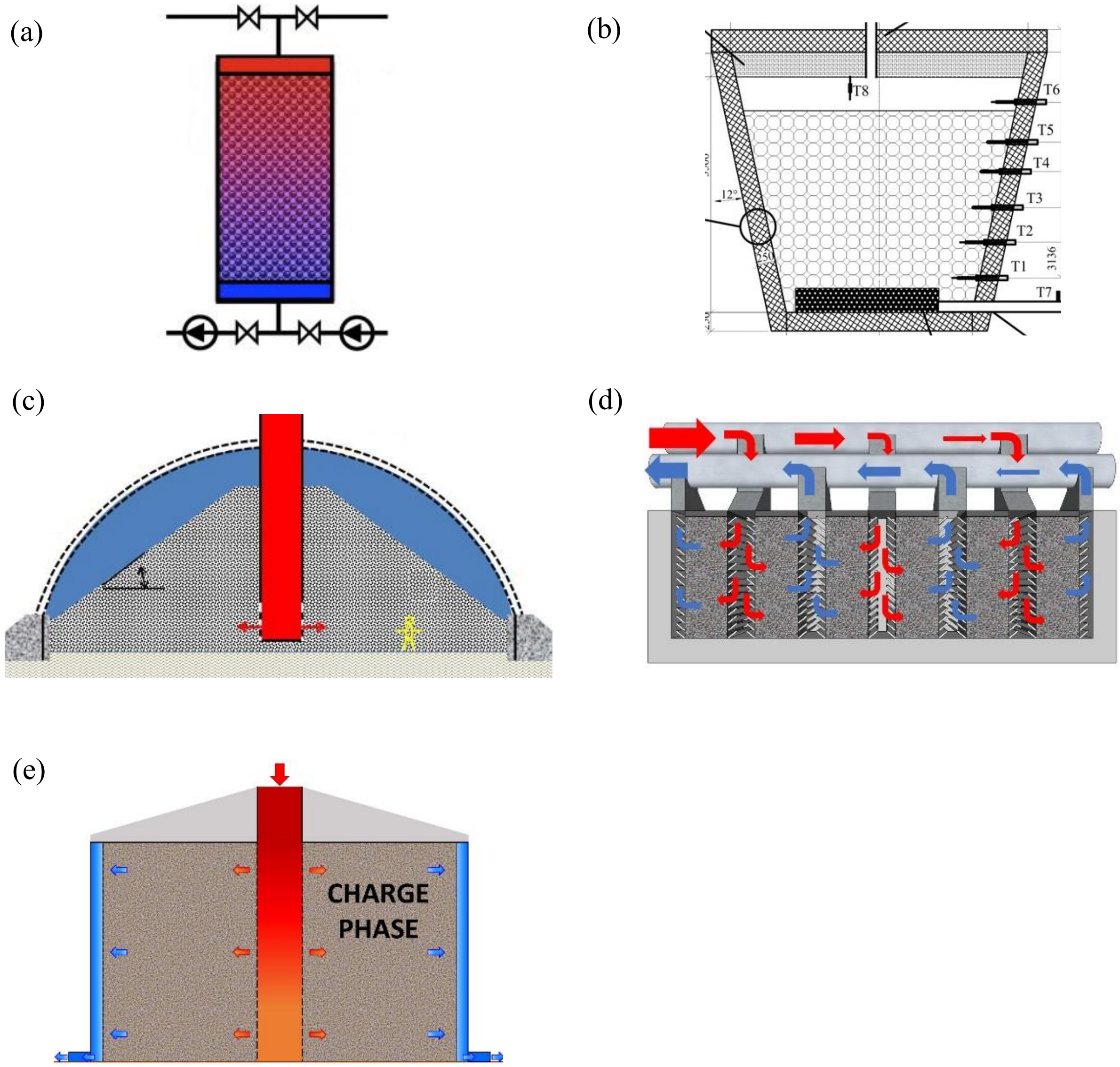

Figure 20 Schematic representation of the three packed bed TES concept designs [22]. In particular, a cylindrical (a), truncated cone (b), unconstrained (c), modular (d) and radial (e) configuration.

2 The storage

The TES under study has been built by the Energy Department at KTH – Royal Institute of Technology and is located at the Solar Lab of the same institute. It consists in 0.2 m^3 packed bed of ceramic spheres, equivalent to about 60 kWh of energy capacity, enclosed in two perforated pipes. The concept is one of a kind, being the first radial packed bed storage built so far, as the concept is new and has never been used before even for experimentations. All its features are described in this section, including geometry, components and materials.

2.1 Working principles

The principle of the proposed TES concept is shown in Figure 21. The packed bed of spherical particles is enclosed between two perforated pipes, the inner/hot and the outer/cold pipe. The HFT crosses the bed in a radial direction as well as the thermocline, which moves outward along the radius during charge and return inward during discharge. During the charge phase, the hot HFT enters the inner channel from the top and then crosses outwards the packed bed, reaching the outer plenum and finally exiting from the bottom of the cylindrical container. During the discharge, the flow is reverted and the cold HTF enters the outer pipe from its bottom and travels through the packed region inwards, exiting from the top of the inner/hot pipe.

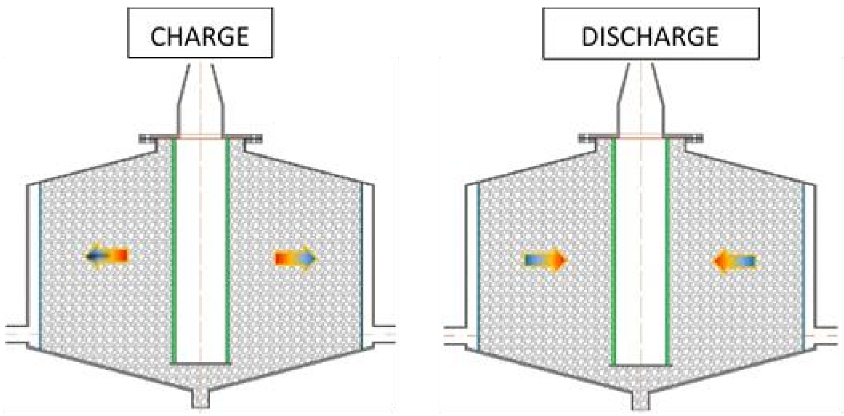

Figure 21 Working principle of the lab-scale TES.

The direct effect of this configuration is a reduced request of insulation, considering that the hottest zone is in the inner region of the storage, while the outer one, in direct contact with the ambient, remains at the minimum temperature. Through this configuration, thermal losses are expected to be minimal. The reduced velocity, consequence of the increased cross section in the packed region, permits a quite stable flow distribution and an increased time of residence, at a price of a slightly reduced heat transfer coefficient. The effect on heat transfer should not be too relevant, considering that the turbulence is partially suppressed by the packed structure. Therefore, this design concept is supposed to result in a roundtrip efficiency comparable with the state-of-art and lower cost.

2.2 Geometry and components

As mentioned before, this concept consists in a radial packed bed configuration. All the geometrical features of the pilot lab-scale TES are shown in Figure 22.

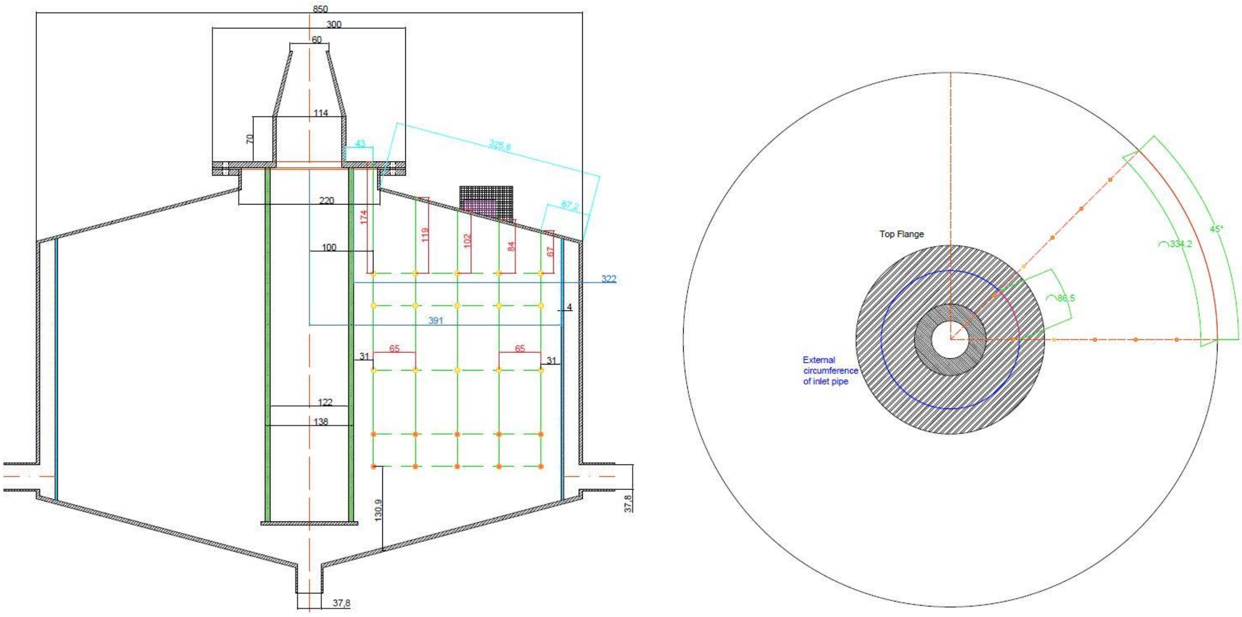

Figure 22 Lab-scale TES: front and top views with dimensions (measured in mm).

From a geometrical point of view, it is basically composed of a cylindrical core and two truncated cones as basis. The packed bed, constituted by a series of poured spherical particles of 6 mm, is enclosed in two cylindrical pipes, delimited by a wired mesh with a wire diameter of 0.25 mm, a mesh size of 40 mm, open rate: 36.76% (defined as the ratio between the void zone and the one occupied by the mesh).

The structure is approximately axisymmetric, presenting a non-symmetry only on the outer channel, which includes 4 exiting tubes in the lower region. The tank is surrounded by a 5 cm insulation layer, to reduce the thermal losses especially during long stand-by periods. On one side, there are 50 thermocouples to measure temperature trends in two different plan; their position will be used to analyze the results in the modeling and improvement sections.

2.3 Materials

Material selection is one of the key points for a packed bed TES and includes not only the filler material, but also the frames, meshes, insulation and external vessel. The solid filler represents the greatest source of expenditure to build a thermal storage, both for to find it and for the manufactory required in order to give the desired shape; therefore, the choice should be made with attention, as it is relevant to maintain a low LCOE. The choice is principally related to the specific function of the component or part of the storage. However, all the materials included in the TES have to fulfil some general requirements derived by the internal conditions [40]:

- Long thermal cycling stability: all the materials adopted to build the storage should present the capability to resist to intense thermal strains. It is important that every component of the storage is capable to handle high temperatures and maintain its integrity and properties over a consistent number of charge/discharge cycles;
- Mechanical properties: good mechanical stability, low coefficient of thermal expansion, high fracture toughness, high compressive strength are principally required for the considered application;
- Chemical properties: the selected materials have to present long term chemical stability, with no chemical decomposition in the range of temperature prescribed. It should be non-toxic and non-explosive in contact with the HTF or the environment. Low corrosion potential or reactivity to HTF and compatibility with it are also relevant;
- Cost constraints: one of the scopes of TES is to store energy at a moderate cost. To do this, cheap and abundant materials represent the best solution. In particular, the choice of a suitable material is also based on the costs of manufacturing, production and transportation associated to it.

2.3.1 Denstone 2000

Denstone 2000 is a ceramic material used for many processes, including hydrocracking [41] . It has been used as solid filler for the TES, for its interesting thermal properties and thermomechanical resistance. It is composed by a combination of silica, alumina, and other components, expressed in percentage in Table 1.

	min (%)	max (%)
SiO_2	67	77
Al_2O_3	18	26
Fe_2O_3	-	1.7
TiO_2	-	1.5
CaO	-	1
MgO	0	1
Na_2O	0	2
K_2O	-	6
$Al_2O_3 + SiO_2$	90	96

Table 1 *Chemical composition of Denstone 2000 in percentage [41].*

This material presents high impact resistance and compressive strength, coupled with high thermal shock resistance. Indeed, it is able to resist without significant damage at temperatures up to 1000 °C, maintaining integrity and stable mechanical properties. Moreover, its high density and specific heat make Denstone 2000 suitable as solid filler for packed bed TES [42] [43].

2.3.2 Inconel 625

Nickel-chromium alloy 625 (also known as Inconel 625) is generally used for its high strength, easiness to manufactory, and outstanding corrosion resistance [44]. Working temperatures range from cryogenic to almost 1000 °C.

This combination of elements is responsible for superior resistance to a wide range of corrosive environments of unusual severity as well as to high-temperature effects such as oxidation and carburization. Inconel 625 presents high tensile, creep, and rupture strength, added to an outstanding thermal fatigue and oxidation resistance; All these characteristics make this material particularly suitable for TES, and for this reason it is used for the wired meshes, the inner and outer pipes, constantly in contact with the HTF at temperatures up to 750 °C.

2.3.3 Fiberfrax Durablanket S

FIberfrax Durablanket S is the material employed for the insulation of the storage. It is manufactured from FIberfrax refractory ceramic fibres and is used for numerous thermal application, due to its superior insulating performance, excellent chemical resistance, flexibility and resilience [45] [46]. All these characteristics, combined with low density and high resistance to thermal shocks, make Durablanket S extremely suitable for TES applications.

	Density [kg/m3]	Specific Heat [J/kg°C]	Thermal Conductivity [W/m°C]
Denstone 2000	2350	720 – 1080	1.46
Inconel 625	8250 - 7900	410 – 580	12 – 25
Fiberfrax Durablanket S	128	1130	0.12

Table 2 Thermal properties of materials.

3 Modeling of packed bed

3.1 Literature review

As packed bed is useful in many engineering applications, numerous studies were performed about fluid flow behavior and heat transfer in this structure. Therefore, numerous numerical models for packed bed have been presented in literature. In this study, the main focus is on TES, so that principally the literature study is referred to that. To model packed bed TES, different approaches can be employed, depending on the accuracy available and on the computational costs affordable.

The first approach consists in the application of simplified energy equations to the components of the storage system, assuming no mass exchange and no heat production inside the storage. In any case, the heat exchanged between solid and fluid is considered proportional to their average difference in temperature. The properties of the materials could be considered uniform and constant or not, depending on the problem. The simplest model consists in neglecting the conduction resistance of the packed bed, with respect to the convection one; it results basically in a 0D elementary model. This approximation is allowable only for very small Biot numbers (<<1). Schumann [47] developed a one-dimensional two-phase model of heat exchange in porous media, consisting in two energy equations, one for each phase, linked by a common convective term. Enhancement of Schumann's model can be implemented accounting for thermal losses, which could affect relevantly the performance. In this case, thermal losses can be expressed by using a global heat transfer coefficient, accounting for the external convective thermal resistance, conduction inside the wall and radiative losses. Sometimes a diffusion term may also be added to better account for stratification during standby periods [48], even if often it is a second order phenomenon during the charge and discharge phase. Votyakov [49] developed a perturbation model, a variation of Schumann's one in which also conduction in fluid and solid phases are considered. The model is based on the consideration that the temperature of the solid differs from the fluid's one by a small perturbation, if compared to the reference temperature. Perturbation models are in general more precise than single phase models. In general, all the models cited before are one-dimensional. However, also some simple two-dimensional models can be achieved with this approach. This is useful in case of flow heterogeneities or relevant radial thermal gradient due to heat losses through the wall. All the parameters could vary in both the two principal directions. These equations permit to obtain a better representation of the phenomena inside the packed bed, allowing also to implement anisotropic effective conductivity if relevant. A three-dimensional model could be achieved from adding a third dimension. Sometimes the heat conduction phenomena inside the particles could be non-negligible: this case is often of interest in large particle Biot number. The model proposed by Handley and Heggs [50] includes this added term by computing, in each elementary layer, the temperature of the fluid and the temperature profile inside a representative solid. This model is applicable under the assumptions of central thermal symmetry of the solid and uniform. All the improvements of the Schumann model can be implemented also in this case, consequently increasing the accuracy.

A totally opposite approach is the complete CFD model, based on the solution of Navier-Stokes equations for laminar or turbulent flow. In this case the packed bed is fully computed by solving the fluid flow and the heat exchange equations around and inside all the particles. This way of modeling is the most accurate possible and particularly suitable for low bed-to-particle diameter ratio, which results in high anisotropic behavior, especially in proximity to the walls. This represents the most accurate approach possible, but it is also very expensive in terms of computational costs. The reason for a full CFD representation derives from the consciousness that the heat transfer mechanism depends mainly on fluid dynamics, or hydrodynamics in case of liquids HTF. Malang et al. [51] introduced the problem with an extensive literature review on CFD modeling applied to packed bed columns, emphasizing the importance of choosing the right model. For fixed bed with small number of spheres, Guardo et al. [52] and Coussirat et al. [53] have investigated the fluid flow and heat transfer mechanisms with CFD models. In Guardo et al., five distinct Reynolds Average Navier–Stokes (RANS) turbulence models (Spalart–Allmaras, standard k–ε, RNG k–ε, realizable k–ε and standard k–ω) were used to study the fluid flow in the packed region, while Coussirat et al. used the most expensive and accurate RSM and Eddy Viscosity Model (EVM) to predict the flow and heat transfer rate. For EVM models, the chosen ones are the one-equation model from Spalart and Allmaras and the two-equations standard k–ε. In both the case it has been shown that CFD represent a useful simulation tool in estimating heat transfer parameters as well as reliable in the calculation of pressure drop in fixed beds. The comparison between standard k–ε and RSM indicated an average error of about 10% from the experimental values. All the evaluations have been done basing on velocity profile, pressure drop, Nusselt number and effective conductivity, and have been compared with some accepted correlations. In another study, Guardo et al. [54] assessed in detail the influence of the turbulence model in predicting the wall-to-fluid heat transfer in packed beds. Dixon et al. [55] focused on the mesh construction, coupling with a k-ω SST turbulence model to evaluate the fluid flow and heat transfer coefficient in a 3D single sphere problem, in order to evaluate the validity of SST model in predicting the Nusselt number with respect to experimental correlations. It has been shown that k-ω SST could be the best one, if a low Reynolds approach is selected. Modeling a single sphere ensure an accurate analysis of the Nusselt number along the profile of the sphere itself, but a complete application to a packed bed structure is necessary to properly validate the model. Jung-Jae Lee [56] used CFD to predict the fluid flow in a packed bed structured core of a nuclear reactor. The bed is composed by a randomly distributed spheres of fuel. Since the core presents fluid flow with high Reynolds number and therefore an accurate treatment of the turbulence is particularly relevant, a k-ω RANS and LES models have been compared with experimental data. As a result, the LES method showed better agreements with the experimental data than the k-ω, which is not able to correctly predict the local heat transfer. On the other hand, the computational cost of the LES method with mesh-size level of accuracy is higher and could be prohibitive in absence of sufficient computer resource. Dixon [57] experimented also the validity of the software COMSOL Multiphysics for detailed simulations of flow, heat transfer and dispersion of species in a 400-sphere random packed bed with low tube-to-particle diameter ratio in laminar and turbulent regimes. For turbulent flow, the standard k-ε model has been used. Dixon showed the potential of the software for this application, showing good agreement with the trends presented in literature. Jafari et al. [58] observed the flow pattern through random packing of spheres using CFD Fluent. The study focused on a parametric study of pressure drop at different Reynolds numbers with regard to interstitial fluid velocity and pore permeability. A model including inertial terms was simulated basing on Navier–Stokes equations, but without coupling any turbulence model. It was noticed that the influence of wall on drag coefficient values decreases with an increase in the D/d_p ratio and the value tends to agree with Ergun's equation. A third general approach, very often used for industrial scopes which includes packed bed structures or flow in porous devices, is the porous media approach. It consists basically in a CFD approach with a simplification in the packed zone. Indeed, in that zone the particles are not computed one-by-one, but are substituted by a uniform homogeneous material identified by certain values of porosity and permeability, to simulate the effect of a fixed bed. This solution is not the most accurate, if compared with the previous approach, but reduces dramatically the computational costs maintaining a reasonable grade of accuracy for first analyses and basic optimization procedures for engineering applications. The cited approach is principally described in the publications of Zanganeh, Zavattoni [59] [60] [61] and Cascetta [62], and has been applied for the construction of industrial scale packed bed TES. The porous media models are based on the Darcy's law and its derived equations, and several studies have been conducted to make the approach as much precise as possible. Nonetheless, some limitations occur, as it is not possible to simulate the local velocity field in the same way of a complete CFD model. The theory behind this approach, such as the assumptions and simplifications, are discussed in the following sections.

Concerning the modeling of radial packed bed TES, studies using the first mathematical approach have been conducted by McTigue et al. [23] and Trevisan et al. [22]. McTigue analyzed a cold energy storage, making an exhaustive comparison with a corresponding axial one. As a result, it has been shown that radial packed bed present smaller pressure losses, mainly due to smaller path of the fluid and lower velocity caused by a larger cross section. On the other hand, the largest thermal front thickness leads to slightly worse performances with respect to the axial TES. Trevisan et al. performed a similar 1D study with a high temperature radial TES. The radial storage presented thicker thermocline, which remains the most critical feature of this concept. However, the author emphasized the reduction of thermal and pressure losses achievable, and the small requirement for insulation related to the shape of the storage. Moreover, a thinner thermocline could be reached with a properly optimized design. Other researches about radial packed bed structures are related to chemical reactors and filters. Among them, Heggs et al. [63] implemented a simplified mathematical model for predicting pressure drop along the radial direction and flow distribution in a multi-layered annular packed bed structure used in air filters, and compared it with experimental data. The model showed good agreement with the data in terms of pressure profile in the bed, but not in the manifolds. The same authors in 1994 [64] conducted an accurate study on the same topic, modeling a mono-layered 2D radial packed bed and comparing different arrangements, such as the "U" (or "Π") and "Z" configurations with normal and reverse flow. Heggs et al. highlight the radial dimensions of the inlet and outlet manifolds, the axial bed length, the surface friction factors associated with the manifolds, the characteristic parameters of the bed packing and the flow rate as the main parameters to investigate for radial packed bed reactors. The principal assumptions of the model consist in considering the fluid isothermal and incompressible, and allowing only radial flow direction in the packed zone. As a result, the longitudinal flow profile is more uniform with a "U" configuration. Ruijiang Li and Zibin Zhu [65] performed a hydrodynamic investigation of multilayer Π-type radial flow reactor. From the model, it resulted that the uniformity of flow distribution was strongly affected by the pressure profiles in the inner and outlet channels along the axial direction; moreover, the uniformity of the flow varies in the radial direction. To a similar study, Mu et al. [66] added a theoretical basis and useful method for the optimum design and operation of radial packed bed reactors, including a design criterion for flow distribution uniformity. Kareeri et al. [67] analyzed a radial packed bed using the third approach, developing a CFD model coupled with a porous media law. As for the previous studies, the Π-type central pipe structure showed a more uniform axial flow distribution with respect to the "Z" configuration. Moreover, the authors suggested to change the porosity of the inner tube, in order to reach a more uniform flow.

As can be observed, not so many CFD models are available for radial devices including packed bed structures and almost nothing about radial TES. Therefore, the present study aims not only to build a CFD model for a laboratory scale storage, but also to propose suitable solutions to improve the performance of radial packed bed structures, including chemical reactors and filters, by making the fluid flow and the temperature distribution in the axial direction as much uniform as possible.

3.2 Theoretical Background

3.2.1 Navier-Stokes Equations and turbulent flow

Predicting the fluid field and heat transfer mechanism inside the TES results in the solution of the Navier-Stokes equations in turbulent regime [68] [69]. They consist in a set of non-linear partial differential equations in space and time. Navier-Stokes equations govern the motion of fluids and can be seen as Newton's second law of motion for fluids. In the case of a compressible Newtonian fluid, this yields:

$$\rho\left(\frac{\partial \boldsymbol{u}}{\partial t}+\boldsymbol{u}\cdot\nabla\boldsymbol{u}\right)=-\nabla p+\nabla\cdot\left(\mu(\nabla\boldsymbol{u}+(\nabla\boldsymbol{u})^T)-\frac{2}{3}\mu(\nabla\cdot\boldsymbol{u})\boldsymbol{I}\right)+\boldsymbol{F} \tag{1}$$

where u is the fluid velocity, p is the fluid pressure, ρ is the fluid density, and μ is the fluid dynamic viscosity. The different terms correspond to the inertial forces, pressure forces, viscous forces, and the external forces applied to the fluid.

These equations are always solved together with the continuity equation:

$$\frac{\partial \rho}{\partial t}+\nabla\cdot(\rho\boldsymbol{u})=0 \tag{2}$$

The Navier-Stokes equations represent the conservation of momentum, while the continuity equation represents the conservation of mass. In case of heat transfer phenomena involved, one or more energy equations have to be added and solved in a coupled or segregated way with the previous general equations.

An accurate prediction of the phenomena involved within the storage requires the solution of the turbulent flow inside of it. In particular, the correct choice of the turbulent model in the inlet and outlet one could influence considerably the heat transfer mechanisms and thus the temperature prediction in the packed zone. To do it, a brief introduction to turbulence and how to model it in a CFD simulation is necessary.

Turbulent flows are characterized by random and chaotic variance in velocity and other flow properties. They also contain rotational flow structures with so called turbulent eddies. Larger eddies are dominated by inertia effects. This leads to that turbulent flows have a higher amount of inertial forces compared with laminar flows. The Reynolds number, which is shown in the following equation, gives a measure of the relative importance between the inertia forces acting on a fluid and the viscous forces [69]:

$$Re=\frac{\rho uL}{\mu}=\frac{inertial\ forces}{viscous\ forces} \tag{3}$$

The Reynolds number thereby gives an indication of a flow is laminar or turbulent. Depending on if the flow is a free stream over a flat plate or a jet flow or inside a pipe, the transition from laminar to turbulent flow occurs at different Reynolds numbers. For pipe flows, this transition happens at a

Reynolds of around 2300: more accurately, this value is indicative, as in practise it occurs within a certain range.

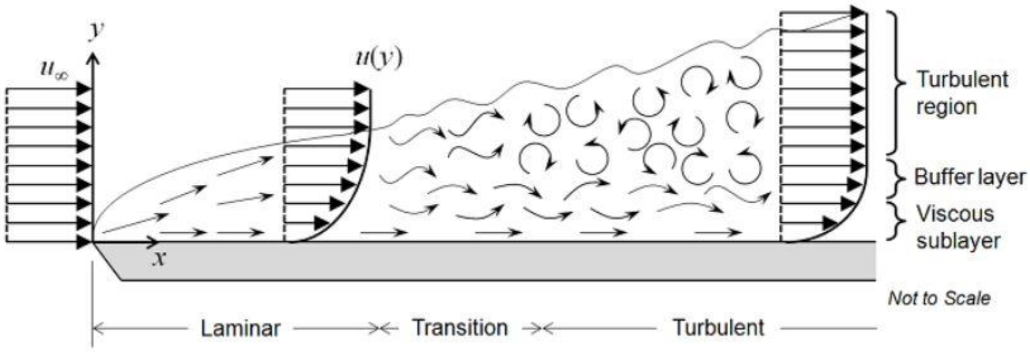

Figure 23 Development of a fluid flow from laminar to turbulent.

Turbulent flows are generally characterized by fluctuating velocity fields. These fluctuations can be both in space and time, and mix transported quantities such as momentum, energy, and species concentration, and cause the transported quantities to fluctuate as well. Since these fluctuations can be of small scale and high frequency, in practical applications they could be too expensive to solve, from a computational point of view. Instead of simulate all of them, the governing equations can be averaged in space and time or otherwise manipulated to remove the smallest scales, resulting in a modified set of equations computationally less expensive to solve. On the other hand, the simplified equations contain additional unknown variables, and turbulence models are needed to determine these variables in terms of known quantities.

The following models are the most used and accepted:

- Algebric yPlus and L-VEL;
- Spalart-Allmaras;
- k-ε models: Standard k-ε, RNG k-ε, Realizable k-ε;
- k-ω models: Standard k-ω, Shear-Stress Transport (SST) k-ω;
- Reynolds Stress Model (RSM)
- Large Eddy Simulation (LES).

Each model has its own characteristics, advantages and weaknesses, and unfortunately there is no single turbulence model which can be considered the most suitable for all classes of problems. The choice of the model depends on many considerations, including the practical application, the physics of the problem, the level of accuracy required, the available computational resources, and the time constraints for the simulation [70]. In order to select the most appropriate model, it is needed to understand the capabilities and limitations of the various options, accounting also for the computational resources used to solve the problem.

3.2.1.1 RANS and LES approaches

A complete time dependent solution of the "exact" Navier-Stokes equations for turbulent flows in complex geometries cannot be affordable at the moment. For this reason, two alternative methods can be employed to transform the Navier-Stokes equations, so that the small-scale turbulent fluctuations do not require to be directly simulated: Reynolds averaging and filtering. Both the two methodologies introduce additional terms in the governing equations that have to be modeled to solve the equations themselves. The Reynolds Averaged Navier-Stokes (RANS) equations simulate transport equations only for the mean flow quantities, with all the scales of the turbulence being modeled. The averaging results in the addiction of some equations, consisting in the six Reynolds stress equations, or in transport equations for scalar quantities (turbulent kinetic energy, turbulent dissipation rate, specific dissipation rate). The approach of computing a solution for the mean flow variables reduces dramatically the computational requirements, making the solution more economical in terms of time consumption. The RANS approach is generally adopted for practical engineering calculations, and mostly used for industrial applications, in which the accuracy requirements are less strict. It uses models such as Spalart-Allmaras, k-ε and its variants, k-ω and its variants, and the RSM. LES method proposes an alternative approach in which the large eddies are computed by using a set of filtered equations. Filtering consists essentially in a variation of the exact Navier-Stokes equations with the aim to remove only the eddies smaller than the size of the imposed filter, which is usually taken as the mesh size. LES method results particular attractive because, by modeling less of the turbulence and solving more, the error induced by the turbulence model is reduced. However, the application of this method for industrial purpose is still not diffused, mainly due to the large computational resources needed to resolve the turbulent eddies.

3.2.1.2 L-VEL and yPlus

The L-VEL and algebraic yPlus turbulence models compute the eddy viscosity using algebraic expressions based only on the local fluid velocity and the distance to the closest wall. These models consist a simple algebraic turbulence model which does not require the solution of any partial differential transport equations. The models solve for the flow everywhere and are the most robust and least computationally intensive among all the turbulence models. While they are generally the least accurate models, they do provide good approximations for internal flow, especially in electronic cooling applications [71].

3.2.1.3 The Spalart-Allmaras Model

The Spalart-Allmaras model is a one-equation model that solves an additional transport equation for the kinematic turbulent eddy viscosity. It represents a class of one-equation models in which it is not necessary to calculate a length scale related to the local shear layer thickness. The Spalart-Allmaras model was originally developed for aerodynamics applications and has been shown to give good results for boundary layers characterized by adverse pressure gradients. The model is relative robust and has moderate resolution requirements. However, experience shows that this model does not accurately compute fields that exhibit shear flow, separated flow, or decaying turbulence. Moreover, the model is still relatively new, and no claim is made regarding its suitability to all types of complex engineering flows.

3.2.1.4 The Standard k-ε Model

The k-ε model belongs to the class of two-equation models, in which the solution of two separate transport equations allows to determine independently the turbulent velocity and length scales. Transport equations are solved for two variables: turbulence kinetic energy, k, and rate of dissipation of turbulence kinetic energy, ε. It represents one of the most employed models of practical engineering flow calculations, due to its robustness, economy, and reasonable accuracy in a wide range of cases, such as in modeling industrial flow and heat transfer simulations. As the model has been widely tested in numerous engineering cases, its strengths and weaknesses are well known. In general, this model is very accurate for bulk flows, and tends to lose precision near to the boundary layer.

3.2.1.5 The RNG k-ε Model

The RNG k-ε model was derived using a renormalization group theory. It is similar in form to the standard k-ε model, but includes some modifications, leading to some differences:

- Improved accuracy for rapidly strained flows;
- Enhanced accuracy for swirling flows;
- Analytical turbulent Prandtl numbers, while in the standard model are constant values;
- Adaption to low Reynolds number, even if it depends on the treatment of the near-wall region.

3.2.1.6 The Realizable k-ε Model

The realizable k-ε model is a relatively recent development and differs from the standard one in two important features:

- A new formulation for the turbulent viscosity;
- A new transport equation for the dissipation rate, ε, derived from an exact equation for the transport of mean-square vorticity fluctuation.

An immediate benefit of the realizable k-ε model is that it predicts with increased accuracy the spreading rate of both planar and round jets. It also performs better for flows involving rotation, boundary layers under strong adverse pressure gradients, separation, and recirculation. Both the realizable and RNG models have shown relevant improvements with respect to the standard one in problems involving strong streamline curvature, vortices, and rotation. Nonetheless the model is relatively new and not tested in many applications, initial studies showed that the realizable model provides the best performance of all the k-ε models for several problems of separated flows and flows with complex secondary flow features. One limitation of the realizable k-model is that it produces non-physical turbulent viscosities in situations when the computational domain contains both rotating and stationary fluid zones. This is due to the fact that the realizable model includes the effects of mean rotation in the definition of the turbulent viscosity.

3.2.1.7 The Standard k-ω Model

The standard k-ω model is based on the Wilcox model. It is similar to the k-ε model, but it solves a transport equation for the specific rate of dissipation of kinetic energy, ω, instead of for the specific dissipation rate. It is a low Reynolds number model, but it can also be used in conjunction with wall functions. It is more "non-linear", and therefore more difficult to converge with respect to the k-ε model, and it is quite sensitive to the initial guess of the solution. The k-ω model is useful in many cases where the k-ε model is not accurate, such as internal flows, flows that exhibit strong curvature, separated flows, and jets. The principal drawback is related to the solution far from the boundary layer, where instead the k-ε is more accurate.

3.2.1.8 The Shear-Stress Transport (SST) k-ω Model

The shear-stress transport (SST) k-ω model was developed to conjugate the robustness and accuracy of the k-ω model in the near-wall region with the free-stream independence of the k-model in the far field. To do this, the k-ε model is converted into a k-ω formulation. The derived SST k-ω model is similar to the standard k-ω one, but includes some different features:

- Adding of a blending function, in order to activate the standard k-ω model in the near-wall region and the transformed k-ε model away from that region;
- A damped cross-diffusion derivative term is included in the ω equation;
- The transport of the turbulent shear stress is accounted;

– Different modeling constants.

These features make the SST k-ω model more reliable and accurate for a wider class of flows than the standard k-ω model.

3.2.1.9 The Reynolds Stress Model (RSM)

The Reynolds stress model (RSM) is the most elaborate turbulence model in many accredited CFD software. Abandoning the isotropic eddy-viscosity hypothesis, the RSM closes the RANS equations by solving a transport equation for each Reynolds stress, together with an additional transport equation for the dissipation rate. As a result, four additional transport equations must be solved in 2D flows and seven in 3D. Since the RSM accounts for the effects of streamline curvature, swirl, rotation, and rapid changes in strain rate in a more rigorous way than the previously mentioned models, it has higher potential to give accurate predictions for complex flows. However, the fidelity of RSM predictions is still limited by the closure assumptions employed to model various terms in the exact transport equations for the Reynolds stresses. The RSM might not always produce results that are clearly superior to the simpler models in all classes of flows to be worth the additional computational cost. However, use of the RSM is a must when the flow features of interest are the result of anisotropy in the Reynolds stresses.

3.2.2 Porous media approach

The main issue in modeling a packed bed TES resides in the choice of how to compute the fixed bed zone, which constitutes the region in which energy is stored and heat exchange with the HTF takes part. As cited in literature review, a complete solution of the packed zone, consisting in explicitly computing the fluid flow surrounding each filler particle, is unaffordable, due to the high computational cost. Hence, an alternative way has been followed. For the present study, in order to ensure an affordable computational time, the macroscopic porous media approach has been exploited, rather than modeling singularly all the elements in the internal domain. In this way, the particles are substituted with a homogeneous continuous media, identified by a porosity and a permeability, and by average properties which accounts for the presence of the solid and the fluid parts.

In porous domains, as in Navier-Stokes, the flow variables and fluid properties are defined at any point inside the medium by averaging the actual variables and properties over a certain volume surrounding the point. However, the basic condition is that the control volume is small enough if compared to the macroscopic dimensions of the problem under assessment, and at the same time large enough to include many solid matrix elements. As a result of this approach, the physical properties of the fluid, such as density and viscosity, are defined as intrinsic volume averages. In this way, the relevant physical parameters are assumed to be continuous with the corresponding parameters in the adjacent free flow and can be evaluated experimentally. The flow velocity, for example, is defined as a volume average, and it corresponds to a unit volume of the medium including both the pores and the matrix (or more adjacent particles in this study).

The approximation constituted by the porous media approach derives from the concept that in packed bed structures with high tank-to-particle dimeter ratio D/d_p the turbulent phenomena tend to be partially (or totally) suppressed, due to the low space among the particle, which reduces the formation of eddies and vortices. As a result, the flow field inside the packed zone is closer to a laminar flow and more homogeneous. This assumption is as less correct as the D/d_p ratio increases, so that in case of higher particle diameter the irregularities of the fluid flow in a generic section perpendicular to the main direction could not be negligible and must be computed with a more expensive approach.

The model is based principally on the Darcy's or on the Brinkman's equation, whose features are explained in the following paragraph. However, dependently on the case, many different laws can be applied [71] [72] [73].

3.2.2.1 Free Flow: The Navier-Stokes Equations

The fluid flow in the river channel is governed by the Navier-Stokes equations, as there in not a porous media in the domain. Depending on the Reynolds number, it is possible to model the problem with a laminar or turbulent flow, without applying the porous media approach.

3.2.2.2 Slow Flow in Porous Media: The Darcy's Law

Within the porous media approach, Darcy's law, coupled with the continuity equation and the equation of state for the pore fluid (or gas) provides a complete mathematical model applicable in a wide range of applications involving porous media flows, for which the pressure gradient is the main driving force and the flow is mainly influenced by the frictional resistance within the pores. This law describes essentially the fluid movement through interstices in a porous material. Considering that the fluid loses considerable energy due to frictional effect within the pores, flow velocity in porous media tends to be very low.

Basically, the Equation Formulation Darcy's law states that velocity field depends on pressure gradient, fluid viscosity and the structure of the porous medium. Darcy's law applies when the gradient in hydraulic potential drives fluid movement in the porous medium. The equation states that velocity is directly proportional to pressure gradient of the gas phase:

$$\nabla p = -\frac{\mu}{\kappa}\boldsymbol{u} \tag{4}$$

Where u is the Darcy's velocity of the fluid, μ the dynamic viscosity of the fluid and κ the permeability of the bed defining the resistance of fluid flow through the medium.
Darcy's equation is applicable only in regions without any boundary shear flow, such as away from the walls. It is a model useful for low Reynolds numbers, used to model low-velocity flows or media with very small permeability and porosity.

3.2.2.3 *Fast Flow in Porous Media: The Brinkman Equations*

The Brinkman equation is normally used to describe fast-moving fluids in porous media. In this case the flow is driven by the kinetic potential from velocity, pressure and gravity. The equation is an extension of Darcy's law able to describe the dissipation of kinetic energy by viscous shear as with the Navier-Stokes equations. The principal difference with the Darcy's Law is represented by the introduction of a Laplacian term, as can be observed in the equation:

$$\nabla p = -\frac{\mu}{\kappa}\mathbf{u} + \mu\nabla^2\boldsymbol{u} \tag{5}$$

As can be seen, in the Brinkman equation there are two viscous terms. The first is the Darcy's term and the second is the mentioned Laplacian term, which is normally included in the Navier-Stokes equation. By using this extension, the sheer stress will be accounted for, forming a relationship between permeability and porosity.
As a result, this model is useful also for transitions between slow flow in porous media governed by Darcy's law and fast flow in channels described by Navier-Stokes equations. Indeed, the Brinkman equations are largely employed coupled with Navier-Stokes ones, in order to represent models in which a fluid in free flow state passes through a porous media. However, for fast flows in highly porous media, it is recommended to directly model the domain and use Navier-Stokes equations, or to use another law to describe the phenomenon.

3.2.2.4 *Variably Saturated Porous Media: The Richards' Equation*

Richards' equation has been used to model flows in partially saturated porous media, such as the movement of water in unsaturated soils.
This law accounts for the changes in hydraulic properties as fluids flow throughout the medium, filling some pores and draining others. Similarly to Darcy's law, the pressure gradient is considered as the main driver of the flow. Richards' equation is nonlinear, due to the fact that the hydraulic properties vary based on saturation, which can make it a bit more challenging to compute numerically with respect to Darcy's law.

3.2.2.5 Two-Phase Porous Media Flow: The Two-Phase Darcy's Law

These equations consist in an extension of Darcy's law, which includes the possibility to model two-phase flows in porous media. These models are particularly relevant and interesting in the petroleum and chemical industry, such as in oil reservoirs. In addition to the normal Darcy's law and the calculation of the pressure and velocity field, the two-phase model solves a transport equation for the fluid content of one fluid phase. Fluid properties, such as density a and viscosity, are averaged based on the saturation and properties of each phase.

3.2.2.6 Porosity models

As can be deduced from chapter 1, porosity is a key parameter to represent the characteristics of a packed bed TES; therefore, the correct estimation of its value and variation inside the storage is particularly important. According to Klerk [30], basically four random packing models can be found:

- Very loose random packing ($\varepsilon \approx 0.43$-0.44), obtained usually by sedimentation or decreasing the fluid velocity in a fluidized bed;
- Loose random packing ($\varepsilon \approx 0.40$-0.41), obtained putting the spheres individually;
- Poured random packing ($\varepsilon \approx 0.375$-$0.391$), obtained pouring spheres into a container;
- Dense random packing ($\varepsilon \approx 0.359$-$0.375$), obtained by shaking down the container with the particle.

However, mean porosity is useful to describe the general particle disposition, while changes in specific zones occurs due to change in geometry. Zavattoni et al. [60] described two fundamental conditions which affects the porosity and changes it with respect to the bulk one:

- The wall effect, or channelling: as mentioned before, in the near-wall region the arrangement of the particles is different, affecting the overall bed until a distance of 5 particle diameters from the wall. In that zone, porosity distribution presents a sharp oscillatory variation, from a value close to unity to a minimum of 0.2, due to the presence of the external walls;
- The thickness or top-bottom effect: it is connected to the effect of gravity, which brings to higher value of porosity on the top of the bed and lower ones on the bottom.

The second effect is considered negligible in almost all the practical cases, except if the ratio d_p/H is higher than 0.05.

To investigate the porosity variation related to the channeling effect near the wall, numerous theoretical and experimental studies have been conducted. Thus, many analytical and experimental correlation are available to model the problem. Basically, the correlations available in literature follows two types of behavior: oscillatory and exponential. In all the correlation considered by [32], the porosity is equal to the bulk one in the inner regions, since there is not wall effect, and increases until the value of 1 in proximity to the wall, with the maximum value corresponding to the contact point. The difference is represented by the trend in proximity to the wall, which tends to be oscillatory in one case, similarly to the experimental measurements available in literature and more accurate, or exponential, leading to a simpler approach.

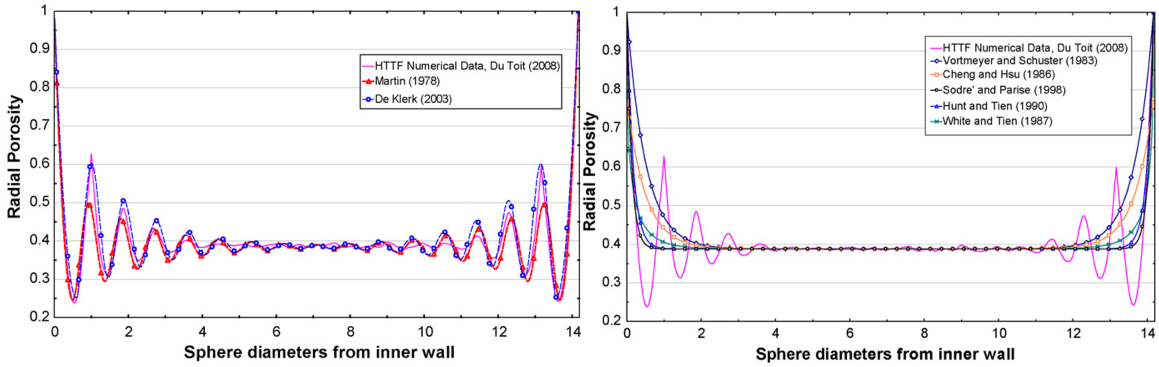

Figure 24 Comparison between radial oscillatory (left) and exponential (right) porosity correlations [32].

Under the conditions mentioned before, the porosity variation could, or could not, influence relevantly the fluid flow in the packed region and the heat transfer.

3.2.2.7 Heat transfer in porous media

Heat transfer in porous media has been an extensively investigated research topic, being associated to several engineering applications, including fluid flow through materials and heat transfer. Indeed, the heat transfer and transport phenomena through porous media are important processes, for example, in heat exchanger, packed sphere bed, electronic cooling, chemical catalytic reactors, and heat pipe technology.

Heat transfer in porous media is a very complex phenomenon, involving fluid flow, conduction and radiation. Due to this fact, it could result very complicated to model, and often requires some simplifications, in dependence on the features of the problem analyzed and on the accuracy constraints. As assumed by Kunii and Smith [74], along the principal direction the following mechanisms are the most relevant:

1) Heat transfer through the fluid in the void space by advection/diffusion, and by radiation between adjacent voids (when the voids contains a non-absorbing gas, such as air). Heat transfer through the fluid is more relevant for not low Biot number, and becomes the only principal mechanism as the Biot number increases.
2) Heat transfer through the solid phase. This mechanism depends on the addiction of different phenomena, such as:

a) Heat transfer through the contact surface of the solid particles. This term is particularly influenced by the contact area of the particle, which depends mainly on their shape and disposition.
b) Conduction through the stagnant fluid near the contact surface.
c) Radiation between surfaces of solid (when the voids are assumed to contain a non-absorbing gas). This term is negligible for low temperatures, and becomes more relevant as the absolute temperature inside the structure increases, depending on its 4^{th} power;
d) Conduction through the solid phase. This term is considered negligible for very low Biot number.

As assumed by Kunii. overall mechanisms 1 and 2 are in parallel with each other. Mechanism d is in series with the combined result of parallel mechanisms a, b, and c. The second phenomenon is accounted by using an effective thermal conductivity for a stagnant fluid, while the first by modeling mass, momentum and energy equations.

The heat transfer equation for porous media is derived from the mixture rule on energies appearing in solid and fluid heat transfer equations. For non-deformed fixed solids, the equation can be formulated as:

$$\rho_s c_{p,s} \frac{\partial T_s}{\partial t} + \nabla \cdot \boldsymbol{q}_s = Q_s \tag{6}$$

and for a fluid domain, with neglected pressure work and viscous dissipation, the equation describing the phenomenon becomes:

$$\rho_{fl} c_{p,fl} \frac{\partial T_{fl}}{\partial t} + \rho_{fl} c_{p,fl} \boldsymbol{u}_{fl} \cdot \nabla T_{fl} + \nabla \cdot \boldsymbol{q}_{fl} = Q_{fl} \tag{7}$$

The mixture rule is applied by multiplying the first equation by the solid volume fraction, θ_p, which is the complementary to 1 of the porosity, and the second one by the porosity, $1-\theta_p$, and then summing resulting equations.

3.2.2.8 Local Thermal Equilibrium

The local thermal equilibrium hypothesis assumes equality of temperature in both fluid and solid phases:

$$\left(\rho c_p\right)_{eff} \frac{\partial T}{\partial t} + \rho_{fl} c_{p,fl} \boldsymbol{u}_{fl} \cdot \nabla T + \nabla \cdot \left(-k_{eff} \nabla T\right) = Q \tag{8}$$

Where:

$$T_{fl} = T_s = T$$

$$\left(\rho c_p\right)_{eff} = \theta_p \rho_s c_{p,s} + \left(1 - \theta_p\right) \rho_{fl} c_{p,fl} \tag{9}$$

Although only one phase is considered, this approximation is considered accurately sufficient for several applications, such as problems without internal volumetric heat production in one of the phases, and in which energy is stored in the same way. For instance, a packed bed TES can be represented with a single equation only for small particle diameter and if only sensible heat is exchanged, thus without phase-change materials. As shown in the following paragraph, the effective thermal conductivity k_{eff} can be calculated in different ways, depending on the heat transfer mechanism taken into account.

3.2.2.9 Effective thermal conductivity

The effective thermal conductivity of the solid-fluid system, k_{eff}, is related to the conductivity of the solid, k_p, and to the conductivity of the fluid, k, and depends in a complex way on the geometry of the medium. The simplest way to calculate the effective thermal conductivity is considering them in parallel (10), in series (11) or with weighted power law (12).

$$k_{eff} = \theta_p k_s + \left(1 - \theta_p\right) k_f \tag{10}$$

$$\frac{1}{k_{eff}} = \frac{\theta_p}{k_s} + \frac{1 - \theta_p}{k_f} \tag{11}$$

$$k_{eff} = k_s^{\theta_p} \cdot k_f^{1-\theta_p} \tag{12}$$

In general, the volume average model provides an upper bound for the effective thermal conductivity, while with series configuration it approaches the lower conductivity between the two materials. However, these simple equations do not account for all the mechanism involved into heat transfer in porous media, such as radiative heat exchange. For this reasons, many models have been investigated in literature, considering different mechanism involved and taking into account also the geometry and the disposition of particles. One of the most used model, developed by Kunii and Smith (ref), has been shown to be very effective for high temperature TES.

Kunii & Smith [74] [60] derived a model to evaluate the k_{eff} considering the packed bed made by homogeneous spheres and the unit cell of the bed constituted by only two particles with one contact point and surrounded by stagnant fluid. With this approximation authors expressed the k_{eff} as a combination of all the heat transfer mechanisms related to the stagnant fluid, including radiation, leading to the following expression:

$$k_{etc}^{0} = k_f \left[\varepsilon \left(1 + \frac{\beta h_{rv} d_p}{k_f}\right) + \frac{\beta (1 - \varepsilon)}{\xi} \right] \tag{13}$$

In which:

$$\xi = \left(\frac{1}{\varphi} + \frac{d_p h_{rs}}{k_f}\right)^{-1} + \frac{2}{3}\frac{k_f}{k_s} \tag{14}$$

Where the radiation heat transfer coefficients for void-to-void (h_{rv}) and solid surface to solid surface (h_{rs}) exchange respectively, are obtained as:

$$h_{rv} = 0.227\left(1+\frac{\varepsilon(1-\Psi)}{2\Psi(1-\varepsilon)}\right)^{-1}\left(\frac{T}{100}\right)^{3} \tag{15}$$

$$h_{rs} = \frac{0.227\cdot\Psi}{2-\Psi}\left(\frac{T}{100}\right)^{3} \tag{16}$$

Where Ψ is the emissivity of the solid part and the parameter φ, which is the most difficult quantity to evaluate, represents the measure of the effective thickness of the fluid film adjacent to the contact surface of the packed bed unit.

To overcome the complexity in the evaluation of φ, Kunii & Smith proposed a simplification based on the assumption that all the packed beds may be considered as at an intermediate of two basic packing states: the loose (φ_1=1.5 and ε_1=0.476) and the close state ($\varphi_2=4\sqrt{3}$ and ε_2=0.26). Hence, for a bed with a given void fraction, φ can be calculated as:

$$\varphi = \varphi_2 + (\varphi_1-\varphi_2)\frac{\varepsilon-0.26}{0.216} \tag{17}$$

If the porosity of the packed bed is above or below the defined range, it is suggested to compute by using the upper and lower porosity level respectively.

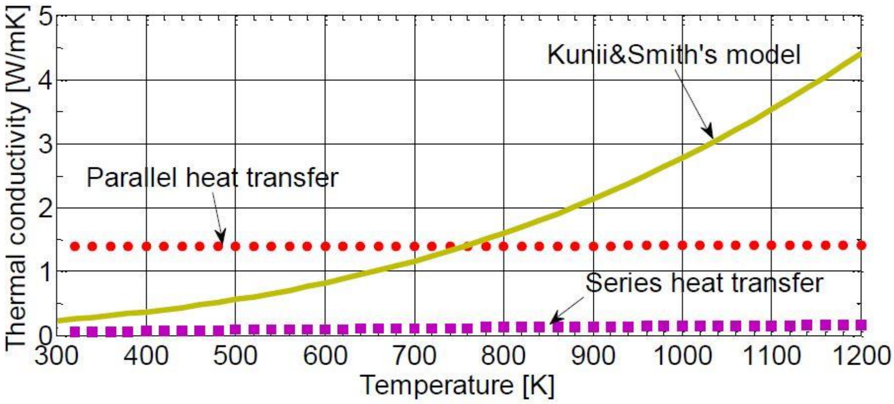

Figure 25 Variation of different ETC models with temperature.

As a result, the effective thermal conductivity result in a trend similar to the one shown in the graph. This way of evaluating k_{eff} has been largely validated and shows good agreement with experimental data.

3.2.2.10 Local Thermal Non-Equilibrium

The Local Thermal Non-Equilibrium theory describes heat transfer in porous media for which the temperatures into the porous matrix and the fluid are not in equilibrium. Non-equilibrium models arise when the transport properties of the various phases are highly contrasted. For instance, the diffusivity of the solid phase is much lower than the diffusivity of the fluid phase. In that case, heat propagates rapidly through the unit cell in the fluid phase and the temperature field relaxes slowly in the solid phase, thus producing a tailing effect. The relaxation process involves many different timescales.

Non-equilibrium heat transfer in porous media for binary systems of rigid porous matrix and fluid phase are governed by two couple differential equations. These are the usual heat equations for solids and fluids, multiplied by the volume fractions θ_p and its complementary to 1 respectively, and with an additional source term used to describe the interaction between the two phases. The solid and the fluid part, respectively, are describe by the following equations:

$$\theta_p \rho_s c_{p,s} \frac{\partial T_s}{\partial t} + \nabla \cdot \left(-\theta_p k_s \nabla T_s\right) = h_{sf}\left(T_{fl} - T_s\right) \tag{18}$$

$$\left(1-\theta_p\right)\rho_{fl} c_{p,fl} \frac{\partial T_{fl}}{\partial t} + \rho_{fl} c_{p,fl} \boldsymbol{u}_{fl} \cdot \nabla T_{fl} + \nabla \cdot \left(-\left(1-\theta_p\right) k_{fl} \nabla T_{fl}\right) = h_{sf}\left(T_s - T_{fl}\right) \tag{19}$$

Where h_{sf} is the interstitial heat transfer coefficient, dependent on the thermal properties of the phases as well as on the specific surface contact area. The term on the right size represent the heat exchanged by the two phases. The mean temperature in the bed is then calculated as a mass-averaged in the porous domain.

4 The Model

In this chapter a model of the previously described system is performed, in order to accurately evaluate and represent all the mechanisms involved during the operation of the storage. As known, the heat transfer phenomenon is mainly affected by the behavior of fluid flow, as the most relevant heat transfer mechanisms are connected to the advection-diffusion phenomenon, and to heat conduction and radiation inside the porous bed. Therefore, a correct representation of these phenomena leads to more accurate results. To predict the behavior of the TES during the charge and discharge phase, a Computational Fluid Dynamics (CFD) approach is employed, by using the heat transfer and fluid flow module of the software Comsol Multiphysics.

Aiming to demonstrate the accuracy of the model, it is necessary to perform a verification procedure. consisting in a grid convergence analysis, based on a robust and widely accepted method. Considering also the lack of publications available about radial flow TES, a validation procedure through measurement in the lab-scale prototype available in laboratory would be useful for future works.

Once the model is verified (and possibly validated), it is a useful tool which allows to investigate how to improve the performance of the storage in the less expensive way, simply by modifying the model itself and varying some parameters within the storage.

The modeling procedure consists in some steps, used to investigate different aspects of the storage, as well as to evaluate the effect of some assumptions on the accuracy of the model. The steps are:

- Step 0: Preliminary analysis of the turbulent models;
- Step 1: 4-hours charge and discharge starting from uniform temperature with adiabatic conditions;
- Step 2: Cycle stability assessment under fixed stop constrains and adiabatic conditions;
- Step 3: Charge, discharge and stand-by phase in a stabilized cycle in presence of dispersion phenomena and an insulation layer.

4.1 Step 0: Preliminary analysis of the turbulent models

4.1.1 Procedure

Although turbulence is partially, or totally, suppressed in the packed zone, the fluid flow is fully turbulent in the central tube and in the external one, where the air is free to circulate without any obstacle. The fluid flow in those zones influences the velocity and pressure distributions at the inlet of the packed bed, influencing consequently the temperature distribution. Thus, the choice of the right model could be determinant.

This preliminary analysis is based only on the fluid flow, and accounts for the accuracy of the solution and the computational cost, as the latter is a relevant parameter for the improving step. The assessment evaluates the performance of different turbulent models in the inner tube, as if it was simulating the fluid flow during the charge phase. The external zone and the discharge phase are not objective of this preliminary analysis, mainly because of the loss of accuracy generated by the axisymmetric approximation (as will be shown in the following paragraph), which makes a turbulent model analysis useless.

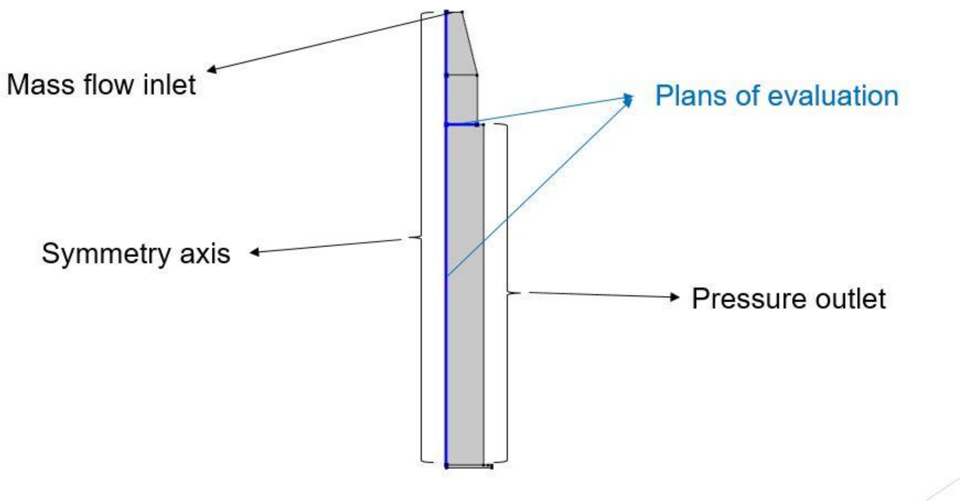

Figure 26 Inner tube geometry and boundary conditions.

Features of the model:

- Steady state fluid flow;
- Boundary conditions:
  - Inlet mass flow rate: 0.035 kg/s;
  - Pressure outlet: 0 Pa (relative pressure);
  - Wall: no slip condition;
- Temperature of inlet flow: 750 °C. Physical properties evaluated at 750 °C.

The boundaries in which the b.c. are applied are visible in Figure 26, while all the other boundaries are automatically walls.

Regarding the models, the LES and RSM ones have been excluded, due to the high computational cost. Others have not been investigated due to similarity with some of the ones considered, but being less attractive in terms of features. Eventually, the models tested are:

- L-VEL;
- Standard k-ε;
- Realizable k-ε;
- k-ω SST.

4.1.2 Results

The comparison is performed basing on velocity magnitude along the evaluation plans illustrated in Figure 26. The choice of the plans is made to roughly analyze the behavior of fluid flow along the vertical and radial direction, to make comparisons among the models. The results are shown in Figure 27 and show substantial differences between the models.

In the symmetry axis, corresponding to a bulk region, it is realistic to believe that the k-ε methods with a wall treatment is more accurate, or at least likely to give a reasonable result. In this case, the two k-ε models are quite similar, while the SST tends probably to overestimate the initial velocity. The L-VEL model is similar to the SST at the inlet, while tends to decrease more than the other models in the rest of the axis. Along the plan in the radial direction, the SST model should furnish the best prediction in proximity to the boundary layer, also due to the different treatment of the boundary layer, while the k-ε models shows the best behavior in the bulk zone. Even in this case, the k-ε shows a smoother trend, while L-VEL has a behavior similar to the SST, but with a slightly increased velocity in proximity of the boundary layer.

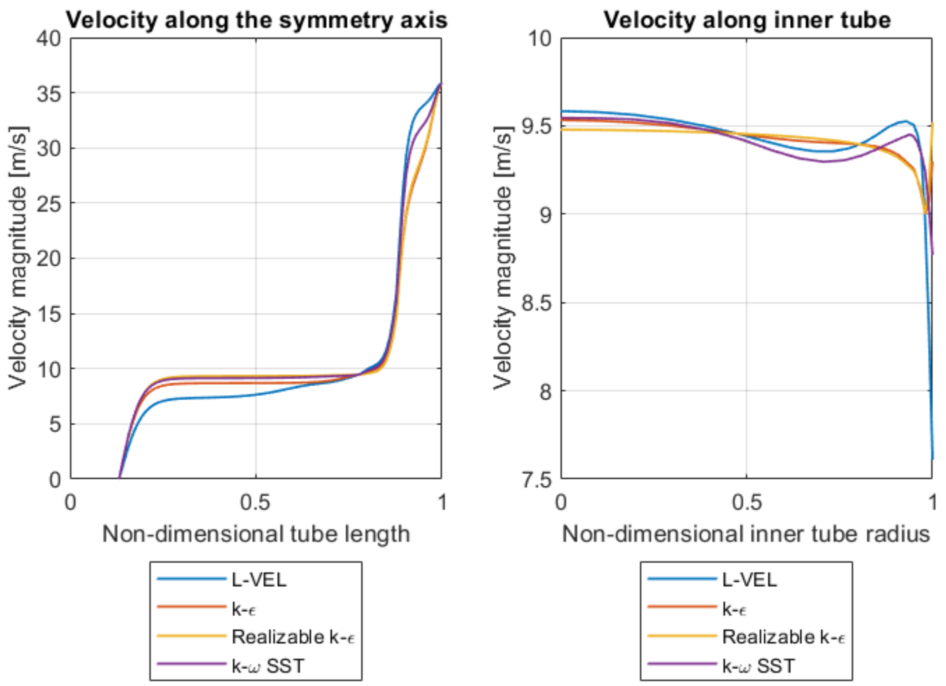

Figure 27 Inner tube, velocity distribution in stationary conditions in the two plans of evaluation.

As can be observed, different models show slightly different results in terms of fluid flow, but it is not so clear which one would represent the best solution. However, these differences tend to be less

relevant in proximity to the porous region, and in the model the influence of the wire meshes decrease even more the difference.
From a computational point of view, it is important to note that the L-VEL model requires 1/3 less time, despite giving acceptable results. The additional computational cost is related to the time of convergence required by the different models, and it is maximum for the SST. The difference in time requirements is even more relevant when the fluid flow is coupled with a heat transfer time-dependent problem. Moreover, an accuracy at k-level does not constitute the major priority of this study, considering the approximations done in the outer channel and in the packed region (see next paragraph). Eventually, reducing the computational time as much as possible facilitate the improvement step, even if the accuracy of the results is reduced.
For all the reasons mentioned above, the L-VEL turbulent model has been selected.

4.2 Step 1: 4-hours charge/discharge

In the step 1, a 4-hours charge and discharge phase are performed. All the features of the model, included the approximations adopted and the limitations of the model, are described in this section.

4.2.1 Geometry

In order to reduce the computational cost as much as possible, many simplifications on the geometry have to be done. Considering the geometrical features and the drivers, in this case corresponding only to the boundary conditions, the problem results intrinsically 3D. Indeed, the flux through the packed spheres is characterized by anisotropies. Even with the simplifications of homogeneous porous medium domain, the design of the external tube (which corresponds to the outlet in the charge phase and to the inlet during the discharge) allows a maximum reduction of the geometry to 1/8 of the total, without affecting the solution. However, this domain is still 3D and the improvement procedure, to be performed subsequently, requires too much computational efforts. For this reason, the problem is studied in an axisymmetric domain, even if this cause a loss of accuracy in predicting the fluid flow in proximity to the external pipe. Figure 28 shows the simplified geometry.

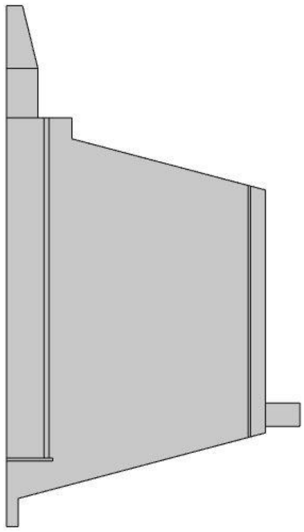

Figure 28 2D axisymmetric simplified geometry of the lab-scale TES.

The effect of the approximation could be not so relevant during the charge phase, but determinant during the discharge, as the fluid flow entering in the packed region could be too much altered with respect to the real one.

4.2.2 Mesh Generation

A triangular based mesh has been used to solve the core of the domain. In particular, the triangular prisms option has been chosen considering it as a good choice for filling all the space in an efficient way, maintaining a good quality of the mesh. The actual mesh used in the simulations consists in 12785 elements, determined as a result of a mesh independence procedure shown in one of the next paragraphs of this section (see 4.3 Verification).

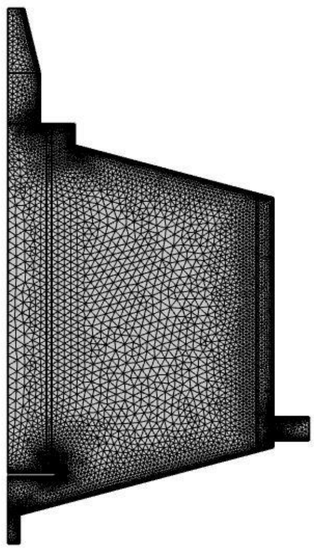

Figure 29 Mesh generation with Comsol Multiphysics.

The prism layer mesh model has been employed to improve the accuracy of the flow solution next to the wall and for better resolving the boundary layer. Being not interested specifically in a great accuracy in the boundary layer and viscous sublayer, the near wall thickness of the first cell in the prism layer has been chosen in order to have a $y^+ > 30$ (high y^+ approach). The boundary layer is then solved with a wall function, without necessity of great refinement. The total thickness of the prism layer has been adapted in order to have a good transition in terms of dimensions of the last prism layer cell and the first core cell.

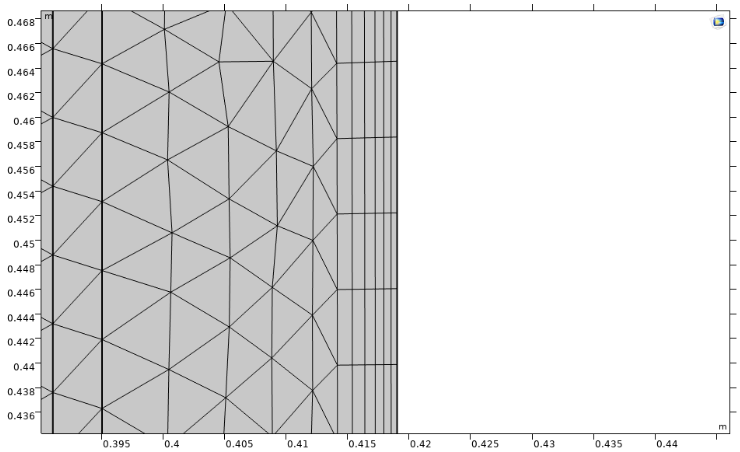

Figure 30 Mesh generation in the boundary layer zone.

4.2.3 Physics

As mentioned before, to model the problem a porous media approach has been adopted, allowing to obtain a homogeneous media in the packed zone, while maintaining a free flow in the non-packed region, such as the inner and the outer channels.

Regarding the physics of the problem, the free and porous media flow option available in Comsol Multiphysics has been employed. According to the features of the interface, a free-flow is used in the channels, combined with a porous media approach in the packed bed and in two of the internal wire meshes. Therefore, for the fluid flow:

- Channels: turbulent Navier-Stokes equations, L-VEL model;
- Packed bed: Brinkman equation coupled with turbulent Navier-Stokes equations to obtain a good transition with the free-flow zone.

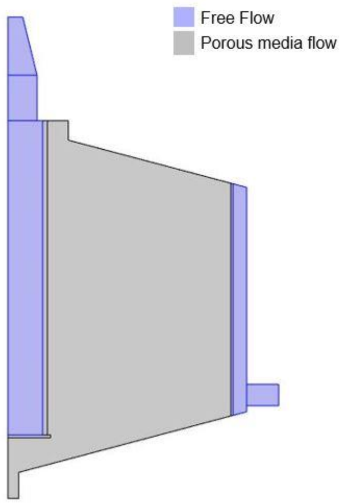

Figure 31 Physics adopted in different domains.

The fluid flow has been considered as weakly compressible, in such a way that the properties of materials are calculated at the actual temperature, instead of at the reference one. Permeability inside the packed bed are calculated with the Kozeny-Carman law, and pressure drop with the Brinkman equation. The fluid flow is coupled with a heat transfer physics, which takes into account the turbulence and the porous zone. The effect of turbulence heat transfer has been considered using Kays-Crawford model. Since the Mach number is minor to 0.3, a segregated approach has been used. Moreover, since the velocity of the fluid through the packed bed is low, the effect of gravity and buoyancy driven forces have been accounted in.

Regarding the materials, air has been used inside the domain, with all the properties found in the Comsol library. All the thermal properties are calculated as temperature-dependent, while the dependence on the pressure has been neglected, considering that the storage works approximately at atmospheric pressure. Also for the packed region all the material properties are temperature-dependent. The packed bed is identified by the bulk porosity, considering that the dimensions of the storage and particles allow to neglect the channelling phenomenon and the effect of the height. Other properties, such as density and thermal capacity, have been volume averaged. The thermal conductivity has been calculated with Kunii and Smith method, to account for all the stagnant heat transfer phenomena, as described previously.

Regarding the wire meshes, some of them have been modelled with the Screen function available in the software interface. This function replaces uniform grille having as only inlet the solidity (complementary to 1 to the open area) and the wire diameter. The drawback of this tool consists in the suppression of the velocity component parallel to the grille. For this reason, only the meshes in the channels are modelled with this tool. To model the ones in contact with the packed bed region, a porous layer of Inconel 625 has been used, considering the porosity equal to the open area of the wire mesh. Furthermore, considering that the real mesh is basically two dimensional (the thickness is negligible) and hence does not influence the heat transfer, the thermal capacity of the Inconel layer has been reduced and the thermal conductivity enhanced.

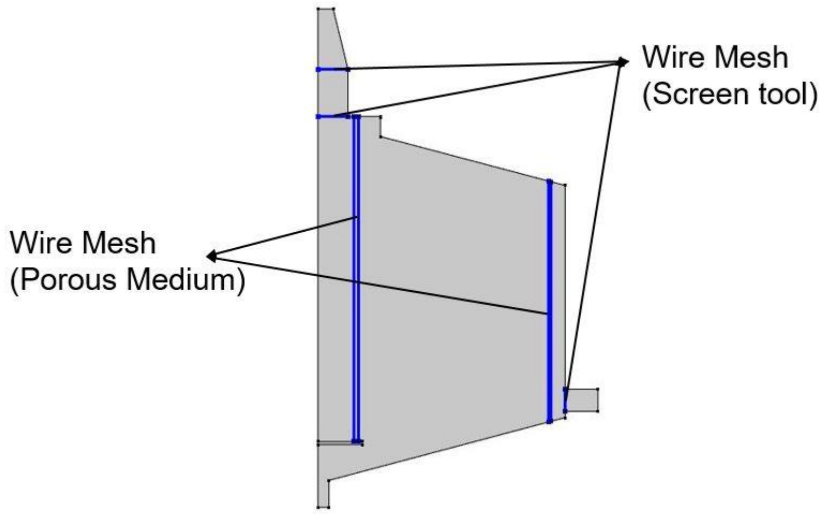

Figure 32 Disposition of the wire meshes in the domain.

4.2.4 Boundary and initial conditions

To make the model working, a set of conditions in space and time has to be imposed. These conditions are different in the charge and discharge phase, as it goes for the boundaries in which they are applied, as shown in the Figure 33. All the conditions imposed are here shown.

Boundary conditions, fluid flow, charge and discharge phase:

- Mass flow inlet: 0.035 kg/s;
- Pressure outlet: 0 Pa (relative pressure);
- Symmetry axis.

Boundary conditions, heat transfer, charge phase:

- Temperature inlet: 750 °C;
- Specific heat flux outlet: 0 W/m^2;
- Symmetry axis.

Boundary conditions, heat transfer, discharge:

- Temperature inlet: 200 °C;
- Specific heat flux outlet: 0 W/m^2;
- Symmetry axis.

Initial conditions, charge phase:

- Initial temperature distribution T(r, z): 200 °C;

- Symmetry axis.

Initial conditions, discharge phase:

- Initial temperature distribution T(r, z): 200 °C.
- Symmetry axis.

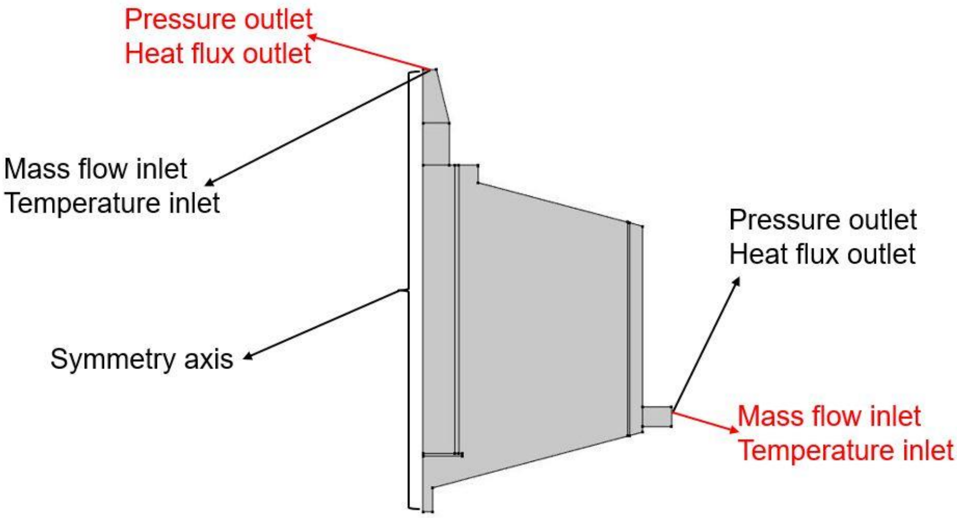

Figure 33 Boundary conditions during charge (in black) and discharge (in red) phases.

4.2.5 Results

The results have been examined in terms of pressure drop distribution inside the packed bed after one hour and local temperature evolution in time. In particular, pressure drop has been evaluated between the inner and outer plans (as visible in the Figure 34), while the temperature has been evaluated in proximity to the thermocouples 3, 8, 13, 18, 23 and along the radial direction. In this way, it is possible to accurately assess the pressure drop distribution and the temperature trend inside the packed bed depending on the interest.

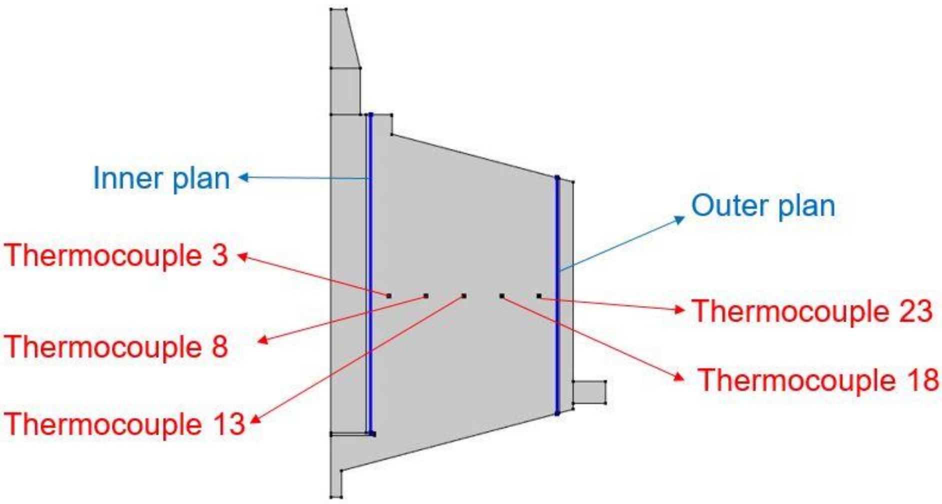

Figure 34 Plans of evaluation of the model's features.

Indeed, for the evaluation of the pressure drop, the interest is more focused on space distribution along the axial direction at different times: this allows to evaluate how much pressure is lost while he HTF passes through the bed and its uniformity in the axial direction is an index of a uniform fluid flow distribution inside the bed itself. Regarding the temperature, it is more interesting to observe the behavior in the radial direction, to assess the thermocline thickness and its evolution in time during the charge and discharge processes.

During the charge phase, it is possible to notice a quite uniformly distributed pressure drop along the axial direction, with a small rise in the upper part of the storage and a slightly more accentuated decrease in the lower one. As shown in Figure 35, an increase in temperature, due to the charge process, results in higher pressure drop and in a more uniform distribution in the z-axis. This major uniformity is also due to a less influence of the variations with respect to the absolute value of the pressure drop.

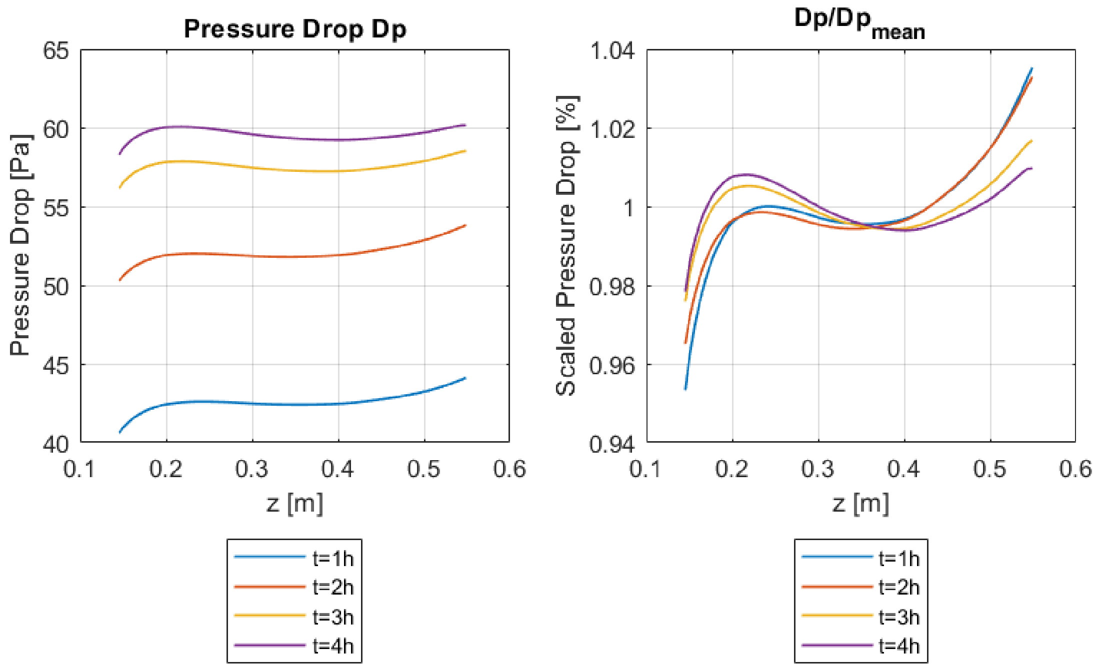

Figure 35 Evaluation of pressure drop, charge phase.

The temperature graphs show an expected trend. Temperature in the thermocouple 3 grows almost immediately, while the others' increase is slower, depending on the distance from the inner channel. As in every thermocline storage, the HTF exchanges heat with all the bed and at different temperatures, as its thermal quality decreases while exchanging heat with the particles. Due to this and to all the heat transfer mechanism involved in the storage, the thermocline thickness increases in after the initial hours and decreases again after stabilizing while the charge phase proceeds, until the relevant thermal gradient goes out of the TES. In the graph on the right the thermocline evolution can be deduced by looking at the temperature slope.

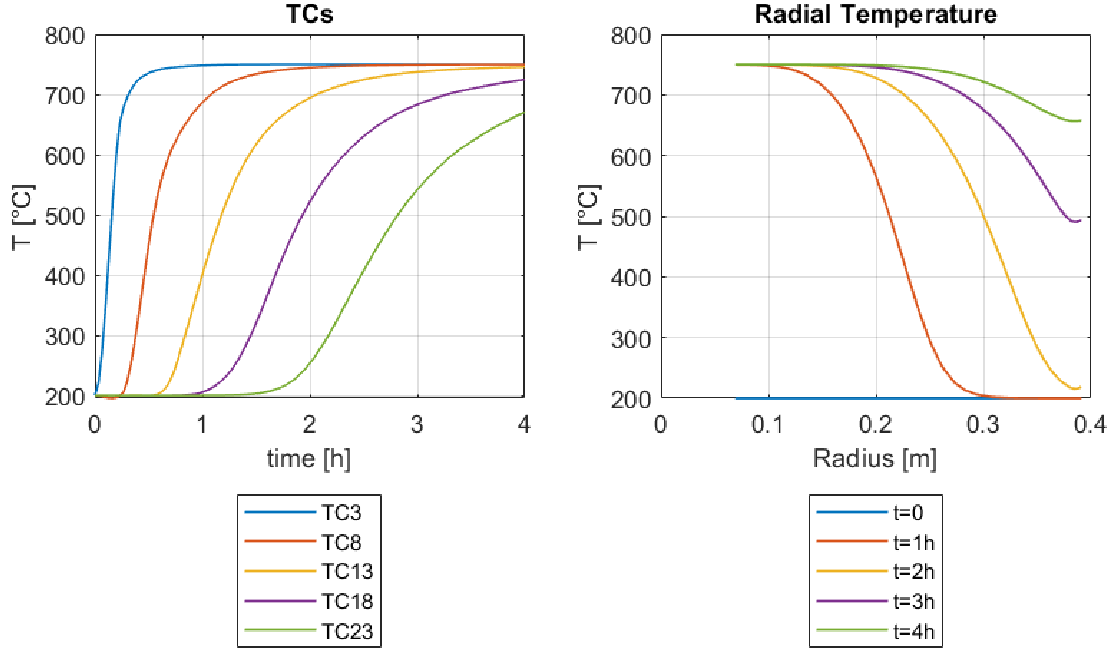

Figure 36 Evaluation of temperature trend in space and time, charge phase.

As for the charge phase, the initial temperature is maintained constant, this time equal to the maximum value. The pressure drop shows an opposite trend with respect to the charge phase, due to the progressively decreasing temperature inside the bed. However, the pressure drop variation in the axial direction is more relevant in this case, and shows a gradually decrease in time (the 4th hour is not relevant, as the storage is completely discharged). The increased variation of pressure drops could be related to the geometry of the storage and in particular due to the position of the inlet, which makes more difficult to have a uniform distribution of the fluid flow. It is important to remind that the inlet fluid flow in this phase lacks of accuracy, due to the 2D axisymmetric approximation in the geometry.

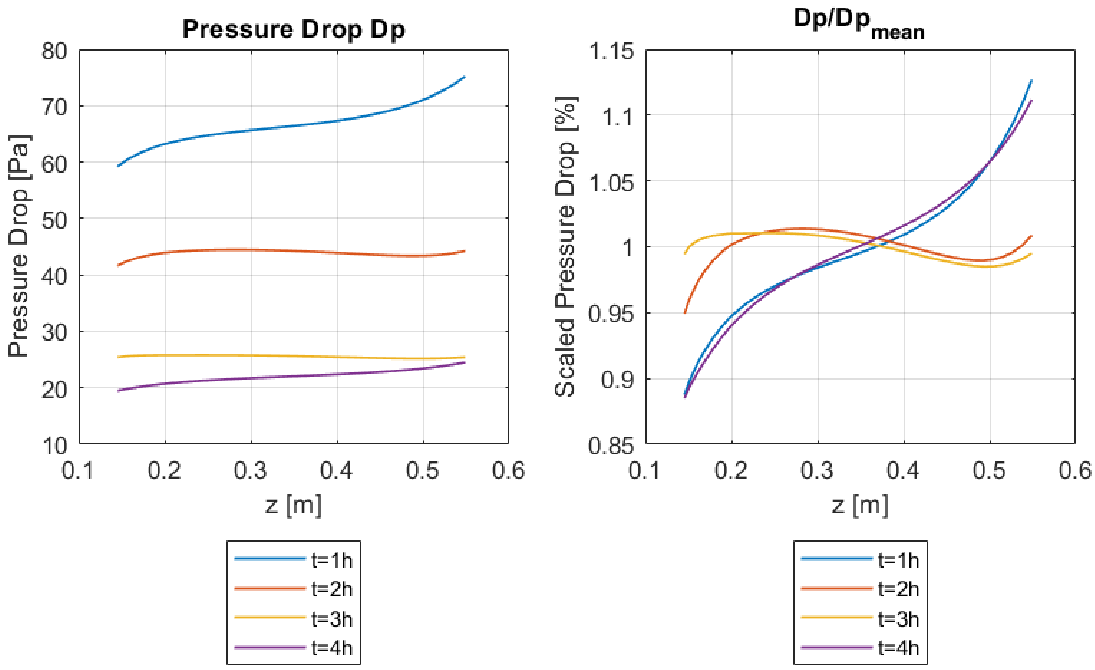

Figure 37 Evaluation of pressure drop, charge phase.

The temperature trend is almost exactly the opposite of the charge phase, but with a noticeable increase of the thermocline thickness, due to irregularities in the fluid flow, lower fluid velocity (resulting in less effective convective heat exchange), not complete exploitation of the storage.

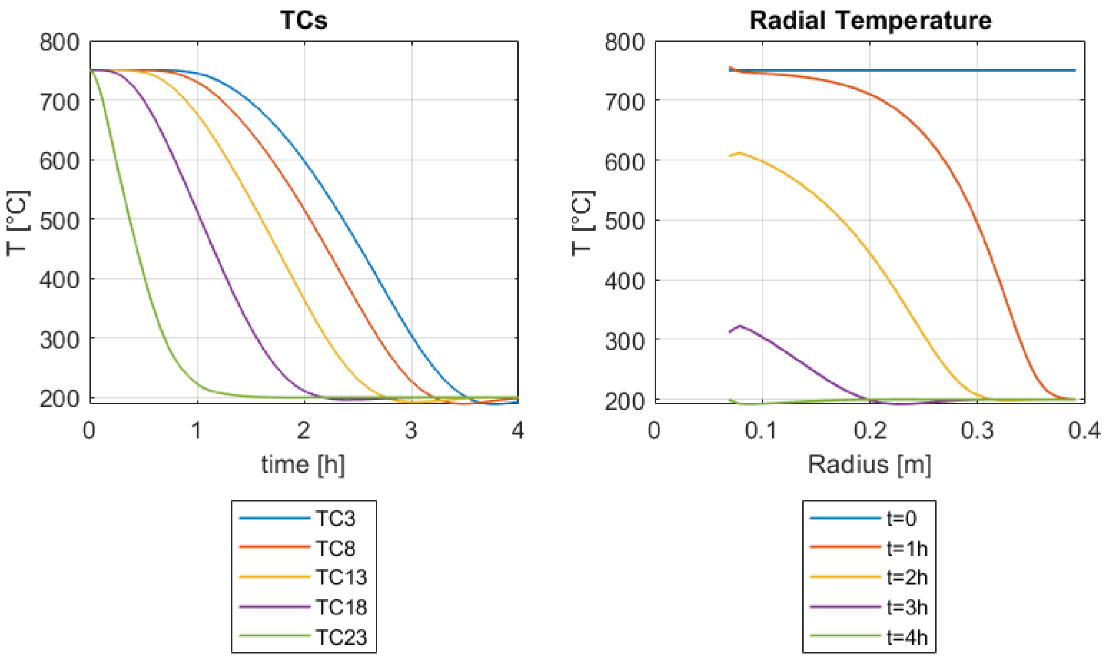

Figure 38 Evaluation of temperature trend in space and time, discharge phase.

4.3 Verification

4.3.1 Procedure

In order to verify the model, a verification procedure has been performed. The verification procedure consists basically in a grid independence assessment, starting from the coarsest mesh and refining it until needed. If the model is properly built, the error will decrease by refining the mesh.

As there is not a particular interest in the boundary layer zone, the only parameter considered for the grid independence is the core mesh dimension, which have an opposite trend to the number of elements. Varying the number of elements, the thickness of the boundary layer tends to change in order to allow a good transition with the first core cell.

The different meshes considered are:

- Coarse: 4627 elements;
- Normal: 12785 elements;
- Fine: 37177 elements.

The physical quantities evaluated are:

- Pressure distribution along the inner and the outer plans after 1 hour of simulation;
- Velocity magnitude along a plan in the middle between the inner and the outer ones after 1 hour of simulation;
- Temperature variation in time in the same position of the thermocouples 5, 13 and 21.

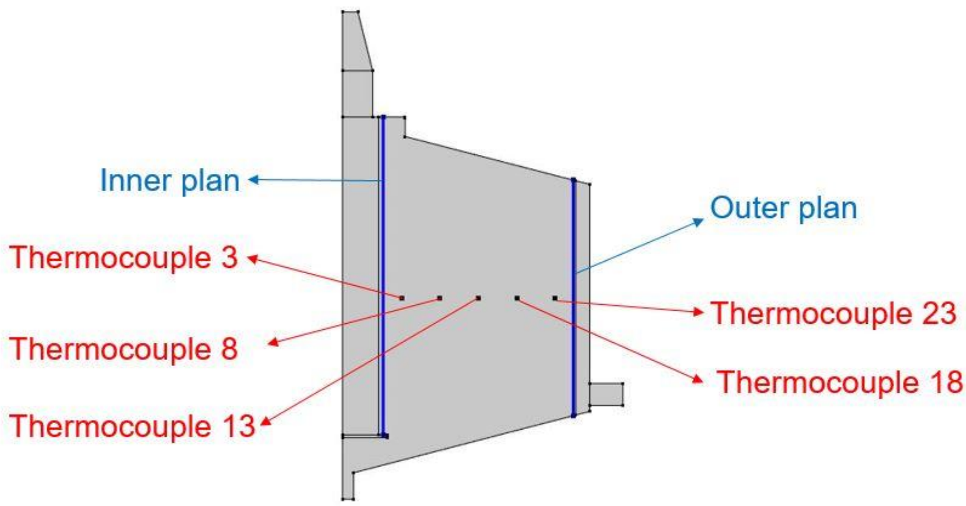

Figure 39 Plans of evaluation of the model's features.

The choice of measuring distribution, thus performing a series of local verification, is based on the fact that the further improvement procedure will involve local values, or local distribution in precise zones, so that averaged and bulk values are not particularly interesting for the analysis.

For the evaluation of the numerical uncertainties, the Richardson extrapolation method has been used, as suggested by the guidelines provided by Journal of Fluid Engineering [75]. In general, it is one of the most robust and has been employed in several CFD cases.

As suggested, the ratio between the mesh characteristic size of two successive meshes is higher than 1.3. This constraint is not strict, but derives from experience. In general, for this application, it is not wrong to use a global (average) cell size. Indeed, it has been calculated as follows:

$$x = \left[\frac{1}{N}\sum_{i=1}^{N}(\Delta A_i)\right]^{\frac{1}{2}} \tag{20}$$

where A_i is the area of the i^{th} cell, and N is the total number of cells used for the computations. To calculate the extrapolated value, the apparent order p has to be calculated. Being $x_1<x_2<x_3$ and $r_{21}=x_2/x_1$, $r_{32}=x_3/x_2$, the following expressions are used:

$$p = \frac{1}{\ln(r_{21})}\left|ln\left|\frac{\varepsilon_{32}}{\varepsilon_{21}}\right| + q(p)\right| \tag{21}$$

$$q(p) = \ln\left(\frac{r_{21}^{p} - s}{r_{32}^{p} - s}\right) \tag{22}$$

$$s = 1 \cdot sign\left(\frac{\varepsilon_{32}}{\varepsilon_{21}}\right) \tag{23}$$

where $\varepsilon_{32}=\Phi_3-\Phi_2$, $\varepsilon_{21}= \Phi_2-\Phi_1$, Φ_k denoting the solution on the k^{th} grid.

The extrapolated valued is calculated as follows:

$$\Phi_{ext} = \frac{r_{21}^{p}\Phi_1 - \Phi_2}{r_{21}^{p} - 1} \tag{24}$$

In this way, the relative error has been calculated with respect to the extrapolated value by means of the following equation:

$$e_{ext} = \left|\frac{\Phi_{ext} - \Phi_j}{\Phi_{ext}}\right| \tag{25}$$

Where e_{ext}^{ij} is the j-th relative error, Φ_{ext}^{12} is the value extrapolated and Φ_j is the value considered for the physic quantity in exam.

For a complete understanding of the procedure, it is suggested to read the cited reference (ref).

4.3.2 Results

In this section the results of the verification procedure are shown. In this case an engineering verification has been performed. It consists basically in presenting the physical quantities discussed before with different meshes, from the least to the most refined, and comparing them with the values obtained by using the Richardson extrapolation. The results are shown both for the charge and discharge phase, as they are different features and represent different problems. The first figures show the trends for the charge phase.

For the relative pressure, it is clear that the coarse mesh is not well representative of the real values, as it is very inaccurate. This could happen because the mesh is not refined enough to correctly solve the internal wire mesh, and this results in a change of the computed pressure. The other meshes are all able to give accurate results if compared to the Richardson extrapolation.

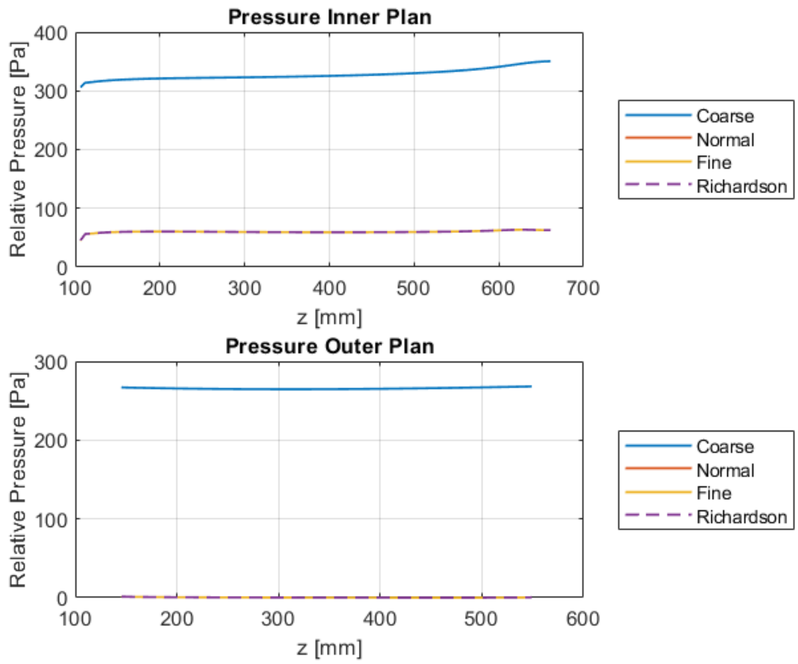

Figure 40 *Verification based on pressure field, charge phase.*

Similar considerations can be done for the velocity magnitude, in which only the course mesh is not able to predict its behavior. However, in this case the error is less relevant, as can be observed in the Figure 41. This is probably related to the plan used for the assessment on the velocity, which is far from the wire grilles. Moreover, although the huge error on the absolute value of the relative pressure, the pressure gradient shows lower errors, resulting in higher accuracy for the computed velocity. Also the velocity shows a convergent trend increasing the mesh refinement.

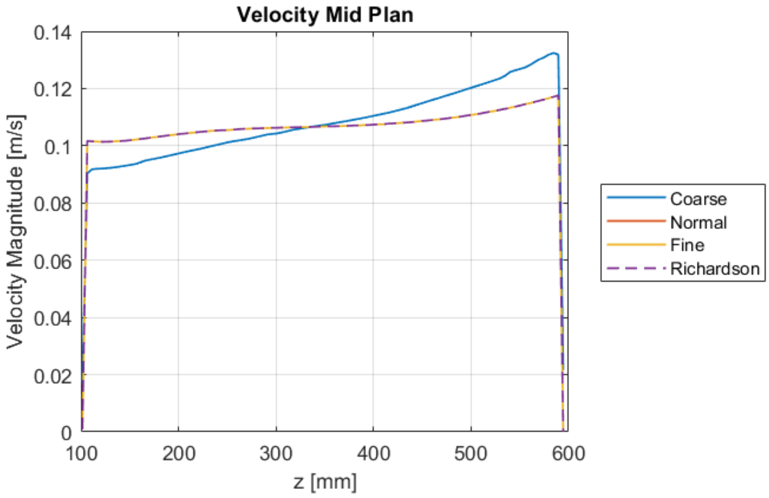

Figure 41 Verification based on velocity field, charge phase.

Regarding the temperature evolution in proximity of the thermocouple 5, 13 and 21, the convergence trend is still visible, but all the meshes in general have good agreement with the corresponding extrapolated values, with the exception of the course one in the thermocouple 21. The higher tendency to approach the correct value could be explained considering all the heat transfer mechanism, which are influenced only in part by the fluid flow (even if it remains a huge part), while the other mechanisms, such as the radiative heat transfer, require less refinement in the mesh.

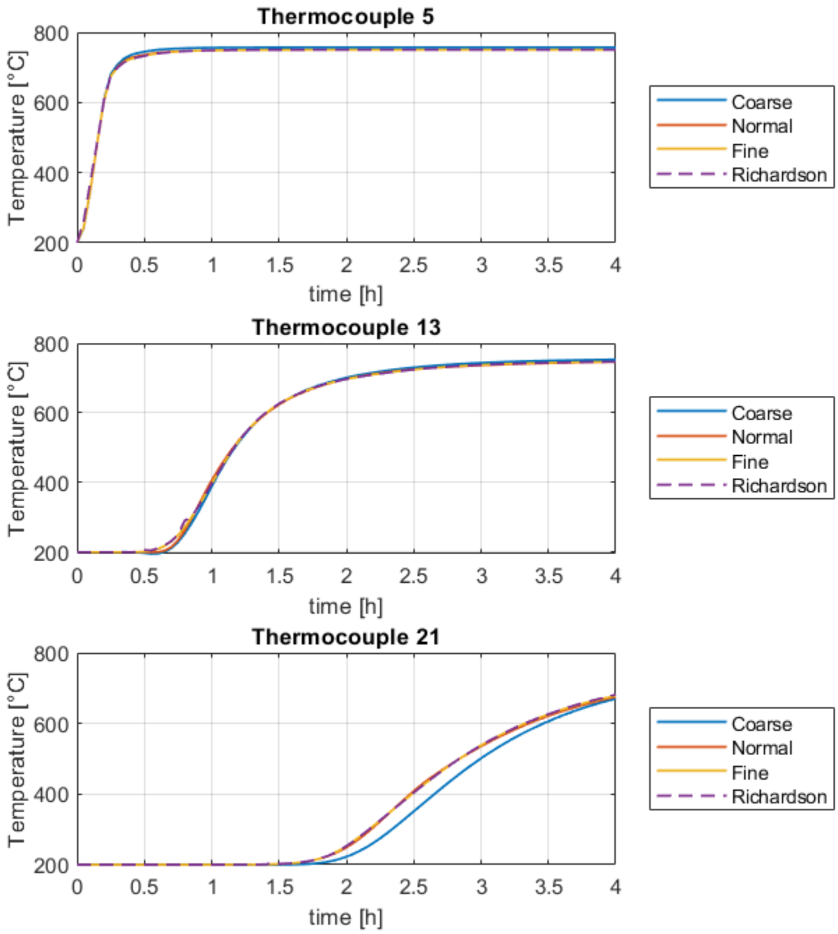

Figure 42 Verification based on temperature trend, charge phase.

The same considerations can be done with the discharge phase, which presents similar dependency on the mesh refinement, except for showing higher accuracy of the coarse mesh in the prediction of the velocity field along the middle packed plan.

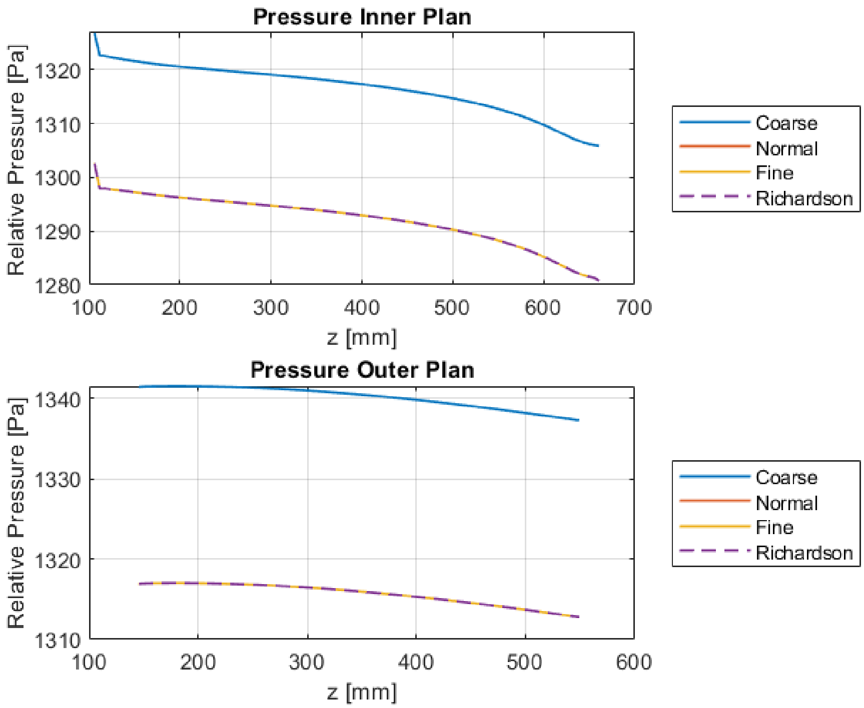

Figure 43 Verification based on pressure field, discharge phase.

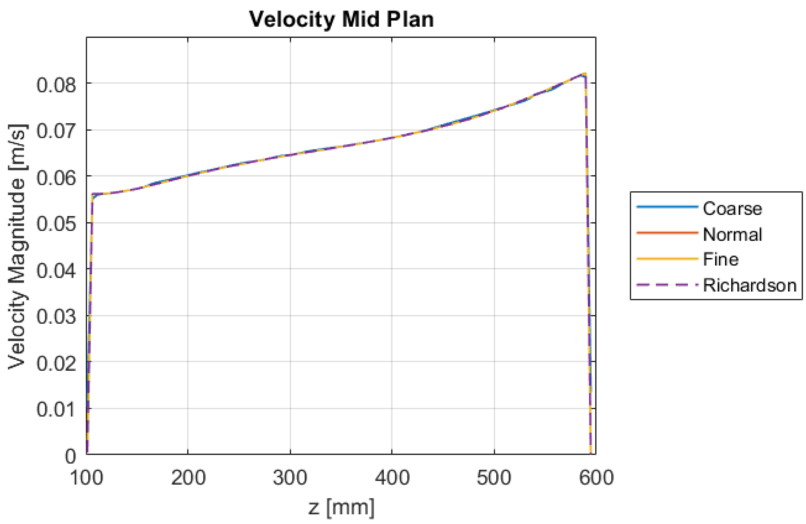

Figure 44 Verification based on velocity field, discharge phase.

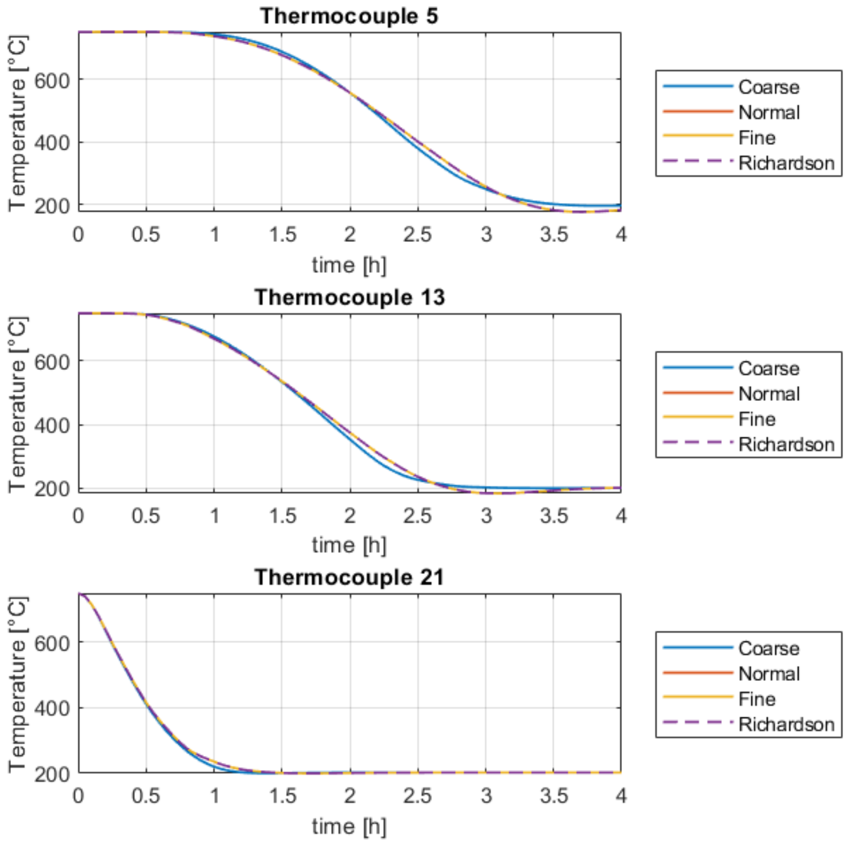

Figure 45 Verification based on temperature trend, discharge phase.

4.4 Step 2: Cycle stability analysis

4.4.1 Procedure

The analysis performed in the previous step is particularly relevant to give an indication of the behavior of the storage during the charge and discharge phase. However, normally the storage works with continuous charge and discharge phases, as expected during operations. As a result of the operation requirements, the storage does not start from a uniform minimum (or maximum) temperature, but presents a different temperature distribution as initial condition. In this case, the initial temperature is expected to be higher in the inner zone and lower in the outer, with the presence of an intermediate thermocline layer.

For the first cycles, the initial temperature distributions, as well as the thickness of the thermocline, are subjected to variations. As a result, the temperature inside the packed bed is variable too. However, it is correct to believe that all the values of interested will tend to stabilize after a certain number of cycles, which could vary in dependence of the features of the model.

To optimize the storage and understand its behavior during plausible working conditions, a cycle stability assessment has been performed. This procedure consists in 10 series of charge and discharge phase using the final temperature distribution of the previous phase as initial value for the following one. As a result, the storage will not start from the same initial conditions, but they will eventually tend to a stable distribution.

A consequence of a similar procedure is that the storage will never be completely charged and discharged, so that it is important to understand when those phase should be interrupted. As those conditions are very dependent on the application, in the present study it has been supposed that the storage is coupled with a S-CO_2 power block, which requires some conditions on temperature to work properly.

Hence, the condition for the discharge phase is clearly limited by the temperature of the heat source required by the power cycle. As can be observed in Figure 5 (chapter 1), a S-CO_2 cycle is able to work at relatively low temperatures, even lower to 400 °C; however, its efficiency is considerably reduced when working far from nominal conditions. Thus, 400 °C on the power block has been imposed as condition. Consequently, taking into account the difference of temperature between the air and the S-CO_2 in the heat exchanger and possible losses, the minimum outlet temperature is fixed to 450 °C. Basically the power block will work at a temperature higher than 450 °C, with the range 400-450 °C used for a smooth shutdown. As noticeable, at the end of the discharge the thermocline is partially out of the storage: this reduces the stability of the thermocline, but allows to better exploit the energy stored in the TES.

For the charge phase, there are not precise stop conditions, since it is not influenced by the power block. Thus, the interruption of the charge phase is based on efficiency considerations. In principle a more extended charge phase permits to better stabilize the thermocline, reducing its thickness, and to get more energy available inside the storage. On the other hand, while the temperature inside the storage is increasing, the heat exchanged between the entering hot air and the packed bed is progressively reduced. This results in a not complete exploitation of the heat source, until the point in which a great part of the energy supplied is wasted. Hence, the charge has to be interrupted at a prescribed condition, to ensure an acceptable tradeoff between the energy stored and the exploitation of the heat source. The energy stored when the charge phase is stopped can be evaluated in percentage with respect to the maximum amount of energy storable, as follows:

$$E_{st}(\%) = \frac{\int_V (1-\varepsilon)\rho_s(T_{end})c_{p,s}(T_{end})(T_{end}-T_{in})dV}{\int_V (1-\varepsilon)\rho_s(T_{max})c_{p,s}(T_{max})(T_{max}-T_{in})dV} \cdot 100 \tag{26}$$

Where T_{max} is the maximum temperature of the storage, corresponding to the temperature of the entering air (750 °C), T_{in} is the initial temperature of the TES at the first cycle, and V the volume of the packed bed. The temperature T_{end} corresponds to the temperature of the storage when the charge phase is stopped, and is variable along the packed region.

The thermal power wasted at the stopping conditions can be evaluated in a similar way:

$$P_{th,w} = \frac{\dot{m}c_{p,f}\left(T_{fl,end}\right)\left(T_{fl,end} - T_{in}\right)}{\dot{m}c_{p,f}\left(T_{fl,end}\right)\left(T_{fl,end} - T_{in}\right)} \cdot 100 \tag{27}$$

Where $T_{fl,end}$ is the outlet temperature of the air at the end of the charge phase.

Eventually, the charge phase is stopped at an outlet temperature T_{fl} of 600 °C, corresponding to E_{st}≈90% and $P_{th,w}$≈70%.

During the cycle stability analysis, the trend of temperature distribution during the subsequent charge and discharge phases is observed at different times. That trend is observed in a radial plan in the middle of the storage, connecting the centers of the inner and outer plans shown in the step 1 analysis. After that, also the thermocline thickness in the radial plan is evaluated. The evaluation of thermocline thickness has been performed by using a Boolean function. In synthesis, temperature is computed at each time simulated along the radial plan. The Boolean function is then set to 1 for temperatures inside the thermocline range and 0 for the ones outside, resulting in a matrix composed of 1 and 0 values. For the choice of thermocline range there is not a fixed rule, but it is normally recognized that it is linked to a high slope on the temperature trend. In this study, after observing the step 1, the thermal front region has been confined as follows:

- 350 °C < T < 650 °C for the charge phase;
- 250 °C < T < 550 °C for the discharge phase.

Once the Boolean matrix is set, its values are averaged in space, as follows:

$$b_i = \frac{\sum_{j=1}^{N} a_{ij}}{N} \tag{28}$$

Where i is the generic time step, j is the generic position in the radial plan, N represents the total number of elements considered and a_{ij} is the element in the ij position of the Boolean matrix.

This procedure permits to obtain a value between 0 and 1 for each time step, as a result of the space averaging. Each of this value indicates the thickness of the thermocline in a precise moment: to give an example, a value of 1 means that the thermocline region is covering all the packed bed in that specific time step. Hence, the lower is the value, the lower is the spreading of thermocline during the operation of the storage.

4.4.2 Results

As shown in Figure 46, the initial temperature distribution is uniform and equal to 200 °C at the first cycle, while it is different in the following ones, reaching progressively a stable distribution. The thermocline thickness tends to increase after the first cycle, until reaching stability as the initial temperature distribution, and thus its evolution in time, becomes stable too.

As can be seen in Figure 46-47, temperature trend tends to stabilize after the firsts cycles and to oscillate around certain values of temperature distribution, which can be considered as approximately stable. The behavior can be observed in both the charge and discharge phases, even if in the second case more cycles are required for a complete stabilization. However, both the two phases can be considered stable after the 10th cycle, meaning that it represents the actual nominal operation of the storage.

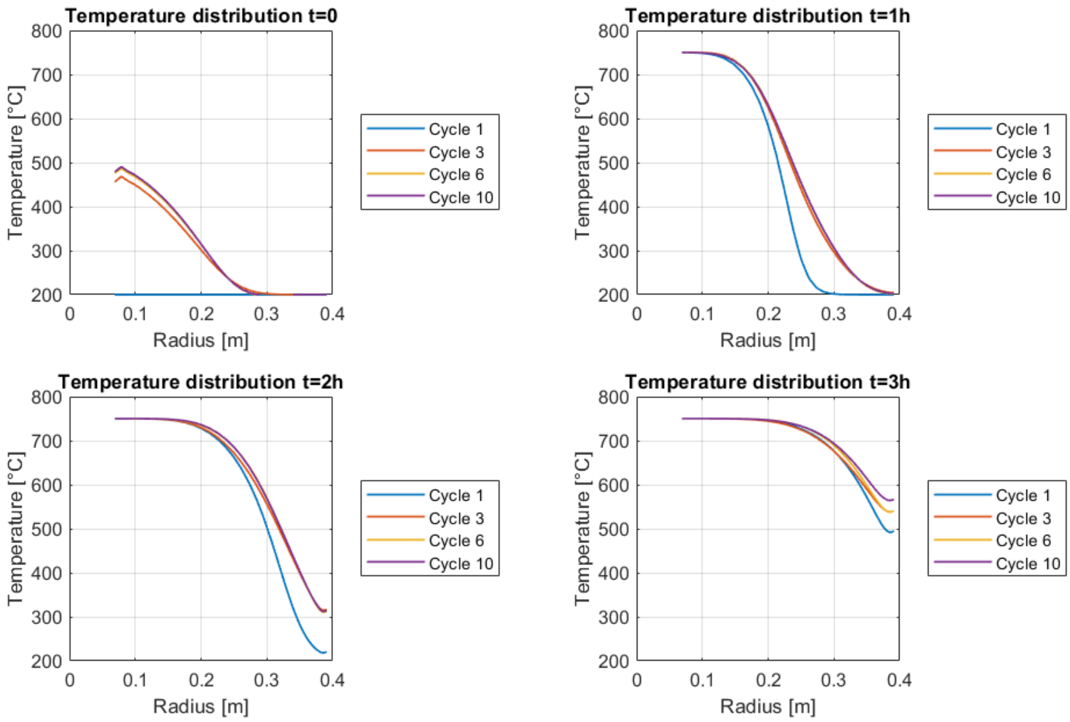

Figure 46 Evaluation of temperature trend during cycle stability analysis (charge phase).

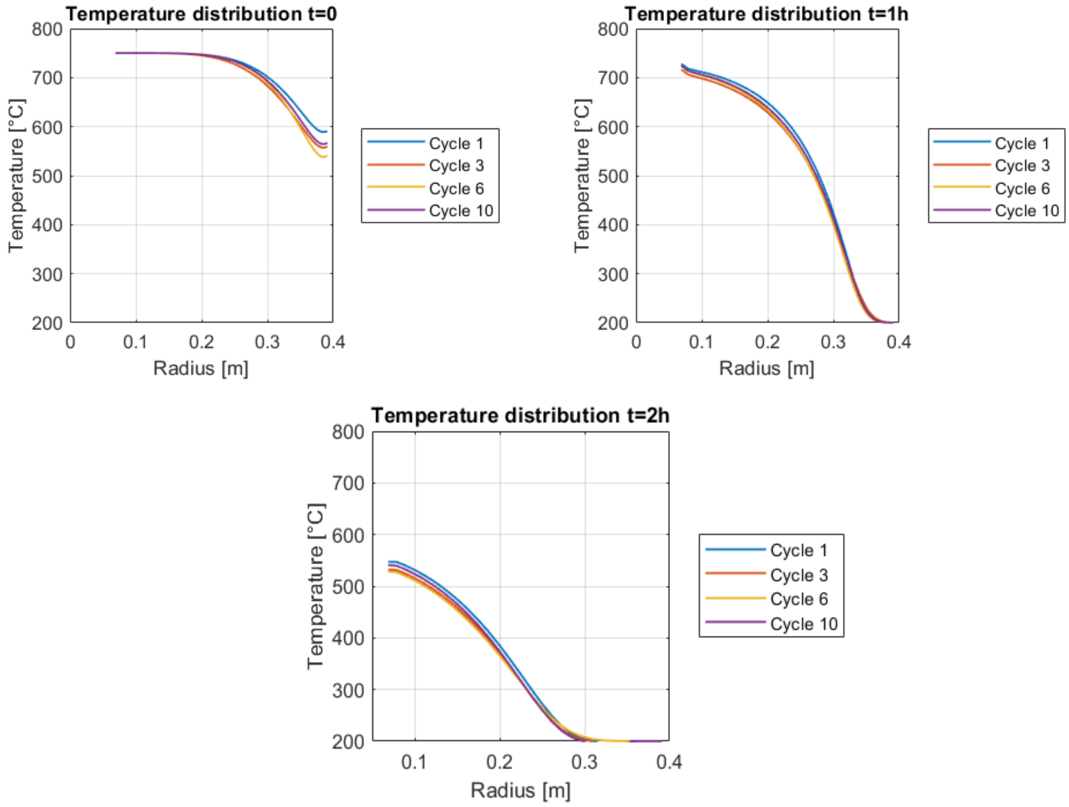

Figure 47 Evaluation of temperature trend during cycle stability analysis (discharge phase).

The thermocline exhibits a stable trend before the 10^{th} cycle. In general, apart from the first cycle, thermocline thickness tends to be quite unchanged during the whole charge phase, with a consistent decrease at the end of it, meaning that the thermal front is going outside the domain of the packed region (Figure 48). Differently, the discharge starts with an almost null spread and it increases continuously until the end of the phase. It can be observed that the thermocline occupies around 60% of the whole packed region at the end of the discharge, while the average value is 30%, as well as for the charge phase.

In Figure 48 it is possible to notice many oscillations in time of the thermocline thickness function; however, those oscillations are not real, and are linked to how the function has been define. Indeed, the effect of the its Boolean definition is a finite step variation, while in reality it should be more continuous and smooth.

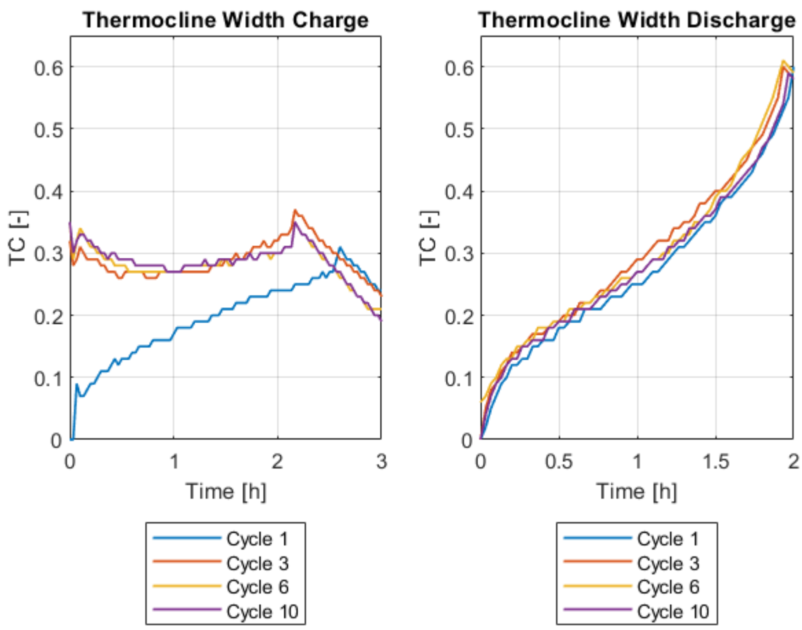

Figure 48 Evaluation of temperature trend during cycle stability analysis.

4.5 Step 3: Insulated tank, charge, discharge and stand-by phases

4.5.1 Procedure

In the step 2 a stability analysis has been performed, in order to identify the behavior of the storage during operation. However, the previous assessment considered a totally adiabatic tank, with no heat exchanged with the external environment, if not considering the inlet and outlet flux. It is also interesting to considered, as added assessment, the effect of the dispersed heat flux through the ambient, as it is a good indicator of the performances in a TES. Of course, the effect of dispersed heat flux is much more relevant in a small prototype TES, rather than in an industrial scale one, in which the volume-to-area ratio is much larger: thus, the results found in this paragraph are interesting for some reasonings, but could be not representative of a possible industrial scale TES of the same typology.

For the analysis, a 5 cm insulation layer has been added, as established by design. For the dispersed heat flux, a heat transfer coefficient of 5 W/m^2K has been set, because the storage is settled inside a laboratory. The external temperature T_a is fixed to 20 °C. Regarding the model, a 2D time dependent heat conduction and convection model has been implemented in the walls' domains, while all the rest is kept as before.

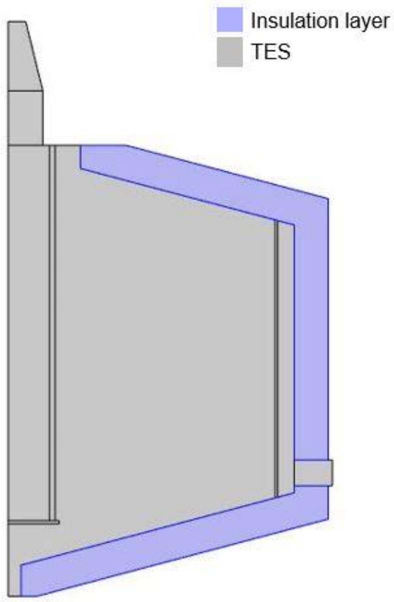

Figure 49 Geometry of the insulated tank, with focus on insulation layer.

The procedure consists in three sub-steps:

- Charge phase;
- Discharge phase;
- 4 hours stand-by.

The principal aim is to measure the flux dispersed through the external walls during the three phases, and to express them in terms of losses in percentage with respect to the total energy stored. Hence, energy dispersed is calculated as:

$$E_{disp,ch}(\%) = \frac{E_{disp,ch}}{E_{f,ch} - E_{in,ch}} =$$

$$= \frac{\int_T \int_A h(T - T_{ext})dAdt}{(1-\varepsilon)\int_V \left(\rho_s(T_f)c_{p,s}(T_f)\cdot(T_f - T_{ref}) - \rho_s(T_{in})c_{p,s}(T_{in})\cdot(T_{in} - T_{ref})\right)dV} \cdot 100 \qquad (29)$$

$$E_{disp,d}(\%) = \frac{E_{disp,d}}{E_{in,d} - E_{f,d}} =$$

$$= \frac{\int_T \int_A h(T - T_{ext})dAdt}{(1-\varepsilon)\int_V \left(\rho_s(T_{in})c_{p,s}(T_{in})\cdot(T_{in} - T_{ref}) - \rho_s(T_f)c_{p,s}(T_f)\cdot(T_f - T_{ref})\right)dV} \cdot 100 \qquad (30)$$

$$E_{disp,st}(\%) = \frac{E_{disp,st}}{E_{in,st}} = 1 - \frac{E_{f,st}}{E_{in,st}} = \left(1 - \frac{(1-\varepsilon)\int_V \left(\rho_s(T_{in})c_{p,s}(T_{in})\cdot(T_{in} - T_{ref}\right)dV}{(1-\varepsilon)\int_V \left(\rho_s(T_{in})c_{p,s}(T_{in})\cdot(T_{in} - T_{ref}\right)dV}\right)\cdot 100 \qquad (31)$$

Where Eq. (-) are respectively the equations for the energy dispersed for the charge, discharge and stand-by phases. In addition:

- E_{disp}, E_{in}, E_f are respectively the energy dispersed, and the energy content at the initial and final moment of the indicated phase;

- T_{in} and T_f are the temperatures at the beginning and end of the indicated phase in a specific point of the domain;
- T_{ext} and T_{ref} are the ambient and reference temperatures, fixed to 20 °C and 200 °C.

A little loss of accuracy could be related to the energy stored and not dispersed by the insulation layer, which could partly return to the packed region, principally at the beginning of the discharge phase, or be maintained inside the layer itself. Therefore, an evaluation of the heat exchanged between the insulation layer and the packed region represents a good alternative. However, due to the very low density, the capacity of the insulation to store energy is particularly low, so that the result of the mechanism mentioned before is negligible.

Another interesting outcome of this assessment is the effect of the dispersed energy on the temperature distribution. Indeed, it is expected that the dispersion phenomenon will create a progressively decrease in temperature near the walls. To evaluate this, the temperature distribution along the radial and axial plan shown in Figure 50 is computed and compared to the one in a stabilized adiabatic cycle.

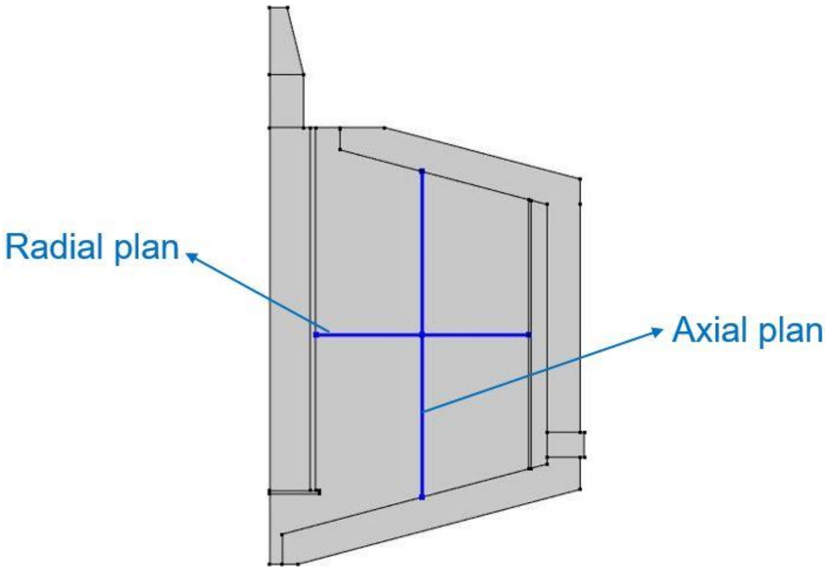

Figure 50 *Plans of evaluation of the model's features.*

It is important to remind that also the temperature assessment is valid only for the analyzed TES, and the differences could be much less relevant or also negligible in an industrial scale one.

4.5.2 Results

As mentioned before, the heat dispersed through the insulation layer is calculated in percentage with respect to the energy stored. The results are the following:

- For the charge phase, $E_{disp,ch}$=12.70%;

- For the discharge phase, $E_{disp,d}$=7.20%;
- For the stand-by phase, $E_{disp,st}$=15.28%.

It is important to notice that the losses are relevant in dependence of the size of the storage. Indeed, for industrial scale TES the volume-to-surface ratio is much smaller, and consequently also the weight of thermal losses is consistently reduced.

Focusing on temperature behavior, the dispersion through the ambient results in no relevant variation in the radial plan during the charge phase, and in an important variation along the axial plan, especially in proximity to the walls. As a consequence, this phenomenon has little or no effect on the thermocline thickness, but it could be relevant in terms of shape, as the temperature near the walls is lower.

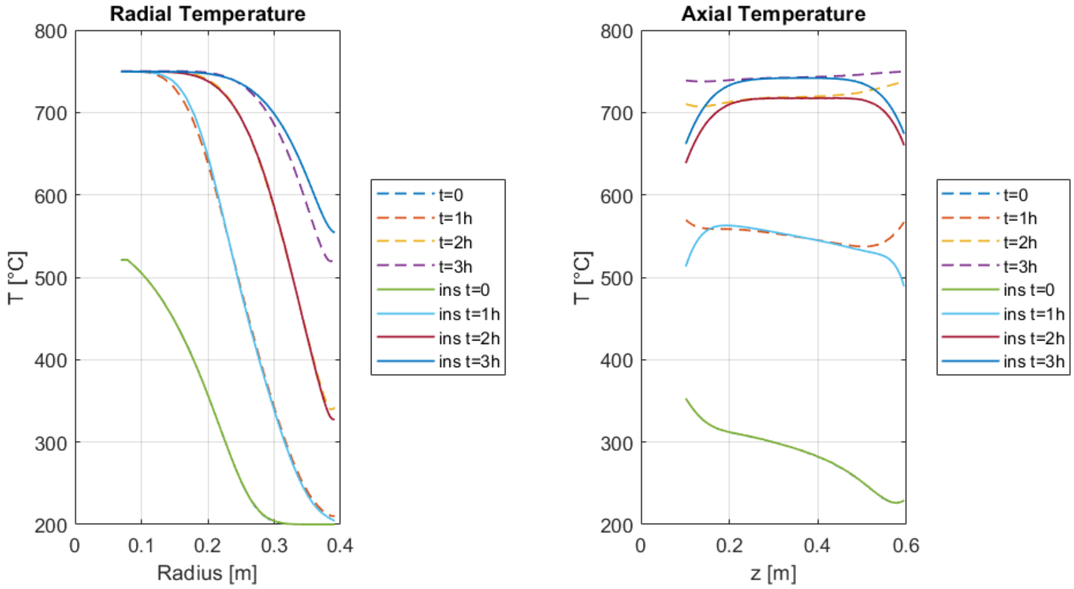

Figure 51 Comparison of temperature trend in adiabatic and insulated cases during charge phase.

Similar considerations are made for the discharge phase, in which the adiabatic configuration shows more constant temperature in thee axial plan, except for the last time shown. However, the effect of the increased temperature in the lower zone of the tank is explainable by a bad exploitation of the lower zone of the storage, so that the temperature in that region is kept higher. This effect is less relevant in the non-adiabatic case, in which that non-exploited heat is in part dispersed in the ambient.

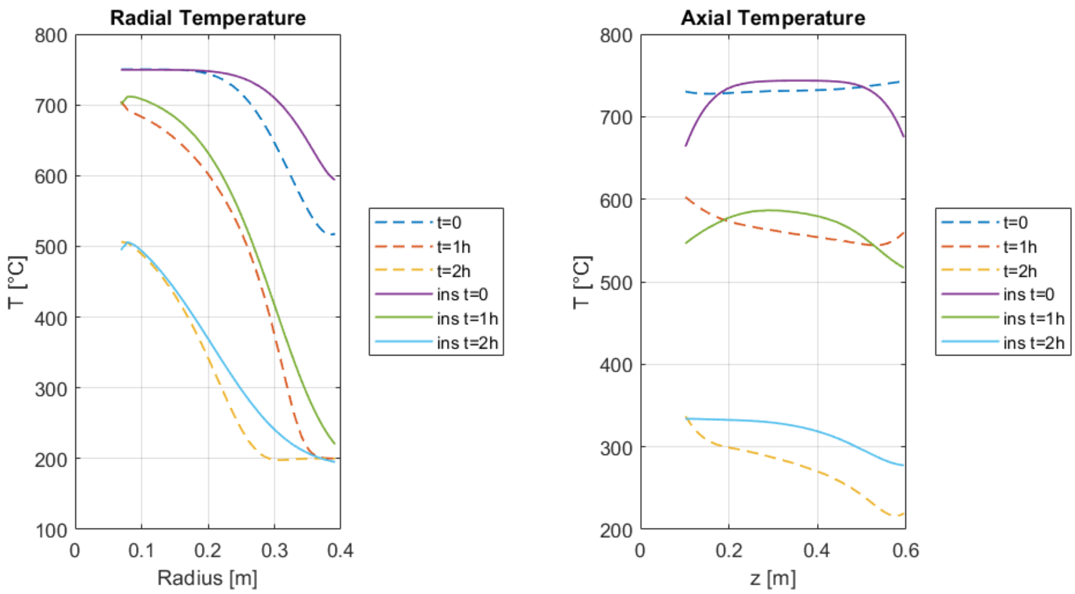

Figure 52 Comparison of temperature trend in adiabatic and insulated cases during discharge phase.

It is noticeable that in some graphs the temperature in the non-adiabatic case is consistently higher. However, this is only in relation to the plans of evaluation, while the outlet temperature of the discharge phase is constantly higher in the adiabatic case.

In the stand-by phase, the temperature distribution decreases significantly along the two plans with increasing times, reaching an inner packed temperature slightly lower than 700 °C after 4 hours. The effect of dispersions influences significantly the temperature shape, especially in proximity to the walls, while other effects, such as fluid mixing or buoyancy, are not visible. The trends are shown in the following figure.

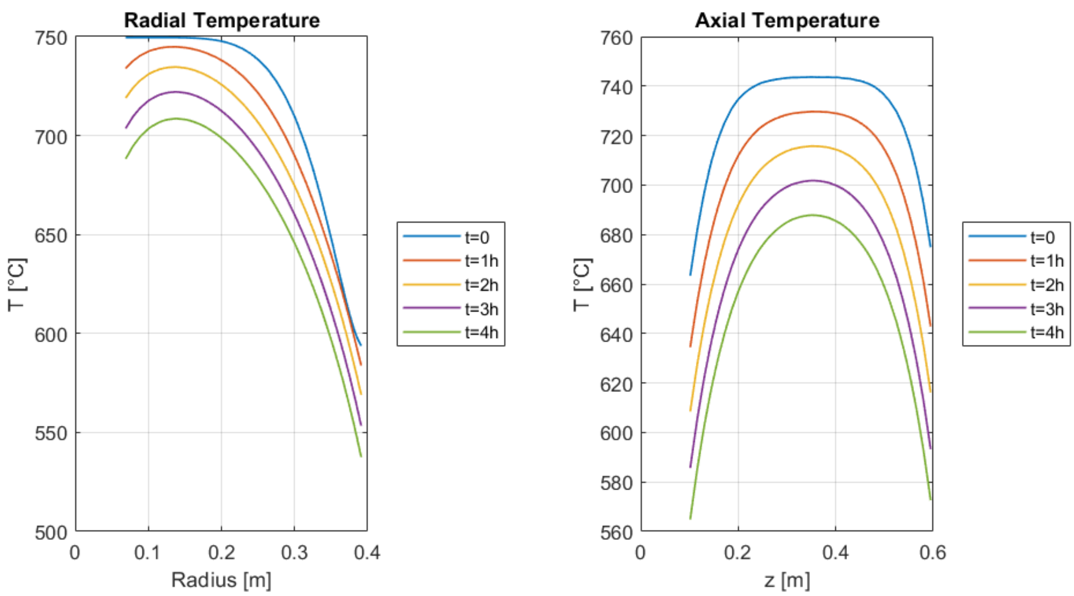

Figure 53 Evaluation of temperature trend during stand-by phase.

5 Improvement

A packed bed TES has many advantages with respect to the current state-of-art, consisting mainly in lower cost and wider temperature ranges. Furthermore, the radial configuration allows to reduce the insulation requirements, leading to even more advantage. However, as mentioned in the introduction chapter, a thermocline storage shows lower efficiency and requires an accurate management of the thermal front. This management is even more difficult in a radial configuration, in which fluid flow is not uniformly distributed along the axial direction, leading to a non-uniform temperature distribution in all the spatial directions, which results in thicker thermocline and not proper exploitation of the stored heat. Hence, after building up a verified model to simulate the packed bed TES, the study is focused on finding suitable solutions which could improve its performances during stable operation. Moreover, it is also interesting to understand how some parameters influence the performances of the storage and the relevance of their variation.

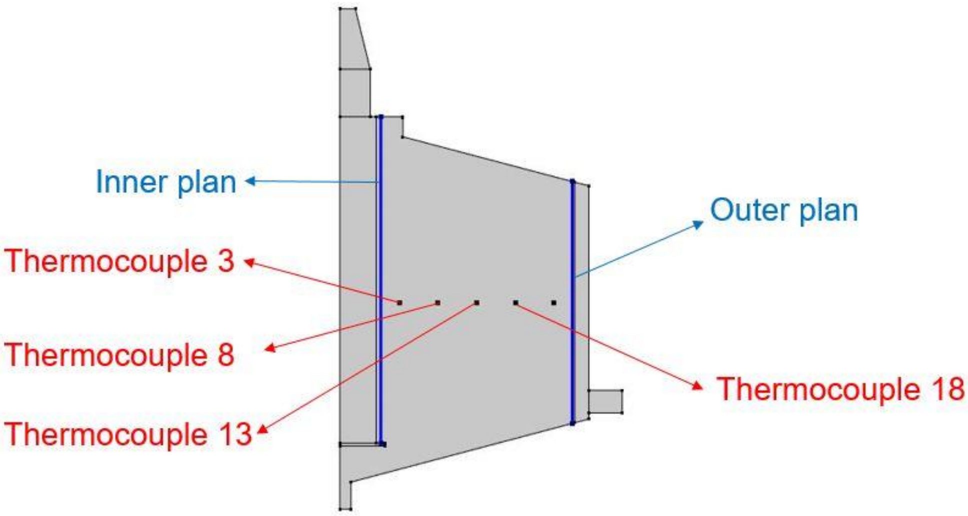

Figure 54 *Plans of evaluation of the model's features.*

The effect of each solution is evaluated basing on how it affects the temperature trend in the thermocouple 3, 8, 13, 18, pressure distribution in the inner and outer plans (see figure …) after 1 hour of charge/discharge, absolute and normalized pressure drop distribution after 1 hour of charge/discharge, thermocline thickness in time, hydrodynamic and thermal efficiency. The choice of a specific hour for the evaluation of pressure drop does not result in an important loss in the accuracy of the evaluation, as the behavior of pressure is not varying in shape during operations, but only in terms of average value.

Hydrodynamic efficiency is an index of the uniformity of pressure drop distribution inside the packed bed, and in this case in the axial direction. It is defined as:

$$\eta_{hydro} = 1 - \frac{\sqrt{\frac{1}{n-1}\sum_{i=1}^{n}(\Delta p_i - \overline{\Delta p})^2}}{\overline{\Delta p}} \tag{32}$$

Where Δp_i is the generic pressure drop between two points located at the same height and respectively at the inner and outer plan, n is the number of points considered for the calculation and $\overline{\Delta p}$ is the average pressure drop, obtained with an arithmetic averaging:

$$\overline{\Delta p} = \frac{\sum_{i=1}^{n} \Delta p_i}{n} \tag{33}$$

Hydrodynamic efficiency results in an averaged value between 0 and 1. The higher is its value, he more the pressure drop at a defined time is uniformly distributed along the z-axis.

In the same way of hydrodynamic efficiency, thermal efficiency determines the uniformity of temperature distribution in some specific zones, being calculated as:

$$\eta_{TCs}(t) = 1 - \frac{\sqrt{\frac{1}{n_{TCs}-1}\sum_{i=1}^{n_{TCs}}\left(T_i(t) - \bar{T}(t)\right)^2}}{\bar{T}(t)} \tag{34}$$

Where $T_i(t)$ is the generic temperature in one of the points considered (and it is time dependent), n_{TCs} is the number of points considered for the calculation and $\bar{T}(t)$ is the average temperature, obtained with an arithmetic averaging, as done for the average pressure drop.

$$\bar{T} = \frac{\sum_{i=1}^{n_{TCs}} T_i}{n_{TCs}} \tag{35}$$

As the hydrodynamic one, thermal efficiency is a value between 0 and 1 and gives similar information, but referred to the temperature. However, this efficiency is not evaluated on a plan, as a continuous function, but among 5 groups of 5 points each one, corresponding on the position of all the thermocouples. In this way, 5 different values are obtained for each time step. The results can be averaged in time, in space, or in both the two, depending on the interest. For a first evaluation, this value is averaged in time and space, in order to obtain one single value which represents the temperature uniformity within the storage during the charge or discharge phase.

All improvement procedure is performed with a parametric (or sensitivity) analysis, which allows to vary some parameters without altering the others, in order to see the effect of each variation on the performances. The parameters considered in the procedure are related to operative conditions, material characteristics and geometry features, in such a way to explore as much improvement solutions as possible. The solutions proposed are:

- Inlet temperature variation;
- Mass flow rate variation;
- Particle diameter variation;

- Emissivity variation;
- Introduction of a conical structure in the inner channel;
- Introduction of a divider in the inner channel;
- Different positions of the outer tube;
- Exploration of different materials.

The evaluation of the performances is based on a stabilized charge and discharge cycle, with the same operative conditions of the last cycle of the stability analysis. One of the consequences is that the storage is considered adiabatic.

5.1 Base case

Before proceeding with the improvements, it is necessary to start analyzing the general characteristics of the base case. As mentioned previously, it corresponds to the last cycle of the stability analysis, and therefore it represents the behavior of the storage during normal operations. Its behavior has been evaluated and described in the previous paragraph, and is here shown basing on multiple parameters employed for the improvement analysis.

It is possible to observe that the pressure distribution, evaluated after 1 hour of charge and discharge, results quite uniform along the axial direction, and this is an index of uniform distribution of the fluid flow within the storage. However, the graphs in Figure 55 shows a not uniform trend in the lower and higher part of the storage, especially in the discharge phase. Hence, there could be possibilities of improvement.

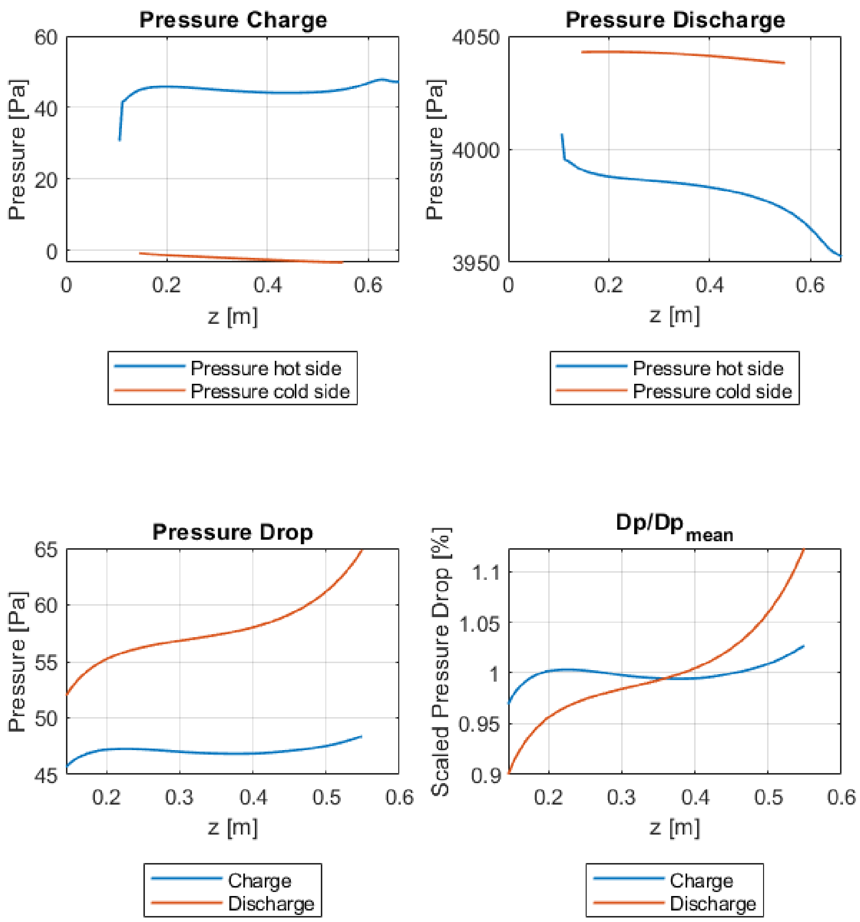

Figure 55 *Evaluation of pressure drop during charge (left) and discharge (right) phases.*

Figure 56 shows the temperature variation in time evaluated in the same positions of the thermocouples 3, 8, 13, 18, corresponding to points at different radius along the above mentioned radial plan. The temperature trend is an index of the thermal behavior of the packed bed, which is influenced not only by the fluid flow, but also by all the mechanisms explained in the previous chapter, including radiative and stagnant convection and conduction inside the bed. As an example, the more a thermocouple is in the prescribed thermocline range (350-650 °C for charge and 250-550 °C for discharge), the more its corresponding zone is affected by this phenomenon during operations and therefor the thermal front is spreading. The ideal behavior would consist in an immediate passage from the minimum to the maximum temperature during charge phase and vice versa during discharge, corresponding also to a perfect stratification. This does not happen in reality, but some improvements could lead to a slight higher slope in the time-temperature curves, as a sign of better performances.

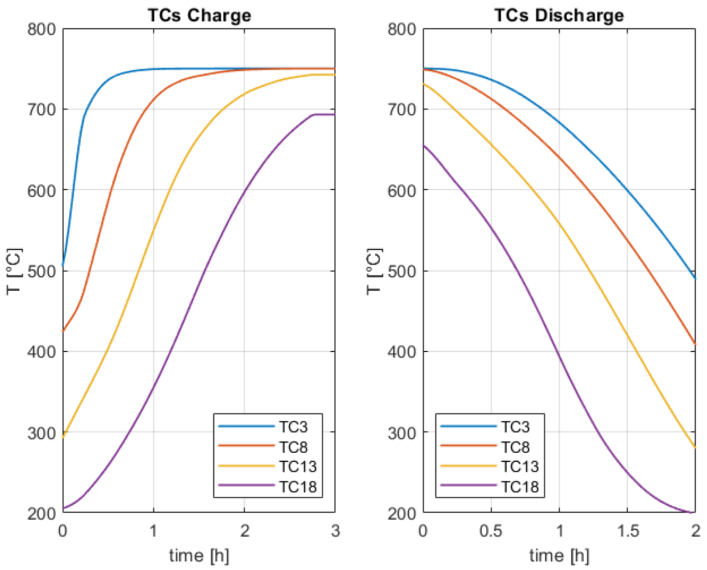

Figure 56 *Evaluation of temperature trend during charge (left) and discharge (right) phases.*

Another parameter considered is the thermocline width. Its evaluation procedure is described in previous chapter and it is a very relevant parameter, as describes directly the thermal front width in a precise moment. As can be seen in Figure 57, at some time the thermocline is large enough to occupy almost 60% of the packed bed, as can be seen during the end of the discharge. However, except in that case, the average is less than 35%.

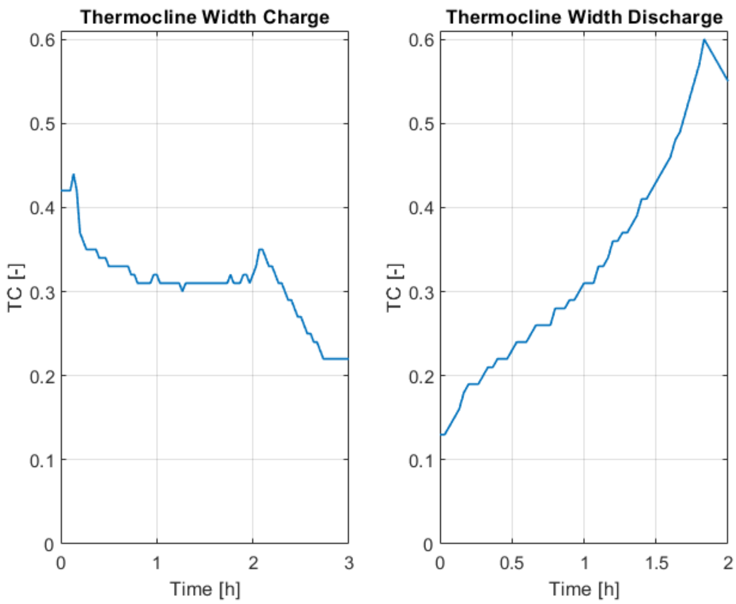

Figure 57 Evaluation of thermocline evolution during charge (left) and discharge (right) phases.

Eventually, the global η_{TCs} and η_{hydro} have been evaluated, as much as the average pressure drop after 1 hour of charge/discharge, with the following results:

Charge: $\eta_{hydro} = 0.9908,\ \eta_{TCs} = 0.9836, \Delta p = 47.1180\ Pa.$

Discharge: $\eta_{hydro} = 0.9526,\ \eta_{TCs} = 0.9792, \Delta p = 57.7569\ Pa.$

Those results show a quite high value of the thermal and hydrodynamic efficiency, and quite low pressure drop. However, some improvements could be done.

5.2 Inlet temperature

5.2.1 Background

Operation conditions are the easiest ones to modify, as they do not require any cost or change in the configuration of the TES structure and/or materials. One of the possible parameters that could be variated is the inlet temperature, as it influences both the temperature and pressure distributions. Indeed, a change in temperature of the inner flow leads to different transients, different thermocline evolution and probably different flow distribution, as the density is related to the temperature. Therefore, a parametric analysis based on variable inlet temperature is performed. As 200 °C is the fixed minimum temperature, the variation is applied only to the inlet on the charge phase, which obviously influences also the discharge phase, considering that the initial distribution during the discharge is strongly dependent on it.

The inlet temperature is varied by 50 °C each time in a range from 650 °C to 850 °C. Consequently, in this case also the thermocline range must be varied, on a base of 25 °C each time. Thus, for the charge phase, the thermocline upper limit varies on a base of 50 °C, going from 550 °C to 750 °C; during the discharge, the same upper limit changes on a base of 25 °C, from 550 °C to 650 °C. This trick permits a better comparison of the thermocline width, while the choice of the upper limits is based on observations.

The stopping conditions are maintained equal for all the inlet temperature, in order to ensure a minimum of two-hours discharge.

5.2.2 Results

Analyzing the pressure, it is immediately noticeable that the different inlet temperature influences mostly the pressure in the hot side, as the cold side is maintained almost at a constant temperature. This results in increased pressure drop, considering that almost nothing is changed on the cold side after 1 hour of charge or discharge. Thus, higher inlet temperatures are associated with higher pressure drops, with not relevant difference in its distribution along the axial direction.

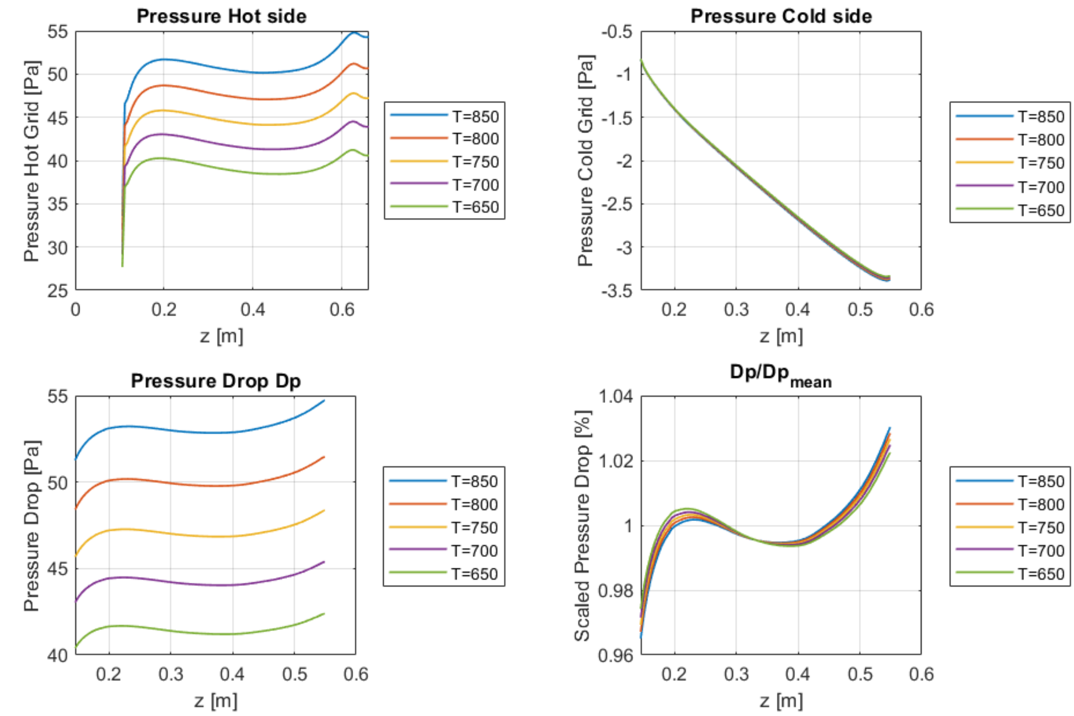

Figure 58 Evaluation of pressure drop during charge phase.

The same considerations are one both in charge and discharge phase, with the difference that in the second case both the hot side and cold side pressure increase. This does not change the higher pressure drop for higher inlet temperature.

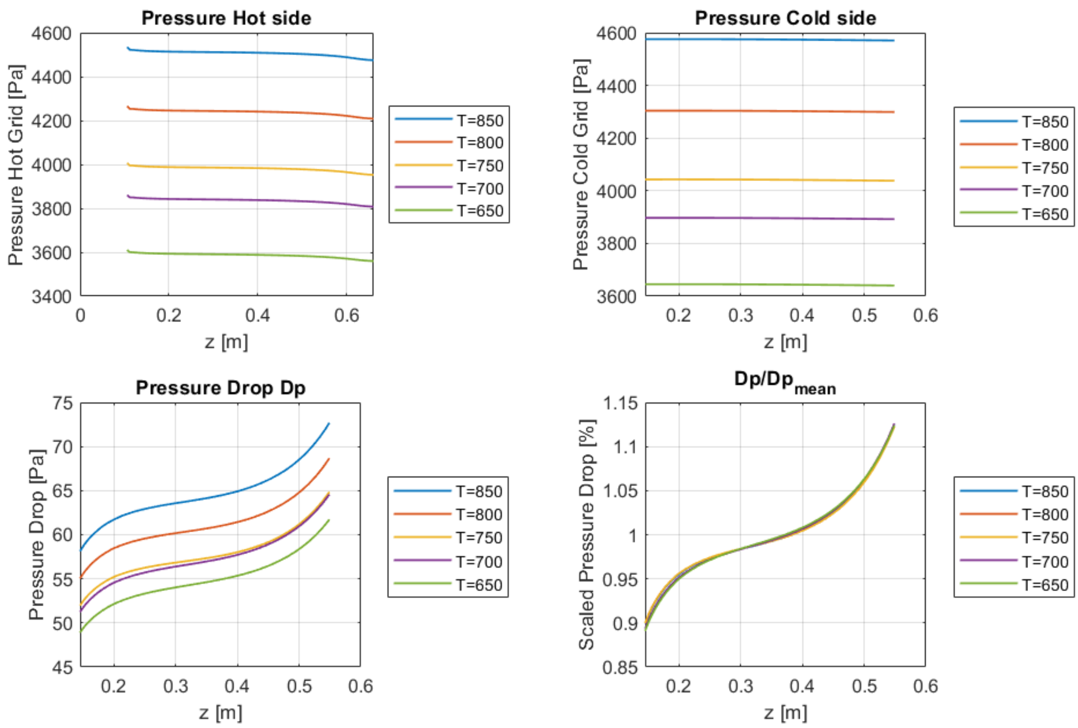

Figure 59 Evaluation of pressure drop during discharge phase.

Looking at the temperature evolution in time, the temperature reached is certainly different depending on the inlet temperature. In the charge phase, the slope of the curves seems to not vary so much in the inner part, which reaches quickly the maximum temperature, while it is more relevant in the external zone.

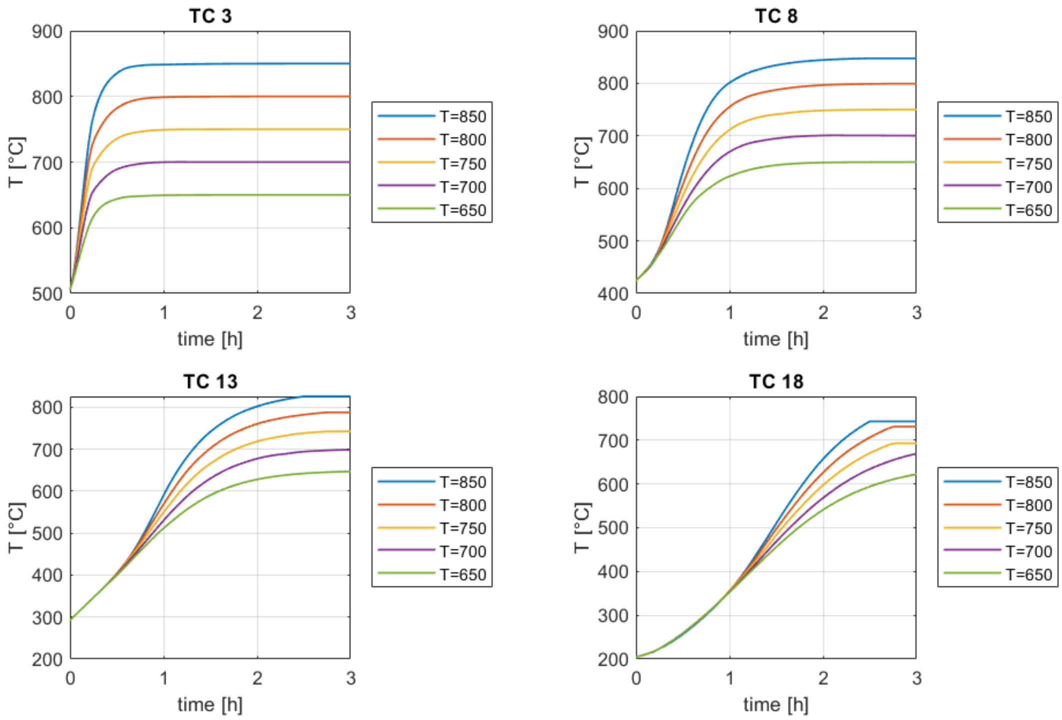

Figure 60 Evaluation of temperature trend during charge phase.

Similar behavior can be observed during the discharge, but with a relevant difference in slope especially for the thermocouples 3 and 8.

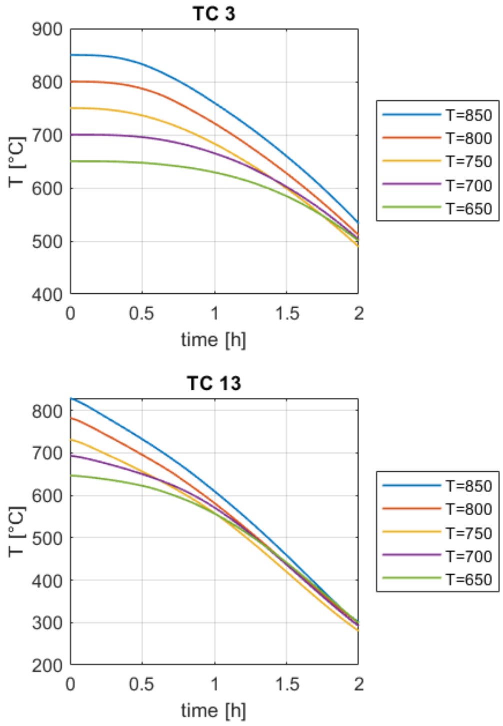

Figure 61 *Evaluation of temperature trend during discharge phase.*

Regarding the thermocline, to lower inlet temperatures correspond a better behavior and a reduced thermal front width, both in the charge and discharge phases. However, the results could also be affected by the choices in terms of temperature range.

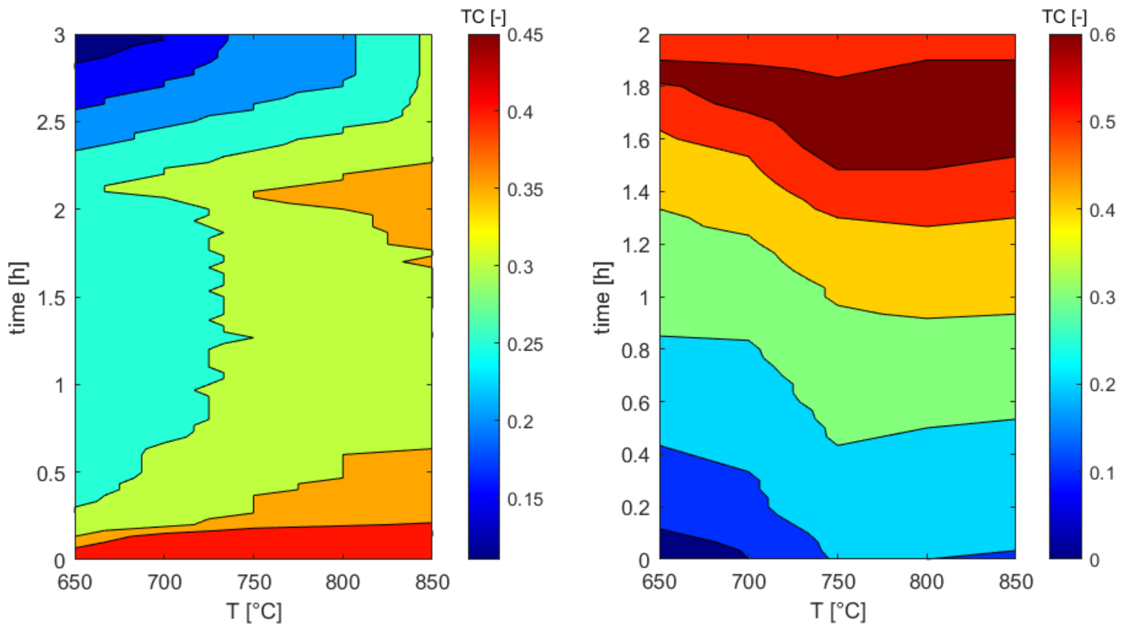

Figure 62 *Evaluation of thermocline evolution during charge (left) and discharge (right) phases.*

Figure 63 summarizes the effect of different inlet temperatures on the fluid flow and thermal distribution during operation. In all the cases, lower inlet temperatures correspond to better hydrodynamic and thermal behavior, also with decreased pressure drop. With increased temperature little improvement on the hydrodynamic efficiency, but it is not relevant, as all the other parameters are decreasing.

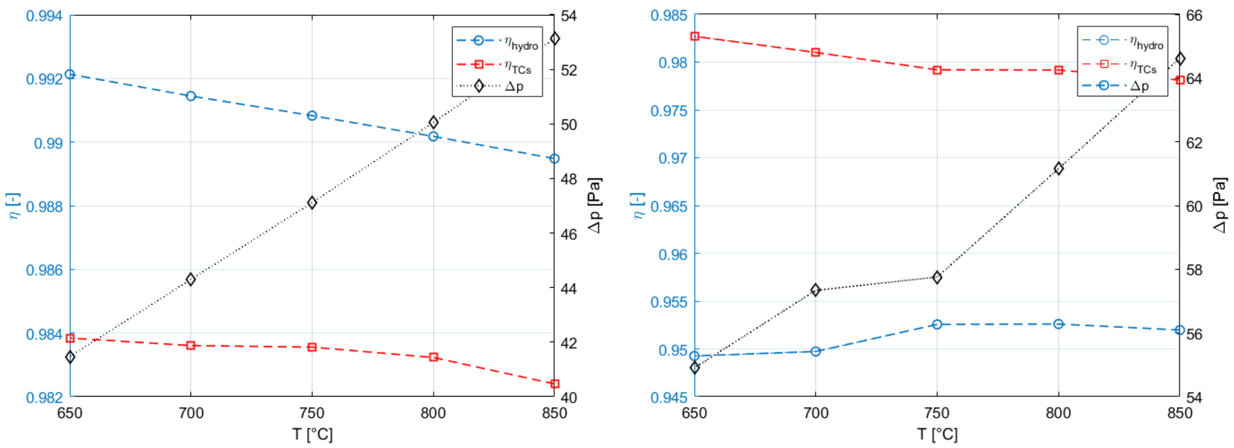

Figure 63 Summary of TES performance comparison during charge (left) and discharge (right) phases.

Eventually, it is important to remember that operative conditions, and in particular temperature range, are usually imposed and it is not possible to modify them. Hence, this measure is advised only in absence of particular restrictions.

5.3 Mass flow

5.3.1 Background

Another operative parameter which can be easily changed is the mass flow rate. In general, the choice of the correct nominal mass flow rate is determinant, as it influences the fluid flow inside the TES, both in terms of average pressure drop and pressure distribution in the axial direction. Moreover, higher mass flow rates result in higher velocities, which have a great influence on the heat transfer coefficient and hence on one of the principal heat transfer mechanisms in a packed bed heat exchanger. On the other hand, lower mass flow rates could lead to better flow distribution and lower pressure drop, which is useful for a better exploitation of the storage capacity. Finally, evaluating the influence of this parameter could allow to understand the performance of the storage in conditions which are far from the nominal ones.

Mass flow rate is varied from 0.025 to 0.04 kg/s, compatible with the dimensions and the features of the storage.

5.3.2 Results

An increase of the mass flow rate leads to a consequent increase in pressure drop, both for the charge and discharge phases. This was expected, as pressure drop is usually dependent on the square of velocity. However, it seems to not have a great influence on the pressure distribution in the z-axis, which presents the similar shape and slope.

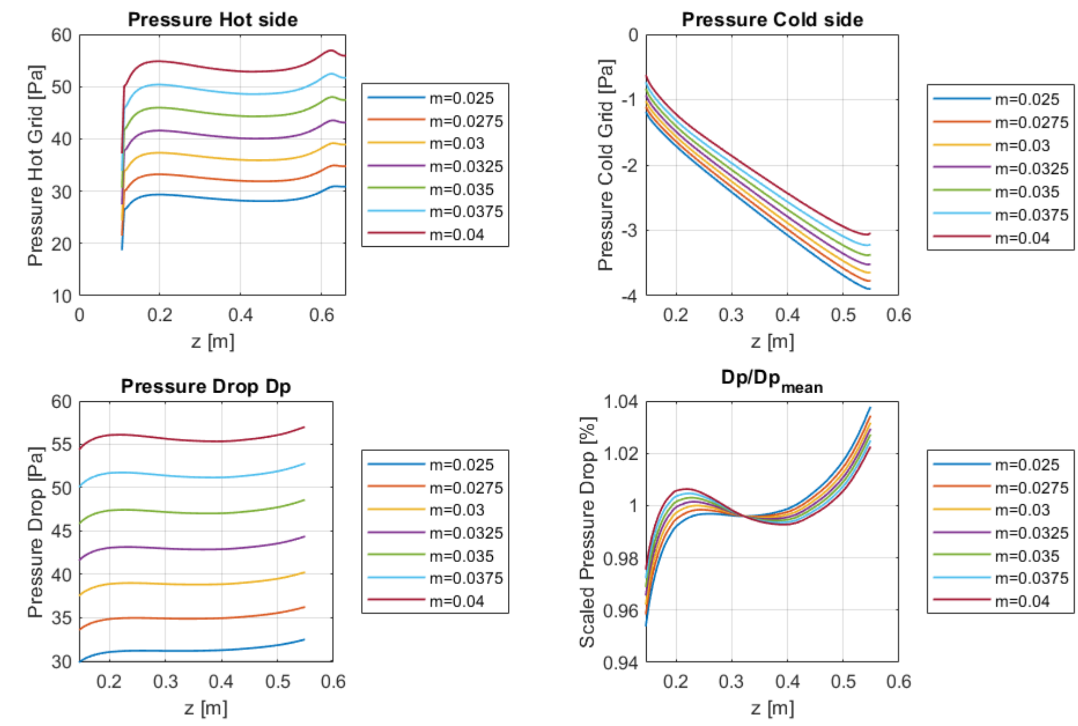

Figure 64 Evaluation of pressure drop during charge phase.

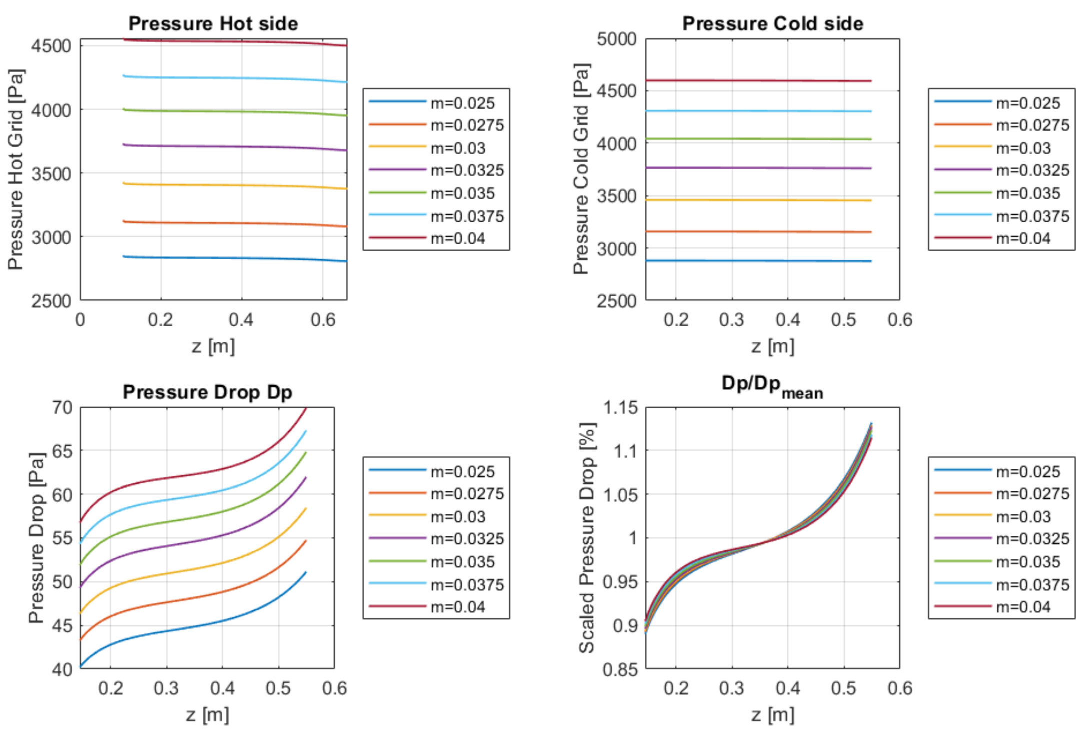

Figure 65 Evaluation of pressure drop during discharge phase.

Looking at the temperature trend, a higher mass flow rate shows results in a quicker increase of temperature in the bed, ensuring a faster charge. The same takes place during the discharge. Therefore, this could be positive for faster responses of the system connected (when charges/discharges are required by the system), but not if energy is required for a long time.

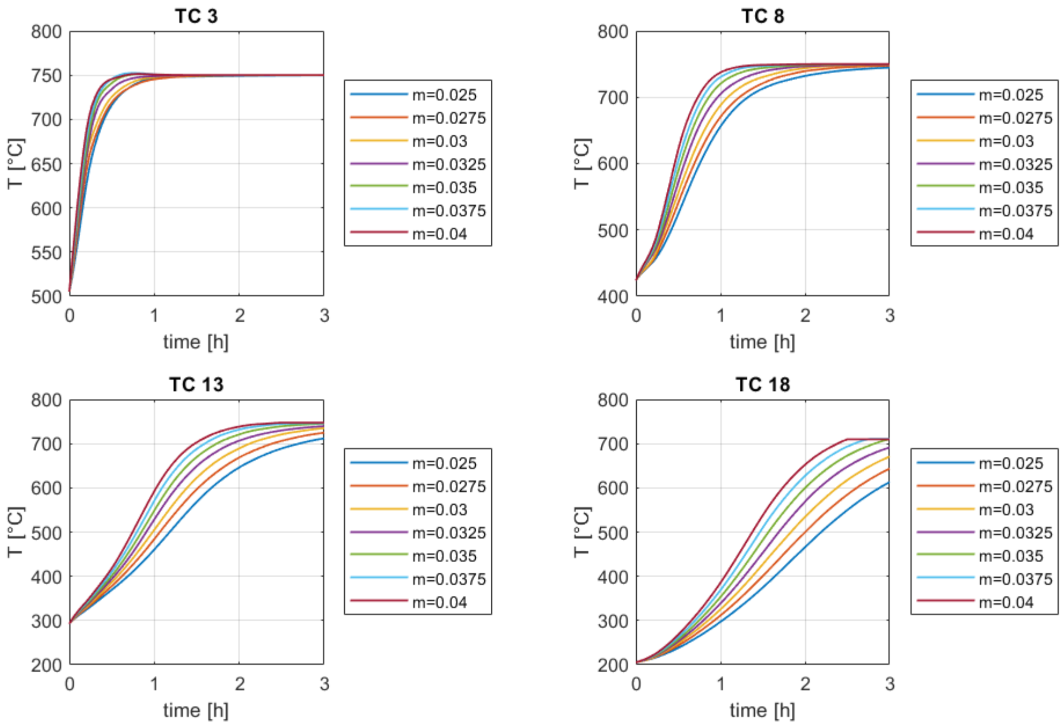

Figure 66 Evaluation of temperature trend during charge phase.

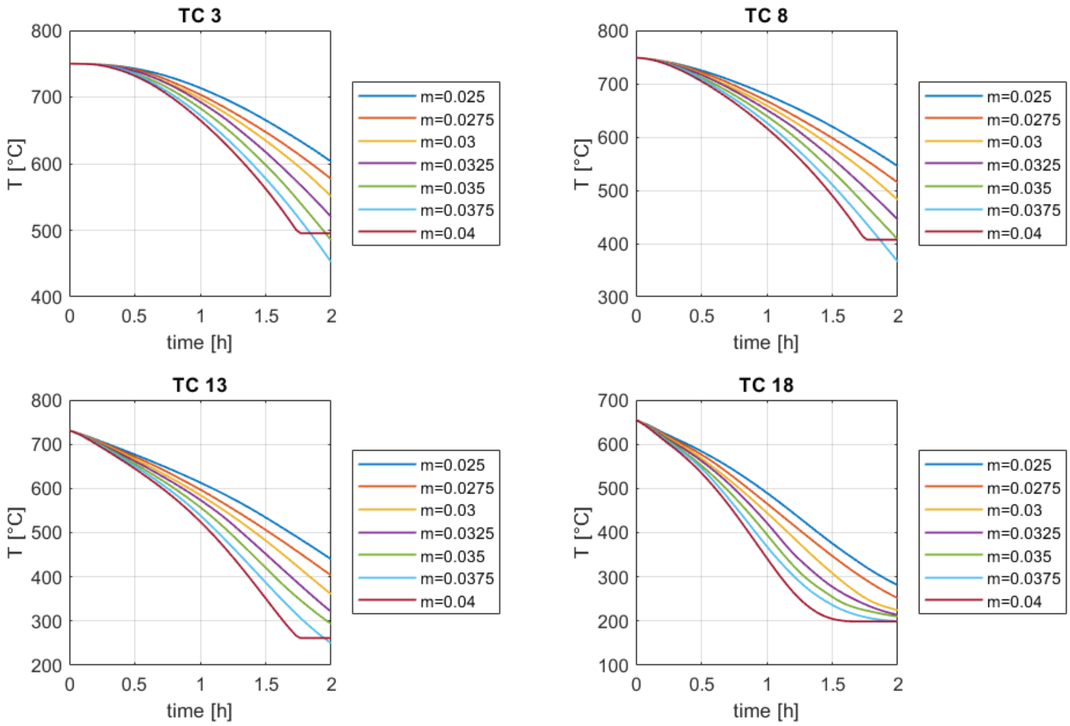

Figure 67 Evaluation of temperature trend during discharge phase.

Regarding the thermal behavior in time, it is possible to observe a totally opposite trend for the charge and discharge phases. Indeed, in the first case a lower mass flow leads to reduced thermocline width, while in the second case that effect is obtained for low mass flow rates.

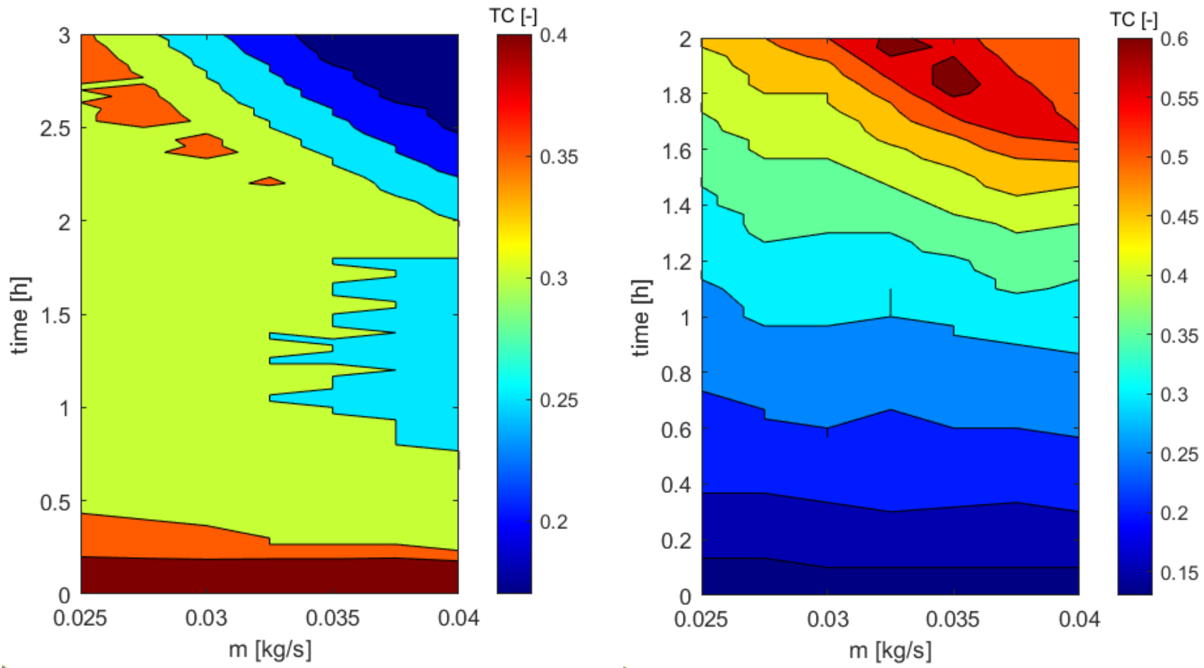

Figure 68 Evaluation of thermocline evolution during charge (left) and discharge (right) phases.

As summarized in Figure 69, the effect of this variation is relevant both on fluid flow and temperature distribution within the packed bed. Higher mass flow allows to obtain better hydrodynamic efficiency, probably due to a less relative difference in pressure drop with respect to the mean value, rather than to a real better flow distribution.

Looking at the thermal efficiency, it has different trends for the two phases, as for the thermocline width. During charge, the inlet flow at a high temperature reaches the inner part of the bed. In this case, the effect of high temperature and high velocity causes an enhancement of the convective heat transfer coefficient, resulting in a better thermal distribution and stratification. During the discharge, the inlet flow temperature is the minimum and meet firstly the colder external zone, while reaching the hot zone when the velocity has been already reduced by the packed bed. Hence, the effect of increased mass flow rate is less relevant, if compared with the one caused by longer times of permanence inside the bed (which is a consequence of lower mass flows). As a result, in this second case the thermal behavior is better for reduced mass flow rates.

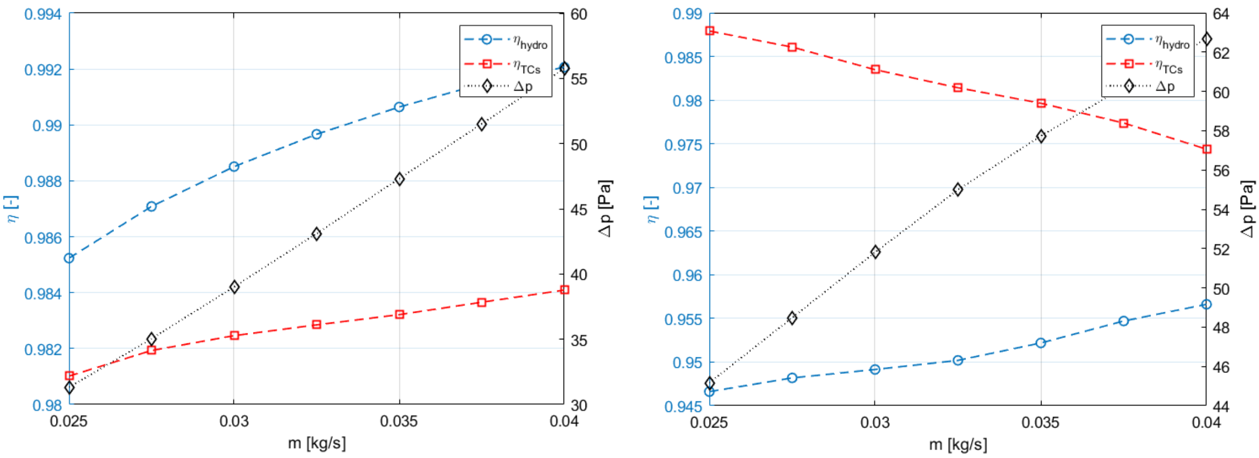

Figure 69 Summary of TES performance comparison during charge (left) and discharge (right) phases.

As visible in Figures 68-69, for better results it is advised to use different mass flows for different phases, but if not possible, a trade-off between charge/discharge constitutes the best option. Furthermore, often mass flow rate is imposed by the system, and it is variable during operations, making the size of the TES a consequence of this parameter. However, it is interesting to observe its influence on the general performances.

5.4 Particles diameter

5.4.1 Background

Design variables are possibly the most influent parameters that can be modified to achieve better performance. Among them, particles diameter is one of the most investigated parameter in literature. Its effect has been evaluated for axial packed bed TES, but not for radial energy storage. In general, higher particles diameters permit lower pressure drop, but worse heat exchange with the HTF, as the contact area is reduced. Over a certain value, conduction inside the particles could be no more negligible, leading to local temperature gradients and less effective heat transfer. On the other hand, reducing the diameter heat exchange is increased, until a value beyond which a greater contact area does not influence considerably the heat transfer mechanisms (mostly convection) and conduction inside the single particle is negligible. However, the drawback related to smaller particles is the higher pressure drop.

This parameter influences also the effective thermal conductivity, but its effect is of secondary importance with respect to the variation of convective heat transfer.

For this study, the diameter has been varied from 4 to 14 mm.

5.4.2 Results

As expected, pressure drop is increasing with smaller particles diameter, with a trend which seems inversely proportional. Indeed, for very small diameters (less than 8 mm) pressure drop grow dramatically, while its variation is a lot smaller for d_p>10 mm. During the discharge phase, almost no effect is visible on pressure distribution in the axial direction, while a more relevant disuniformity is observable during discharge for low d_p.

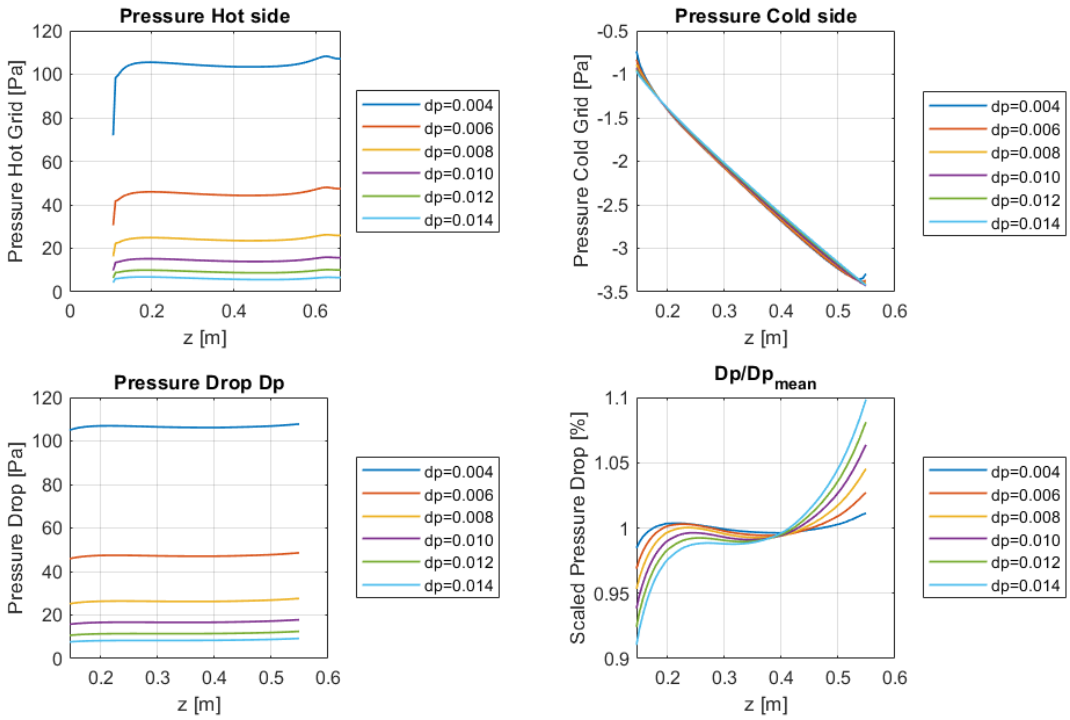

Figure 70 Evaluation of pressure drop during charge phase.

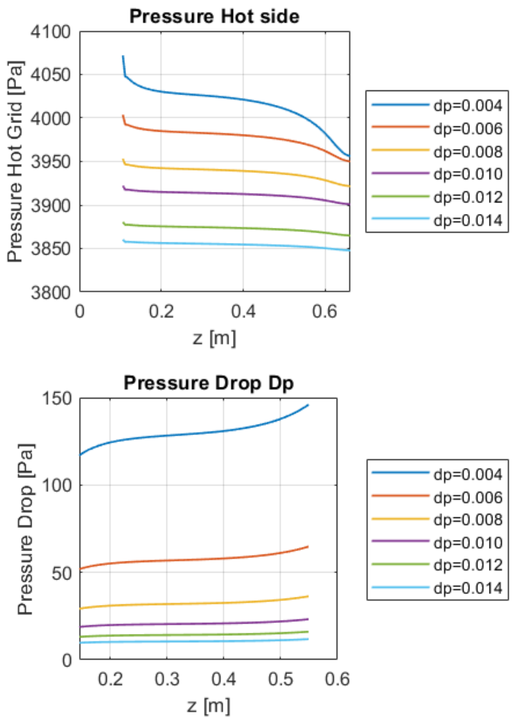

Figure 71 Evaluation of pressure drop during discharge phase.

Focusing on temperature variation in time, the slope of the curves seems to be smoother for higher particles diameters, thus this parameter influences both the charge and the discharge phase in terms of thermal behavior.

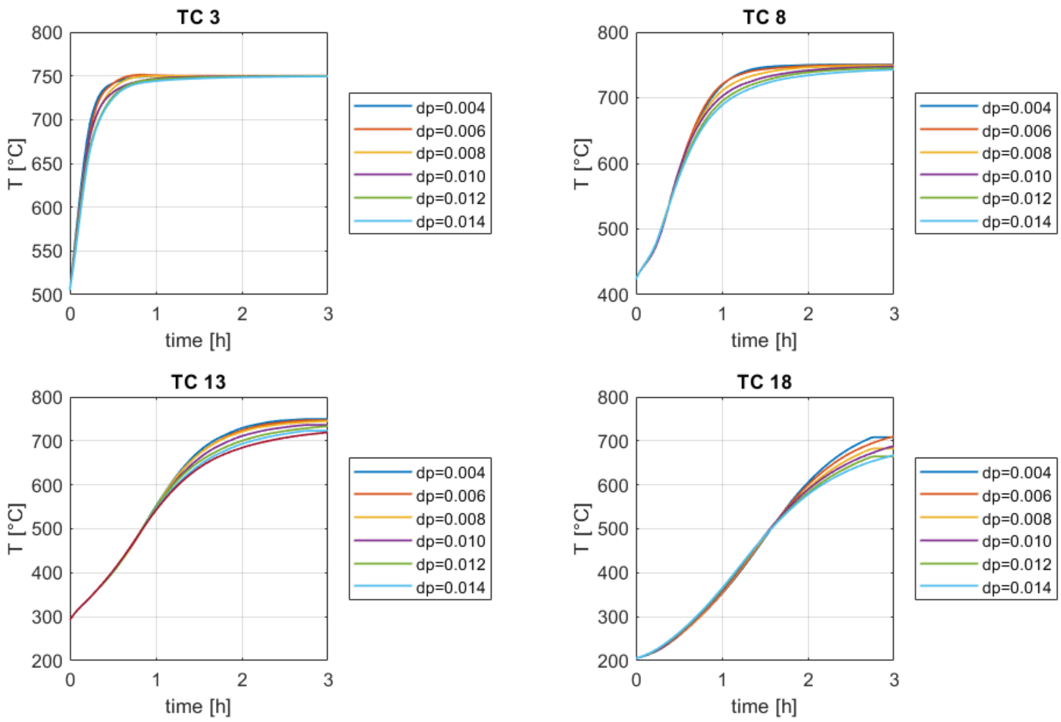

Figure 72 Evaluation of temperature trend during charge phase.

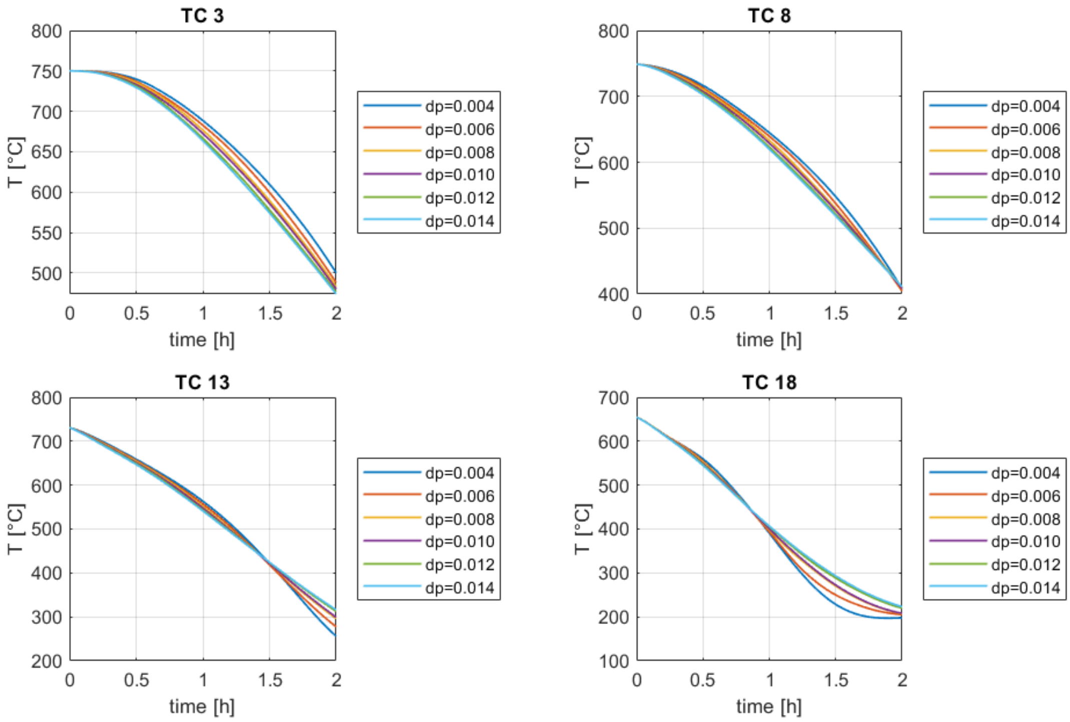

Figure 73 Evaluation of temperature trend during discharge phase.

As mentioned before, the temperature trend in time is smoother for higher d_p, resulting in a more consistent thermocline spread during operation. This effect is clear both in the charge and discharge phases, and it is mostly related to smaller contact area between the solid filler and the HTF, and due to internal conduction inside the single particle, as asserted in the background section. Unlike previous measures, the effect of d_p on thermocline thickness is quite relevant, and the choice of this parameter is a key point in the design of a packed bed TES.

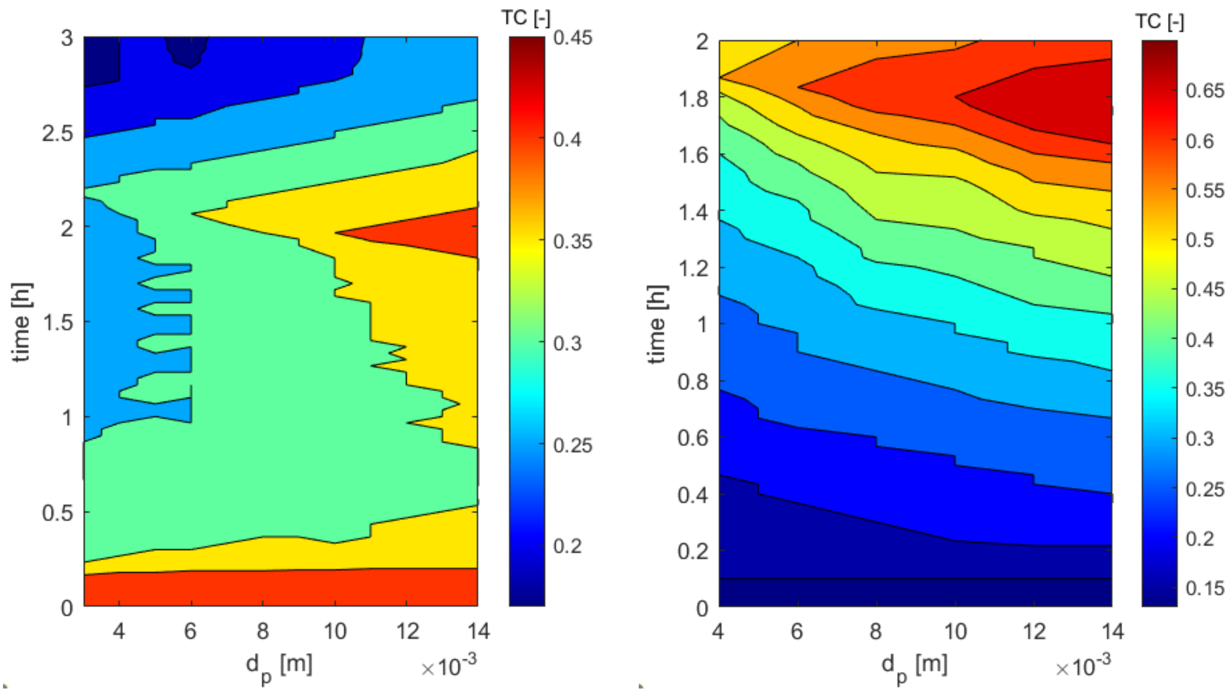

Figure 74 Evaluation of thermocline evolution during charge (left) and discharge (right) phases.

According to the expectations, during charge phase larger particles cause non-uniform flow distribution, while it seems to have almost no effect on the thermal efficiency in the axial direction. The opposite behavior is observed during the discharge, in which both the thermal and hydrodynamic efficiencies are increasing with the d_p. The anomaly of the discharge could be related to the disuniformity caused by the low inlet pipe (the outer one): the flow entering, which is not uniform, has more possibilities to distribute toward the axial direction with larger particles. Smaller ones tend to link more the fluid flow to pressure distribution, reducing the possibility of a proper diffusion in the z-axis.

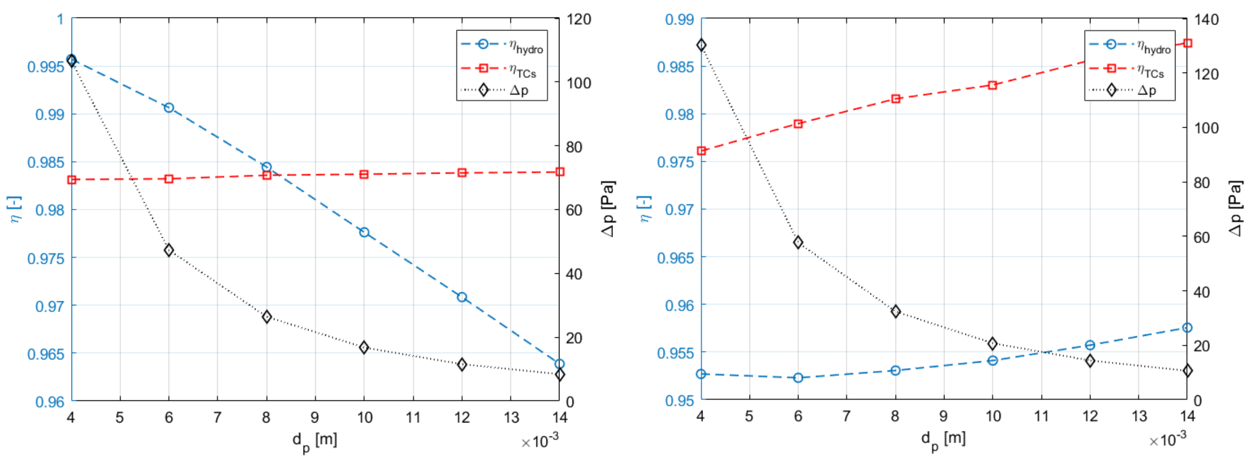

Figure 75 Summary of TES performance comparison during charge (left) and discharge (right) phases.

Considering all the parameters analyzed to explain the performances of the storage, a particle diameter of around 8 mm could represent the best trade-off. Indeed, for this value the pressure drop is low enough and the thermocline thickness maintains an average spread in the range of 30-35%.

5.5 Surface emissivity

5.5.1 Background

Radiation is one of principal heat transfer mechanisms in a packed bed TES. This phenomenon starts to be relevant at a temperature higher than 350-400 °C and gains importance with increasing values, as it is generally dependent on the absolute temperature's fourth power. Thermally emitted radiance for any surface depends also on surface emissivity, which is a function of material properties, surface roughness, electromagnetic spectrum and temperature. Surface emissivity can be varied by adding an external coating through mechanical/chemical procedures.

Emissivity has a relevant influence on effective thermal conductivity, as can be seen in figure …. This could result in an enhanced heat transfer inside the bed, leading to faster charge/discharge, but increasing mixing and diffusion between the hot and cold regions. Therefore, the effect of surface emissivity on TES performance needs to be assessed.

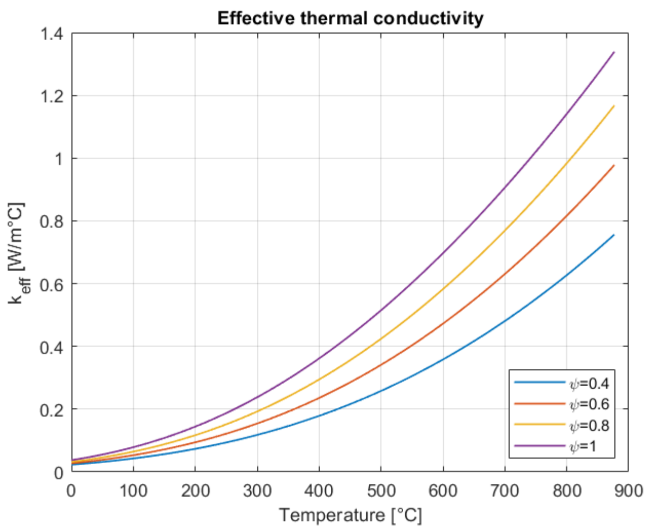

Figure 76 Effect of surface emissivity on effective thermal conductivity in dependence of temperature.

Therefore, the effect of different thermal emissivity on the TES performance are investigated, varying it from 0.4 to 1.

5.5.2 Results

The measure does not modify the shape of pressure distribution along the axial direction, as no physical parts has been added or changed in this measure. However, seems that higher emissivity results in lower pressure drop, which is an indicator of a lower average temperature inside the packed bed. This should be an effect of the increased thermal conductivity, which enhances the heat transfer between the hot region and the intermediate/cold ones. This consideration is valid for the discharge phase, and partially explains the TES behavior during charge.

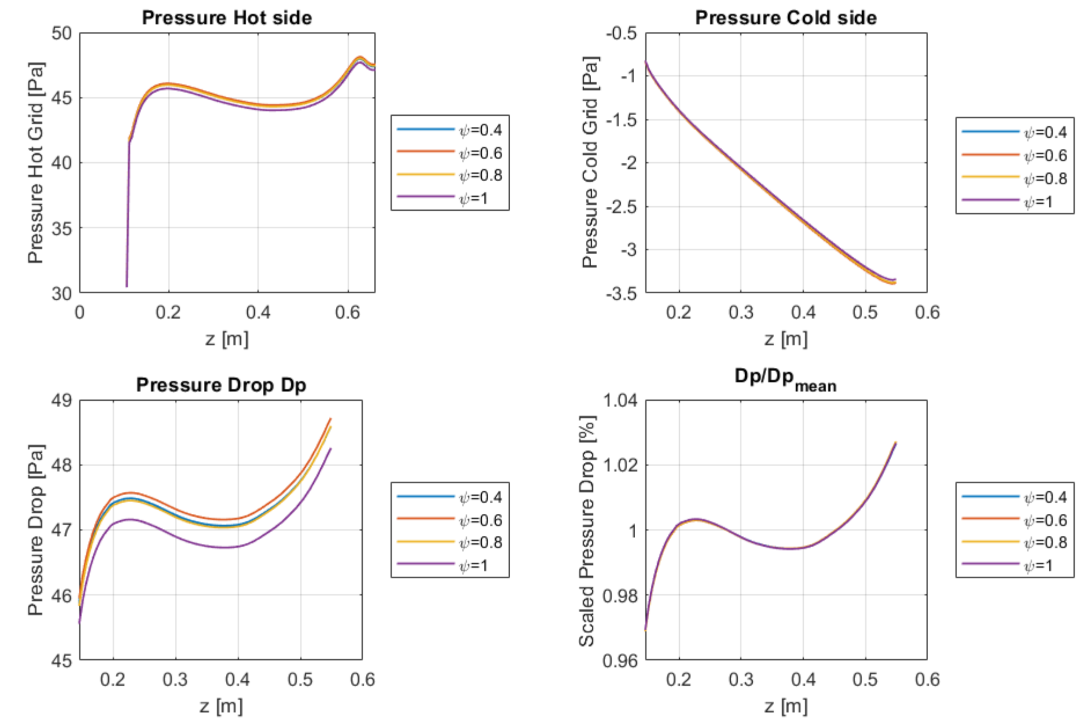

Figure 77 Evaluation of pressure drop during charge phase.

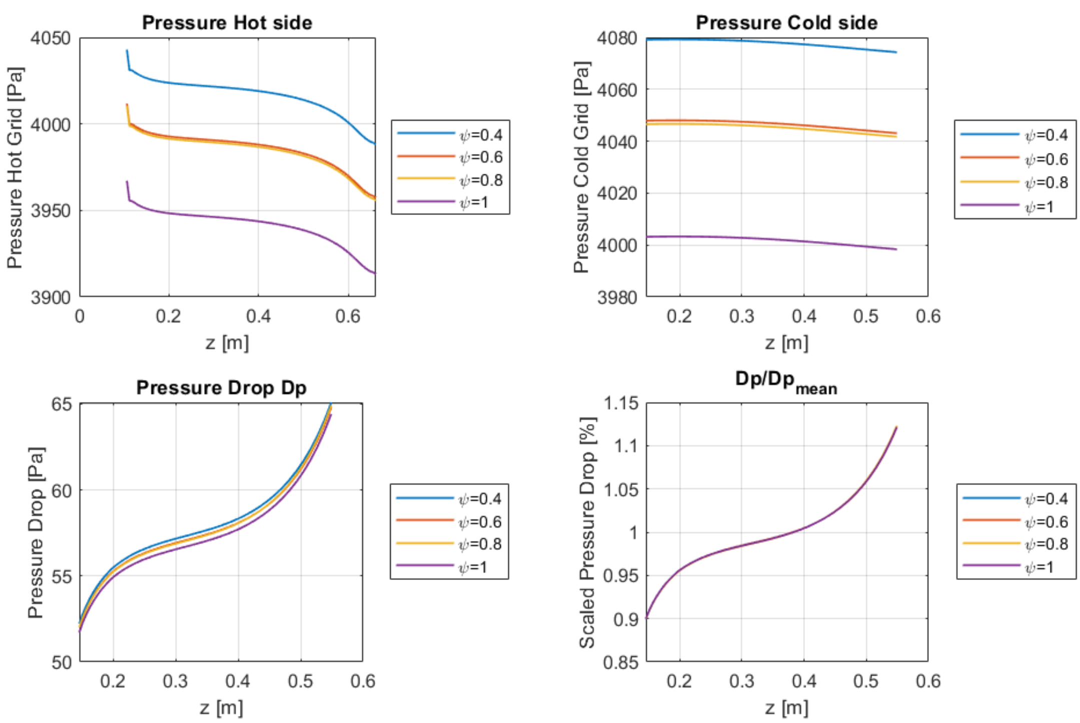

Figure 78 Evaluation of pressure drop during discharge phase.

Looking at the temperature, its trend seems to be slightly smoother for higher values of emissivity. As the effect of emissivity is more relevant at higher temperatures, the inner region is more conductive, and it is possible that tends to transmit more to the outer regions. Furthermore, the curve in the thermocouple 18 shows a flat temperature at the end of the charge process: this is the output obtained if the charge phase is ended. Therefore, with higher emissivity, a shorter time interval is required to charge the storage.

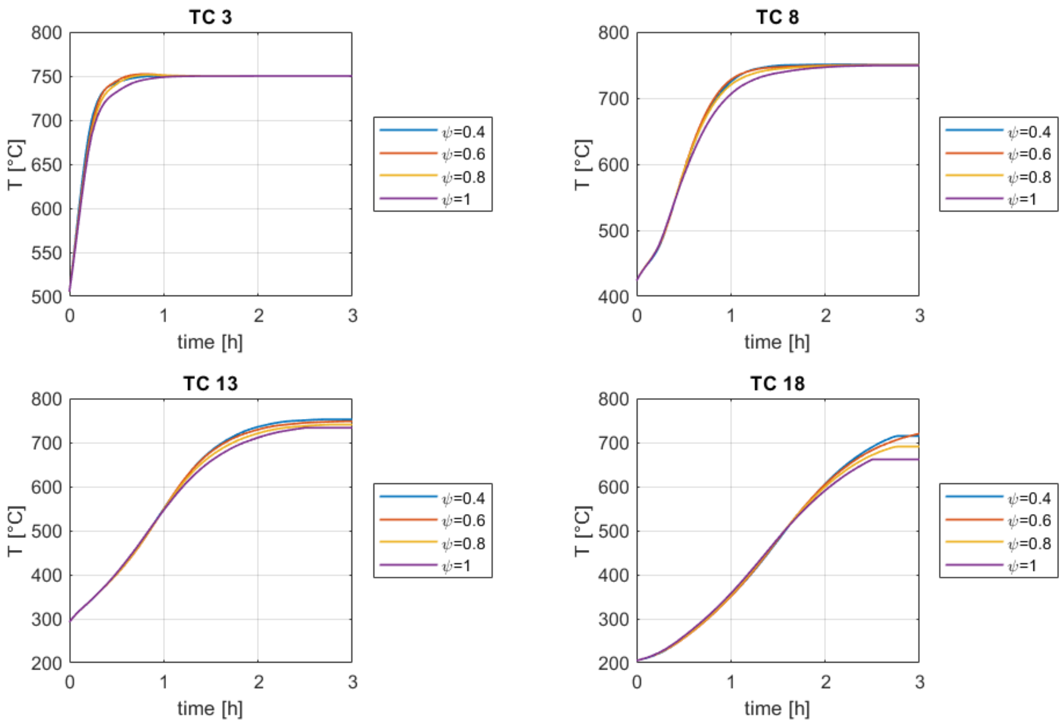

Figure 79 Evaluation of temperature trend during charge phase.

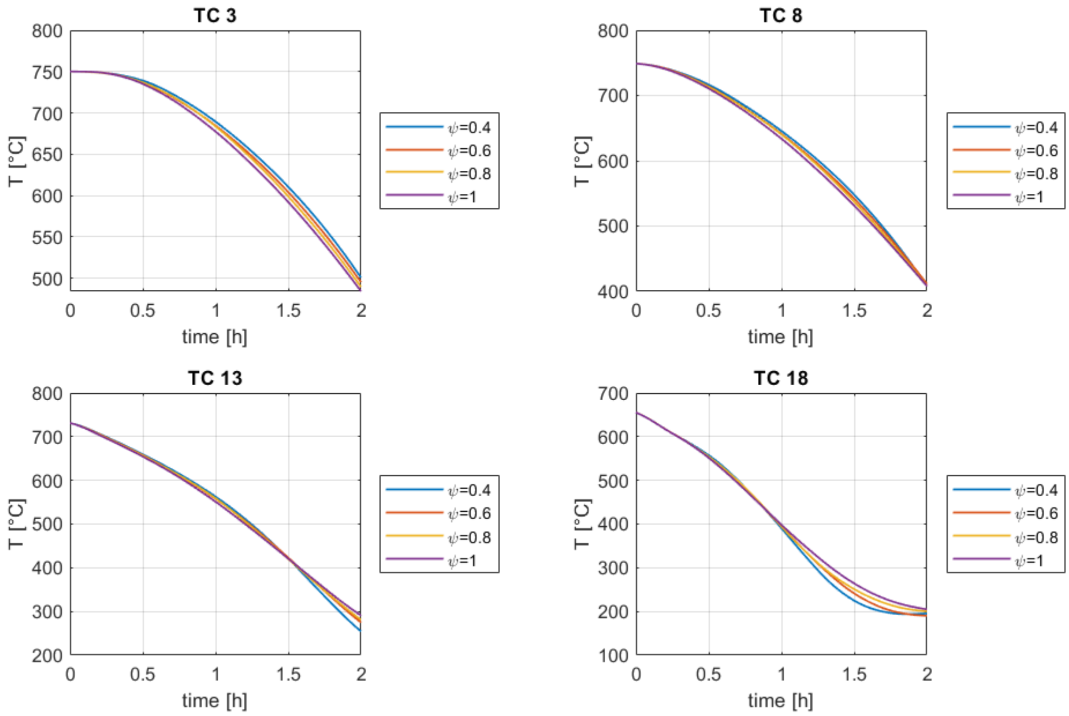

Figure 80 Evaluation of temperature trend during discharge phase.

On the other hand, the smoother trend of temperature curves leads to wider thermoclines, in both the two phases, as the temperature in the outer region tends to stay in the thermal front region for more time. As a consequence, lower emissivity results in a better thermocline behavior, contrarily to what is generally wanted while designing an energy storage.

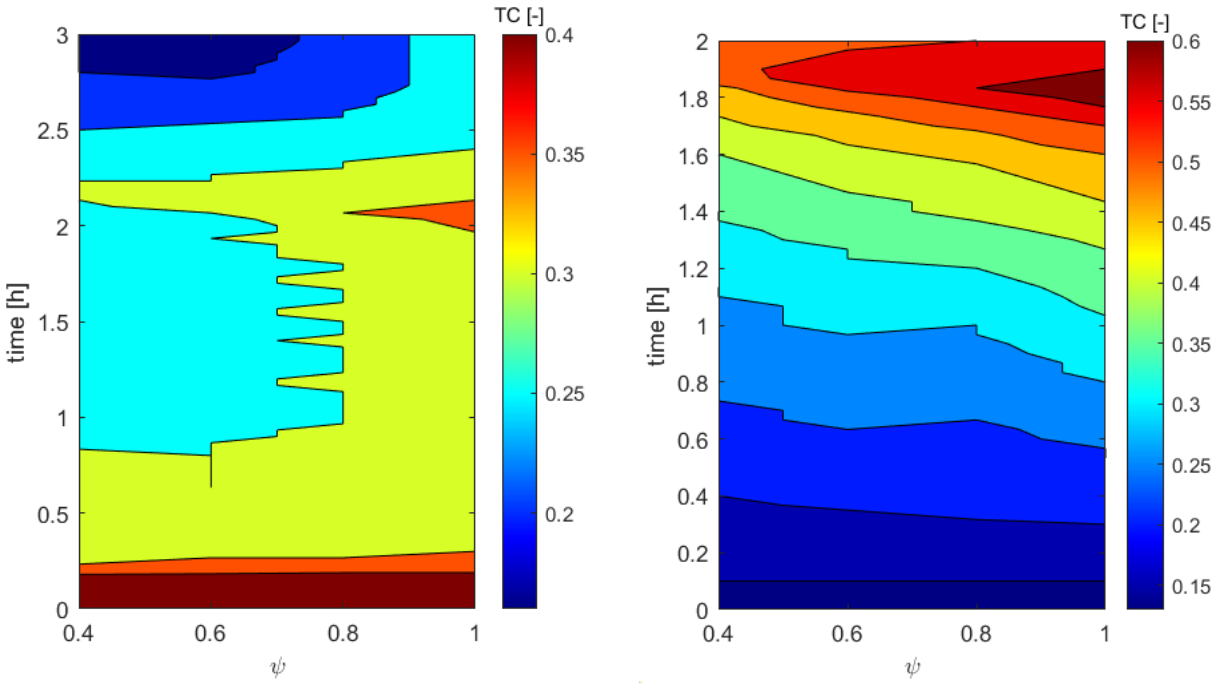

Figure 81 Evaluation of thermocline evolution during charge (left) and discharge (right) phases.

Along the z-axis, the temperature and flow uniformity tend to be slightly improved with increased emissivity, as the higher effective conductivity in the hot region creates a better thermal distribution. However, these variations are almost negligible and cannot justify the increase in thermocline thickness.

Eventually, as the effect of surface emissivity has been included in the effective thermal conductivity by using the model proposed by Kunii and Smith, its effect could not have been calculated accurately. Therefore, as some of the results are different than what expected, further experimental and numerical investigations are necessary.

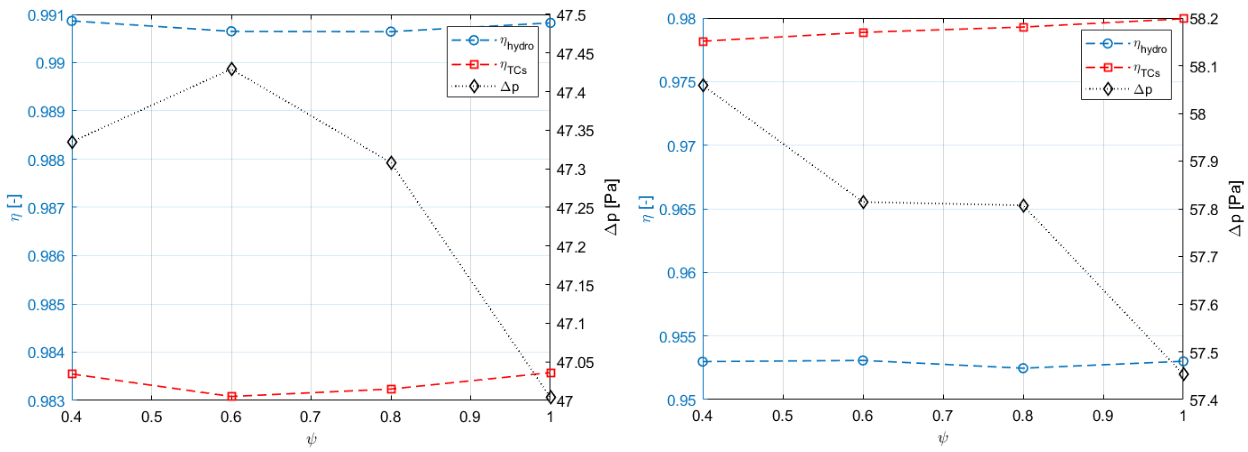

Figure 82 Summary of TES performance comparison during charge (left) and discharge (right) phases.

5.6 Conical structure

5.6.1 Background

Fluid flow distribution within the storage can be considered quite uniform in the base case. However, some modifications are tried in order to improve it further. One of those changes consists in adding a conical structure in the inner channel. In this way, the pressure distribution and the fluid flow along the z-axis is supposed to be more uniform, as the aim of the structure should reduce the pressure drop in the higher part of the TES while increasing its value in the lower zone.

The cone, which is considered not relevant in terms of heat transfer (the cone is empty), has a weight equal to the inner channel, and it is varied in width, changing the radius from 10 to 60 mm. The following figure shows the new TES design.

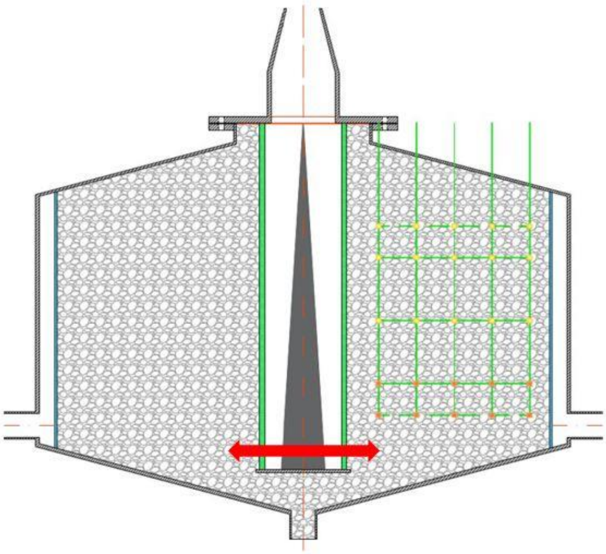

Figure 83 Introduction of a conical structure with different radius.

5.6.2 Results

Analyzing the results of the charge phase, it is clear that the pressure on the hot side, and consequently the pressure drop, is reduced on the top of the storage. This leads to a more uniform pressure drop in that region, which was the aim of the measure. However, the cone structure, whatever is its radius, causes a less uniform trend of pressure drop in the rest of the storage.

During the discharge, no effect on pressure drop is observed, as can be seen in Figure 85.

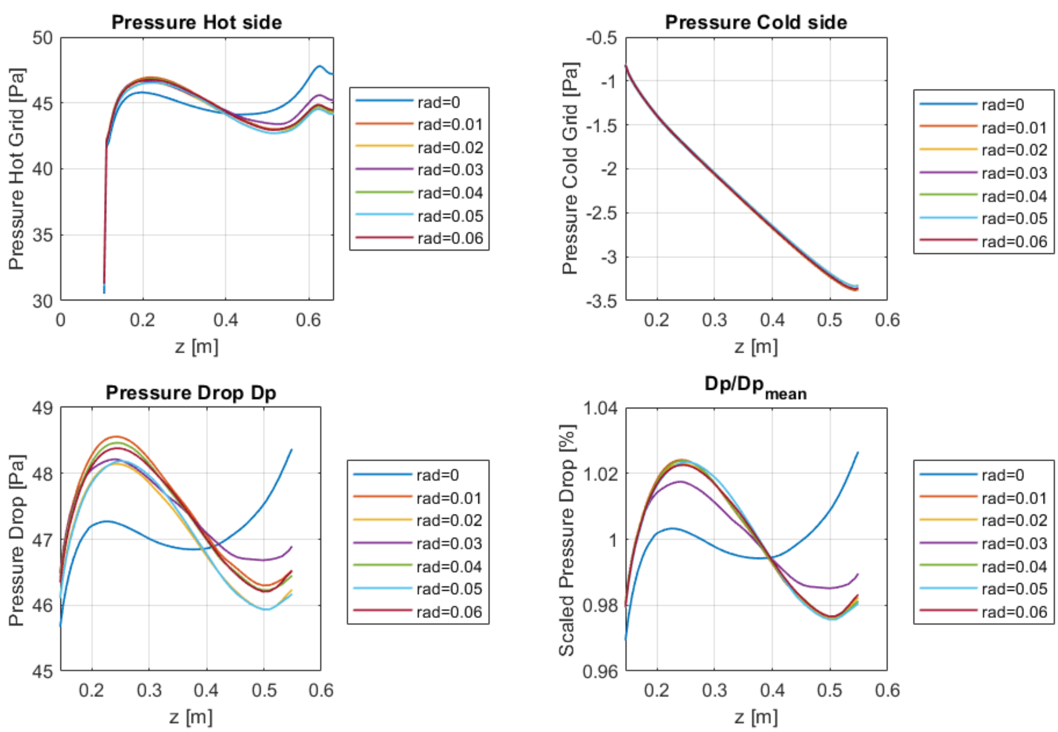

Figure 84 Evaluation of pressure drop during charge phase.

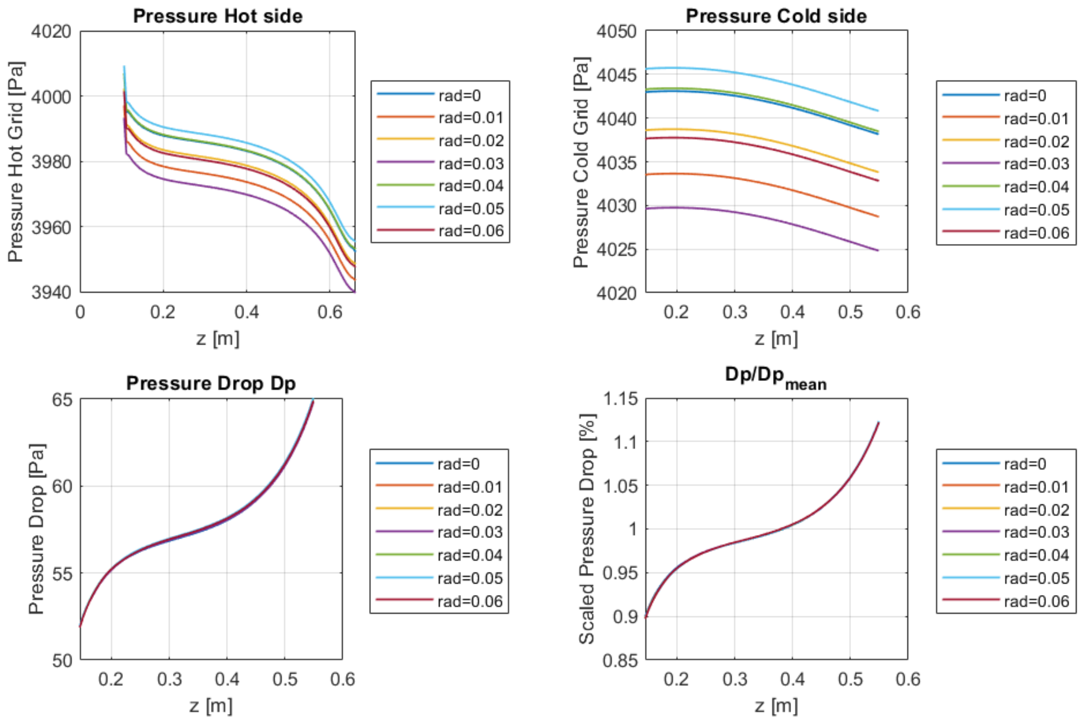

Figure 85 Evaluation of pressure drop during discharge phase.

The conical structure seems to have no effect on the temperature trend in time, as visible in Figures 86-87. Indeed, being the effect on pressure drop distribution, and consequently on fluid flow, not so influent, its effect on temperature is negligible. This fact is observable also looking at the thermocline thickness in time, which is almost constant, and thus not dependent on the diameter of the conical structure.

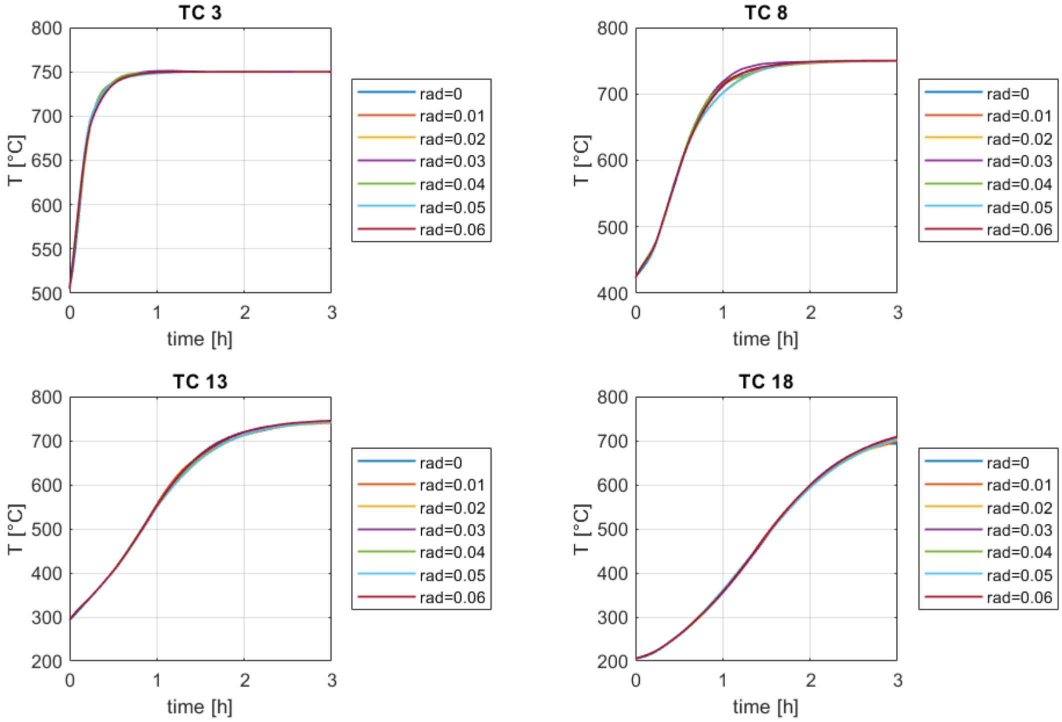

Figure 86 Evaluation of temperature trend during charge phase.

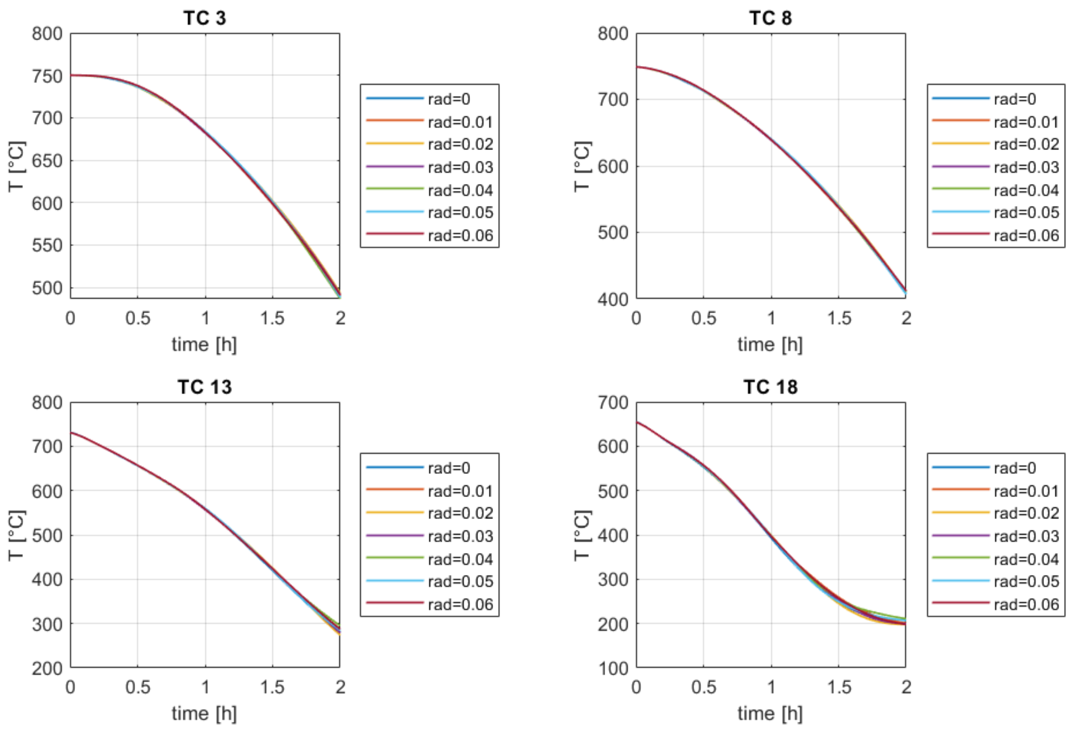

Figure 87 Evaluation of temperature trend during discharge phase.

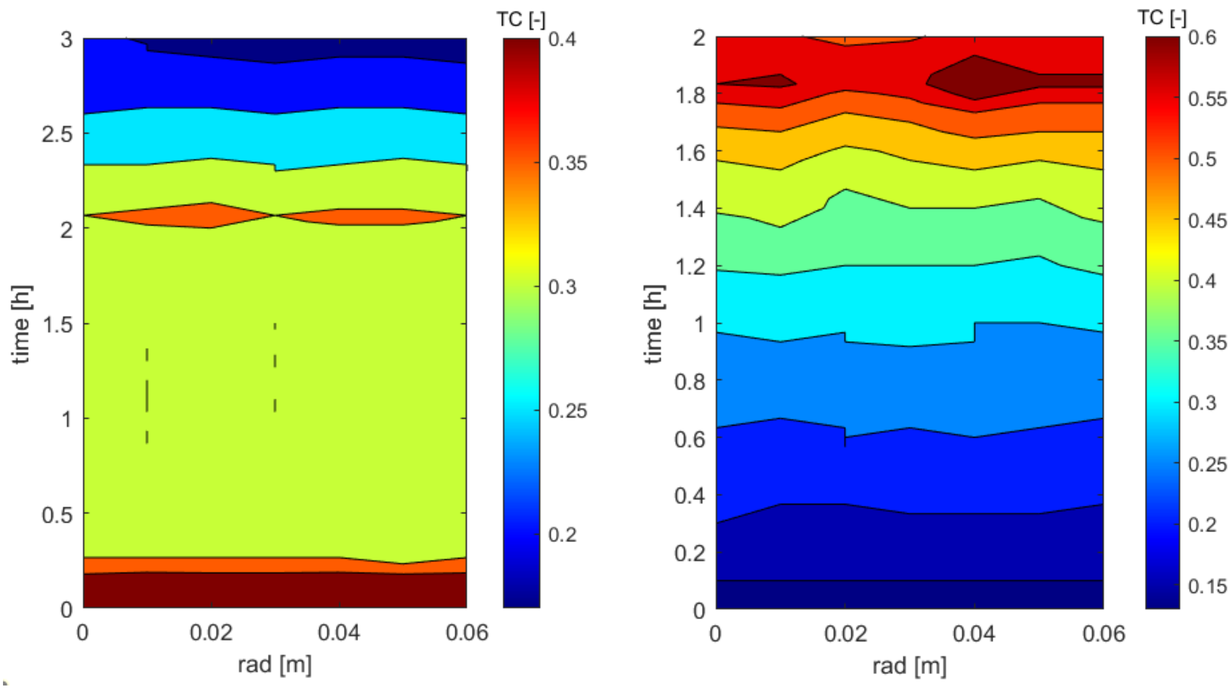

Figure 88 Evaluation of thermocline evolution during charge (left) and discharge (right) phases.

As summarized in Figure 89, the effect of introducing a conical structure to uniform the fluid flow in the axial direction has little or no effect on the storage. In particular, during the charge phase, both the hydrodynamic and thermal efficiencies show a slightly worse behavior with the conical structure rather than in the base case. In the discharge, the effect of the modification is negligible.

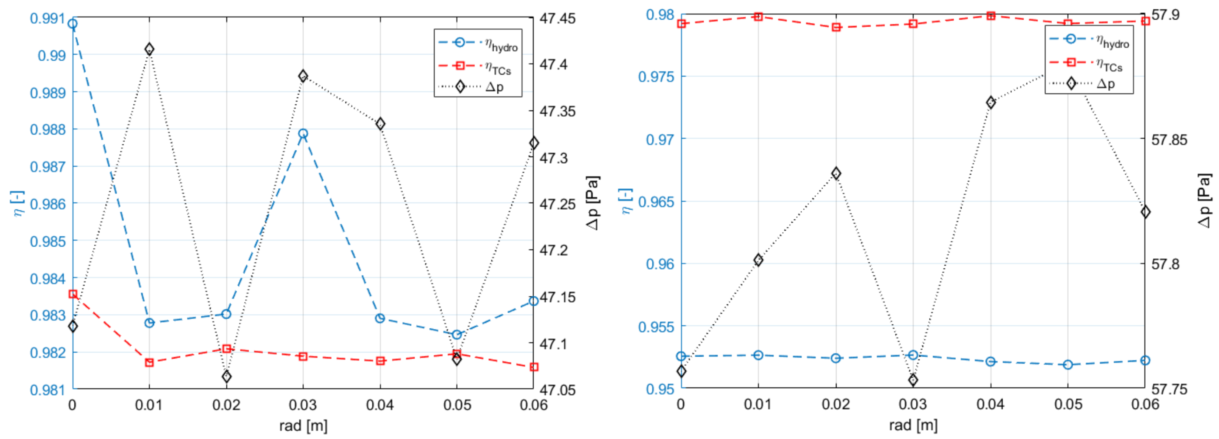

Figure 89 Summary of TES performance comparison during charge (left) and discharge (right) phases.

5.7 Divider inner channel

5.7.1 Background

Another possibility to try to obtain a more uniform fluid flow distribution has been assessed in this section. The measure consists in the introduction of a cylindrical divider in the inner channel, for the purpose of separating the fluid flow in two parts. As for the inner cone, the aim is to reduce the pressure drop gap between the lower and the upper part of the storage, possibly without influencing too much the middle region, which shows uniform distribution. Figure 90 shows the divider and how it is positioned into the storage.

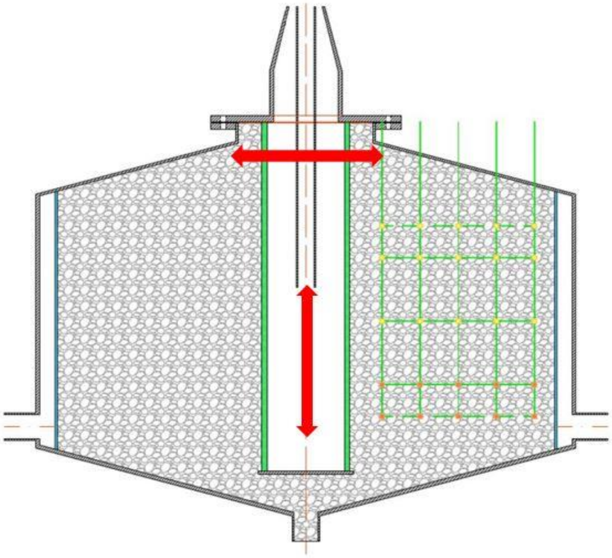

Figure 90 Introduction of an inlet divider with different heights and widths.

The divider geometry can be varied in radius and height. Modifying the height, it is possible to decide at which height the flow inside the inner cylinder can interface with the packed zone; varying the radius, the amount of HTF passing through the divider changes.

5.7.2 Results

The performances have been evaluated at three different heights and widths (inner radius), corresponding to ¼, ½ and ¾ of the channel length and of the inner channel radius (in case of the width). As expected, dividing the flux in two parts the pressure drop distribution changes significantly, depending on the dimensions of the divider; however, seems that the solution adopted destabilize the pressure distribution instead of making it more uniform along the axial direction. The only case of more stable pressure drop during the charge phase happens for a divider with height equal to ¾ of the inner channel and an inner radius corresponding to ½ of the channel's one. This partial improvement is not visible in the discharge phase, in which the introduction of the divider generates an enhanced difference in pressure drop between the lower and the higher regions.

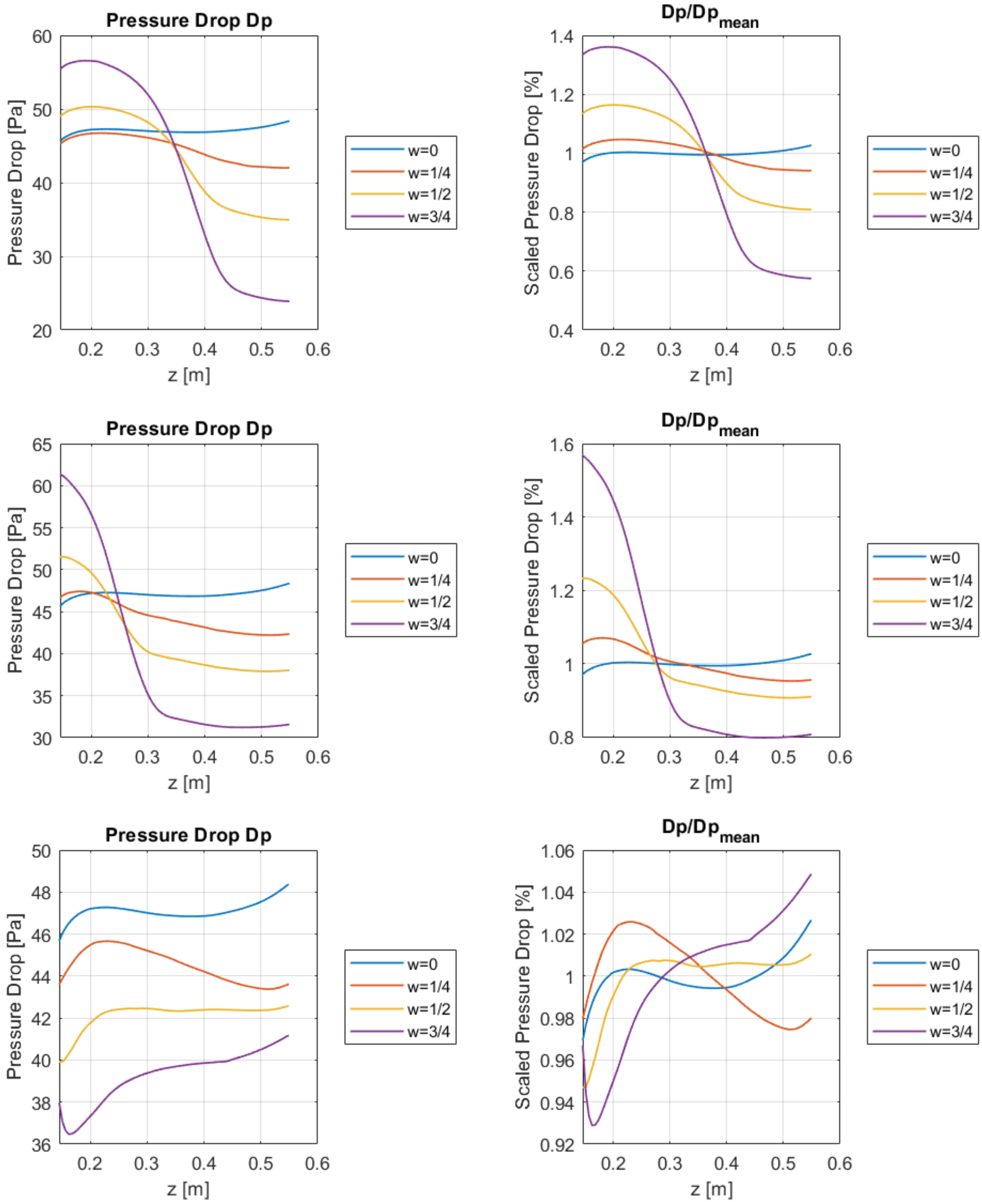

Figure 91 Evaluation of pressure drop during charge at different normalized divider heights: ¼ (top), ½ (middle), ¾ (bottom).

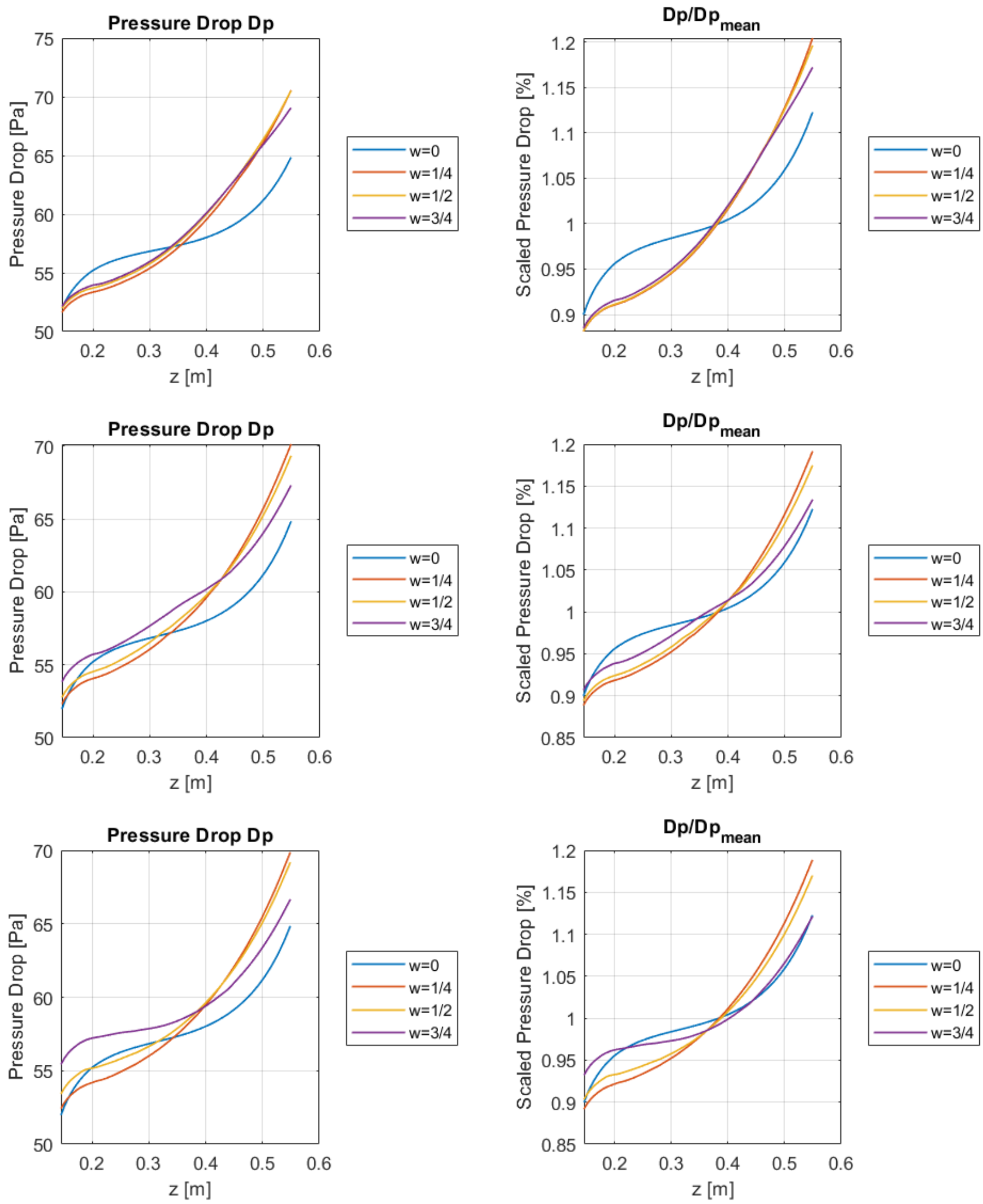

Figure 92 Evaluation of pressure drop during discharge at different normalized divider heights: ¼ (top), ½ (middle), ¾ (bottom).

A worsening with the introduced measure is generally observable in the temperature trend, as during charging it appears to be smoother with the divider, whatever are its dimensions. The discharge phase seems to be less influenced, but the temperature trend is still slightly smoother.

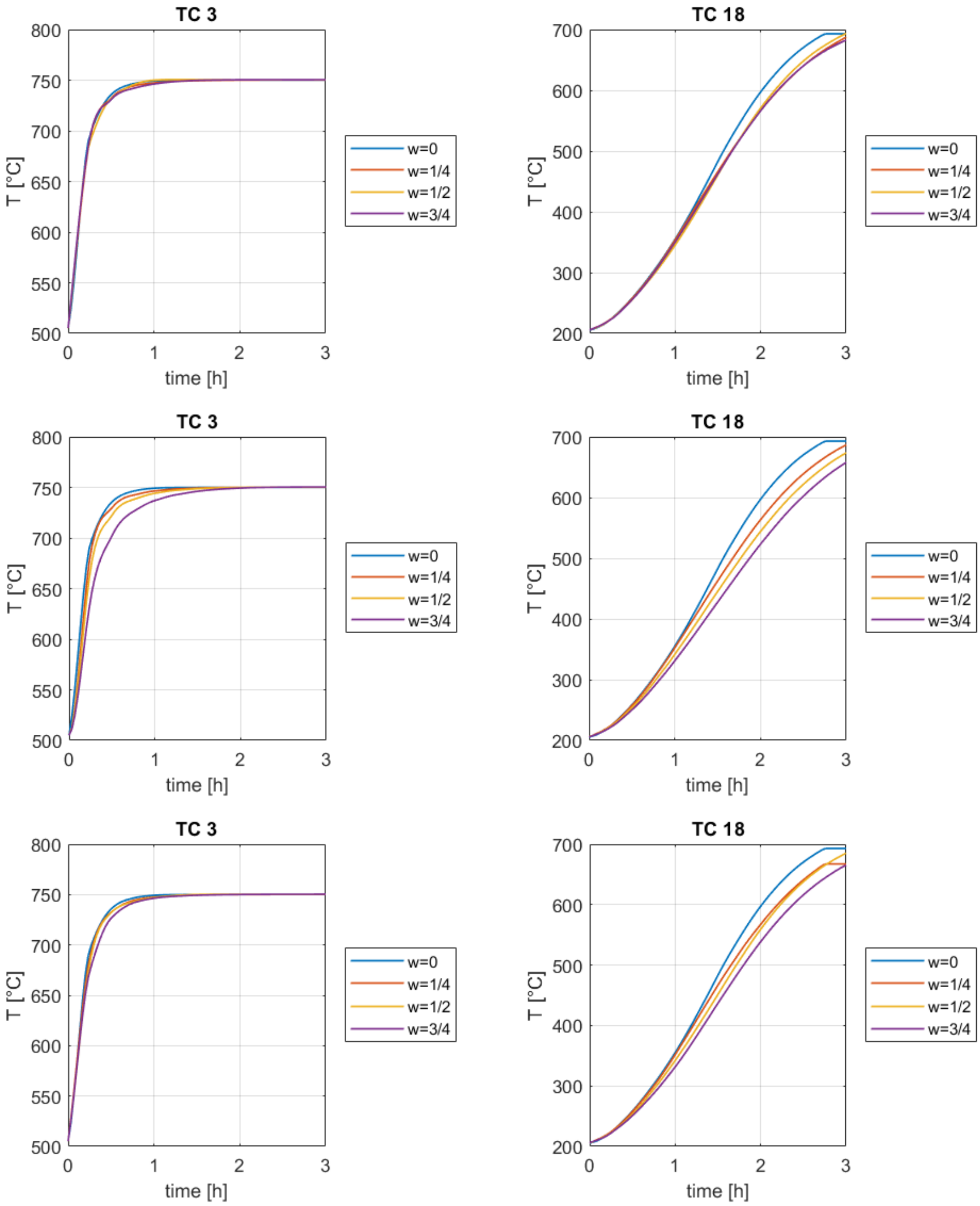

Figure 93 Evaluation of temperature trend during charge at different normalized divider heights: ¼ (top), ½ (middle), ¾ (bottom).

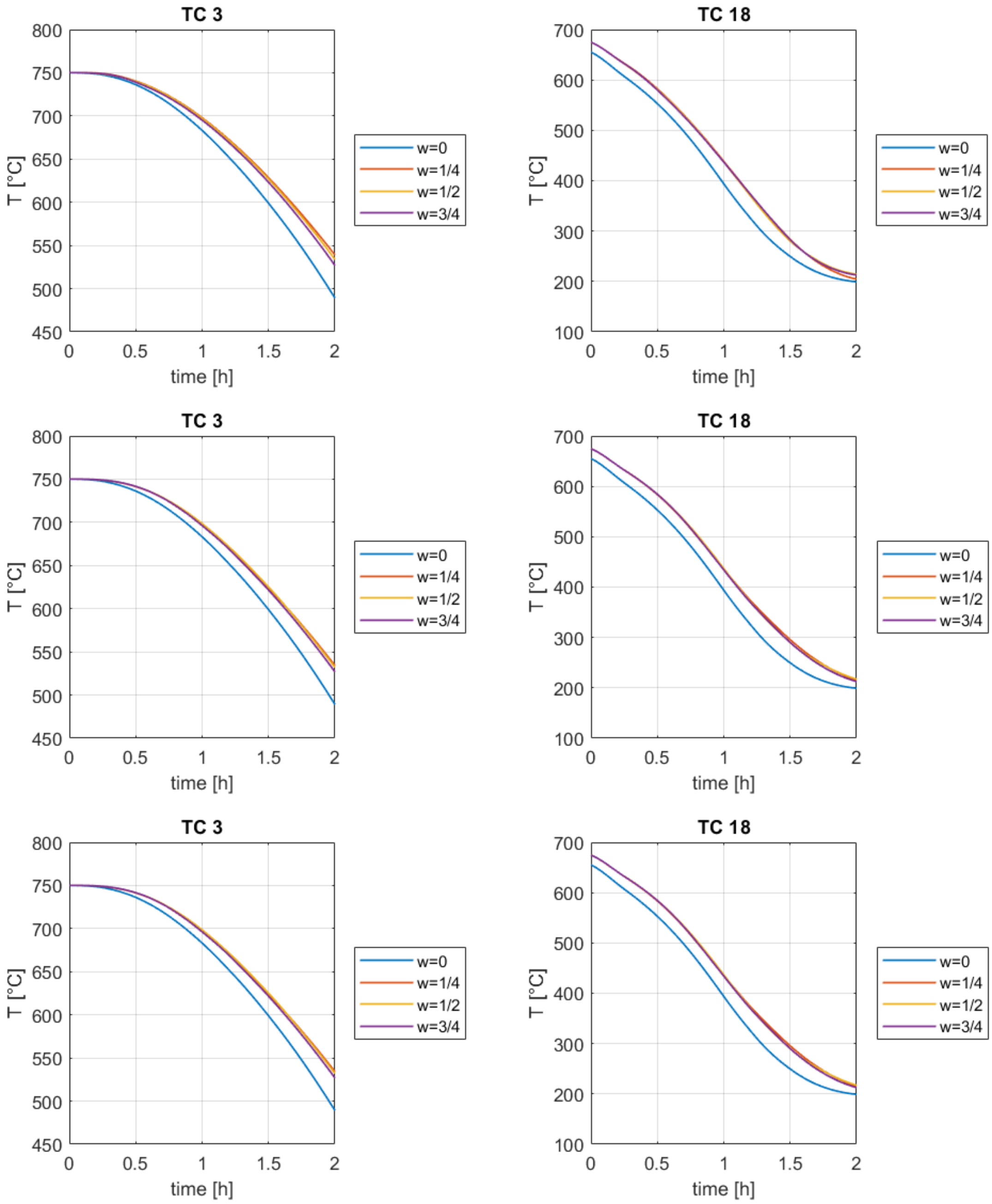

Figure 94 Evaluation of temperature trend during discharge at different normalized divider heights: ¼ (top), ½ (middle), ¾ (bottom).

Figures 95-96 show the thermocline spread during charge and discharge for all the configurations, comparing them with the base case. In all the configuration, the results suggest to not introduce the divider, as the non-uniform pressure distribution causes increased thermocline spread. Its effect is less visible in the discharge phase, in which the divider is posed at the exit of the storage, considering the HTF entering from the outer channel.

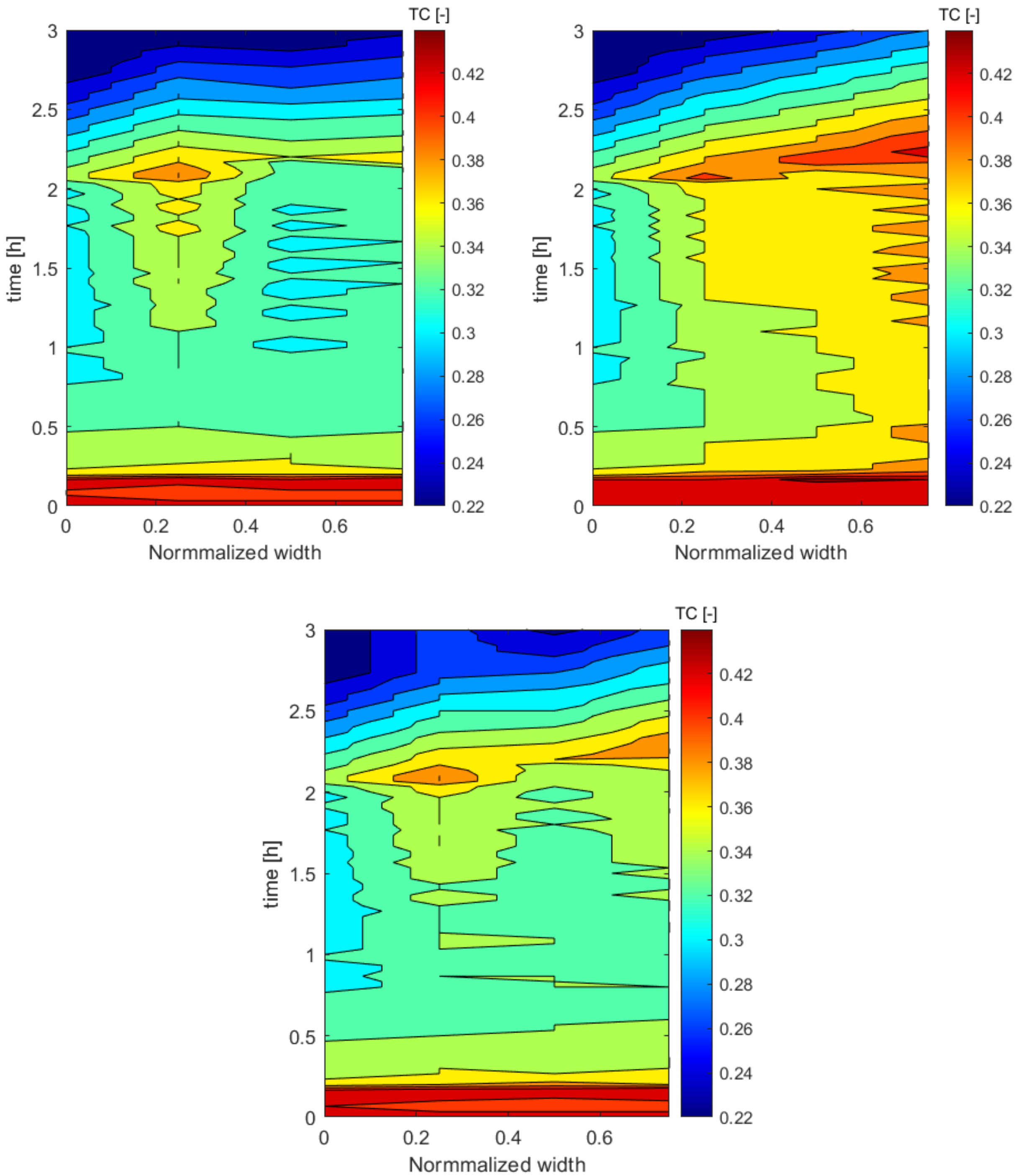

Figure 95 Evaluation of thermocline evolution during charge at different normalized divider heights: ¼ (top), ½ (middle), ¾ (bottom).

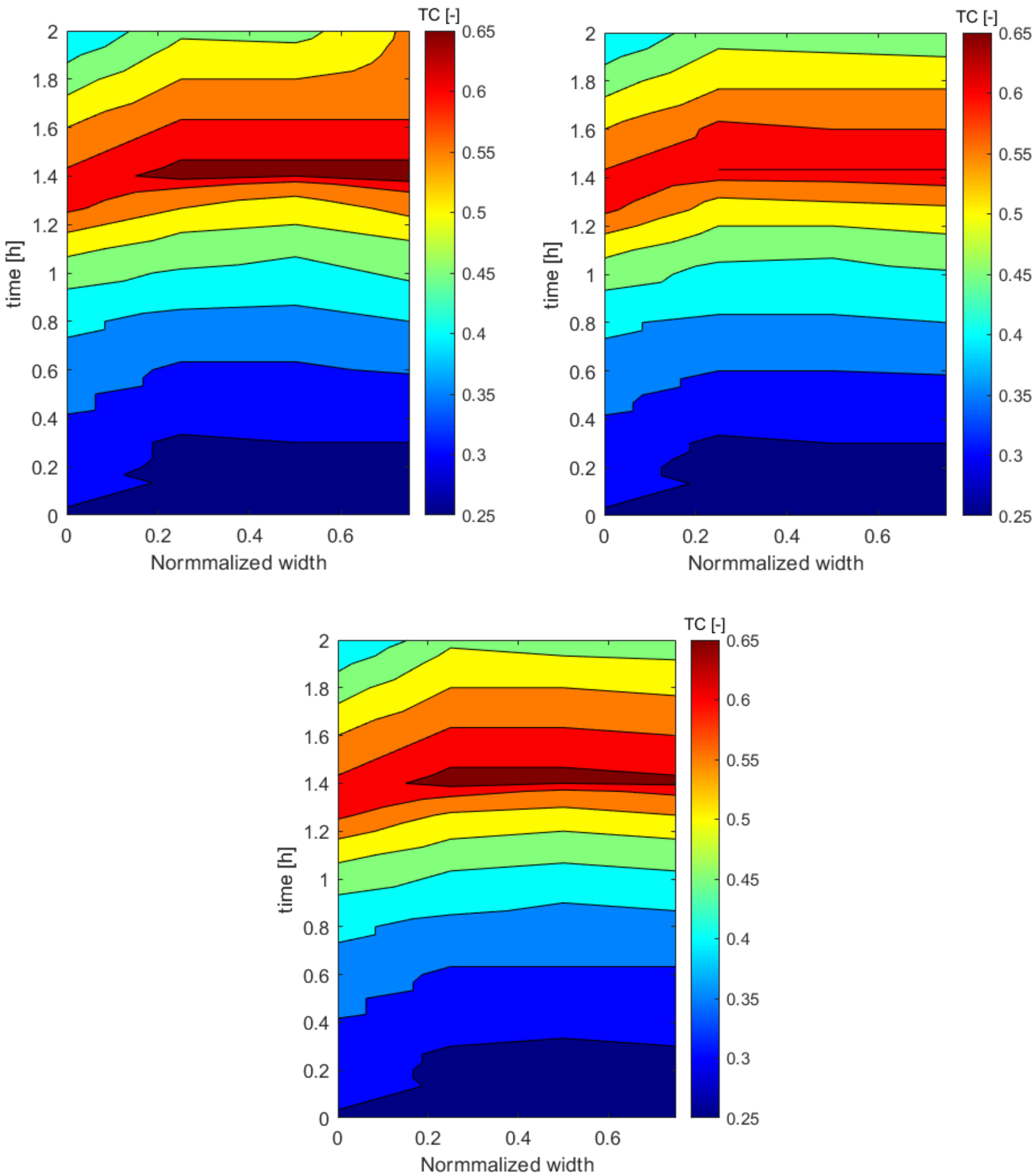

Figure 96 Evaluation of thermocline evolution during discharge at different normalized divider heights: ¼ (top), ½ (middle), ¾ (bottom).

Finally, as summarized in Figures 97-98, it is clear that this measure does not results in a better behavior of the TES, as the fluid flow, and the thermal distribution, is clearly less uniform and stable. This is visible looking both at the thermal and hydrodynamic efficiency, which are decreased or at least not significantly influenced by the presence of the divider.

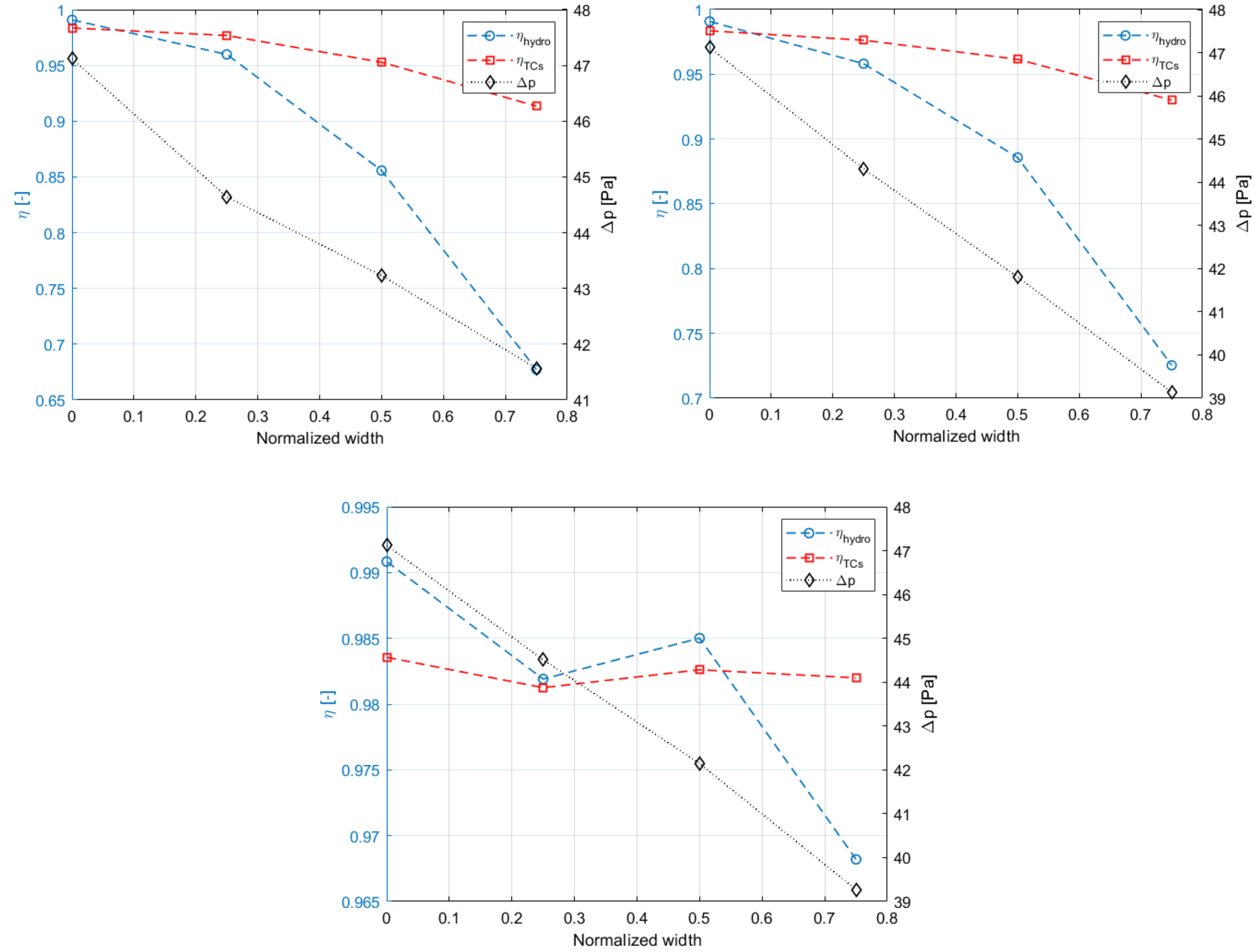

Figure 97 Summary of TES performance comparison during charge at different normalized divider heights: ¼ (top-left), ½ (top-right), ¾ (bottom).

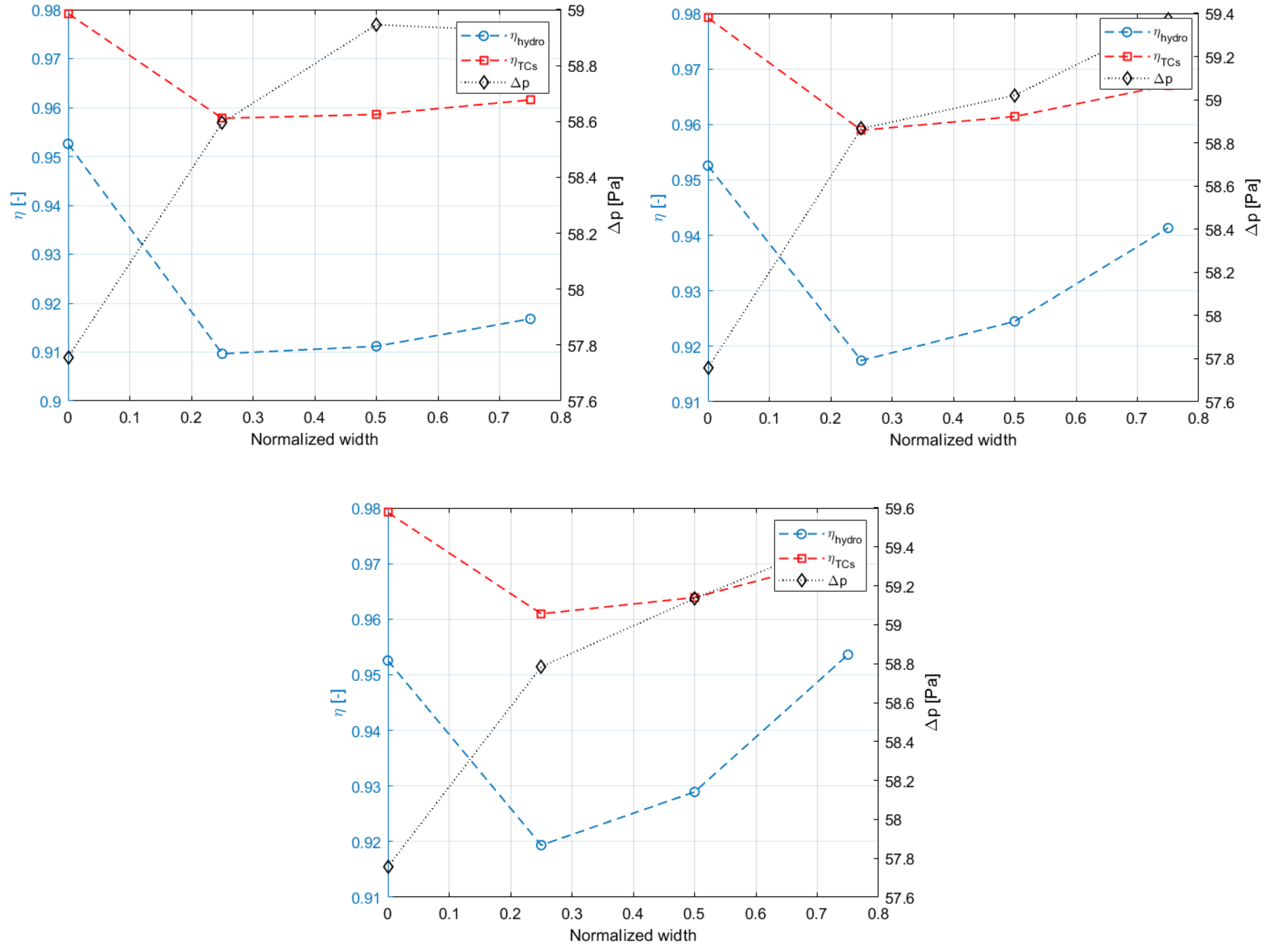

Figure 98 Summary of TES performance comparison during discharge at different normalized divider heights: ¼ (top-left), ½ (top-right), ¾ (bottom).

5.8 External channel

5.8.1 Background

In the section related to literature review many publications on radial chemical reactors (including filters) has been considered. Those studies showed the influence of the outer channel's position, both with a standard and reversed configuration (with the flow entering from the external channel). Nonetheless the results of those literature studies are only related to the fluid flow and influenced by strong assumptions, it has been observed, and it was expected, that this parameter has a strong influence on the evolution of the fluid flow. Being the flow strongly connected with the thermal behavior of a TES, it is worth to perform an analysis on the height of the external channel. While only "U" and "Z" structures have been considered in literature, during this assessment also a middle-height and a triple exit channel has been investigated, as can be seen in Figure 99.

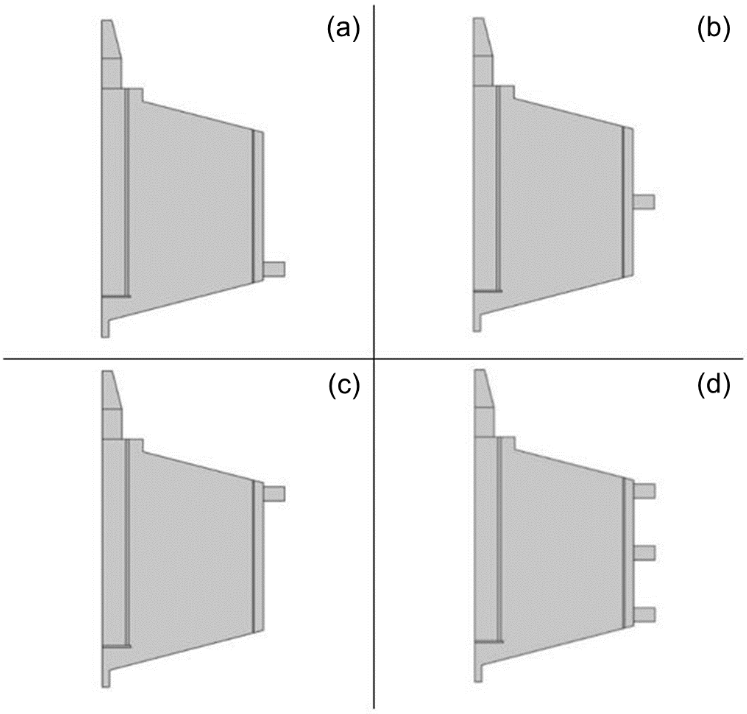

Figure 99 Analyzed configurations with different external channel positions. In particular, Z (a), central (b), U (c) and triple (d) exit configurations.

5.8.2 Results

The charge phase shows a relevant impact of the modification on the pressure flow distribution. Contrarily to what has been found in literature, pressure drop distribution is less uniform for "U" configuration, even if in absolute value it is reduced. The triple exit channel, while increasing the average pressure drop, presents the most uniform distribution: the triple outer channel creates three principal paths instead of one, creating a more equilibrated flow.

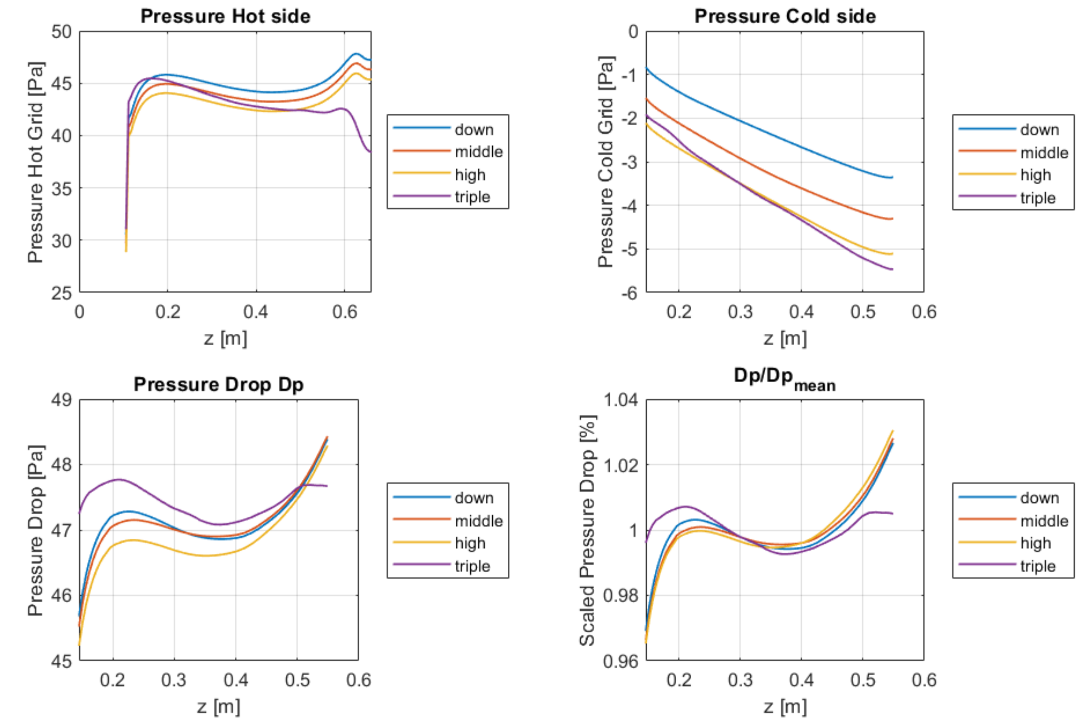

Figure 100 Evaluation of pressure drop during charge phase.

For the discharge phase, the effect of the measure seems not relevant in terms of pressure drops, even for the triple inlet, probably due to the low inlet velocity, which makes the outer pressure more uniform than the inner one in the charge phase.

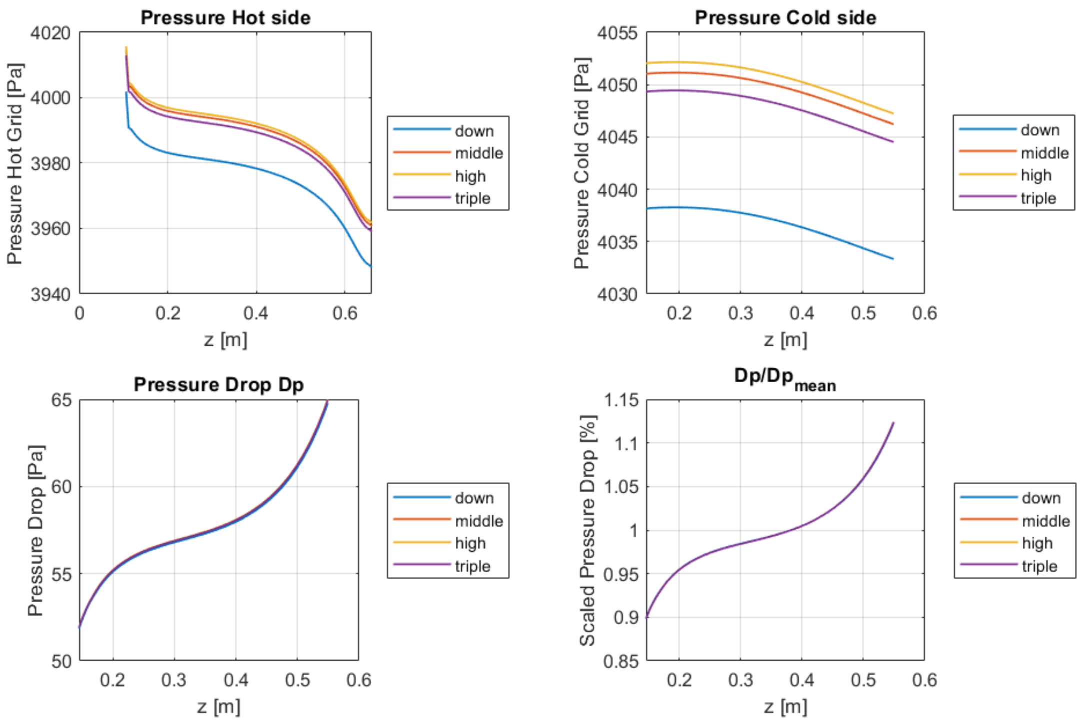

Figure 101 Evaluation of pressure drop during discharge phase.

The height of the external channel seems to not have a great influence on temperature profiles, with the exception of a slightly smoother trend for the high and middle positions during the charge phase. As for the pressure drop, its influence on temperature is negligible during discharge.

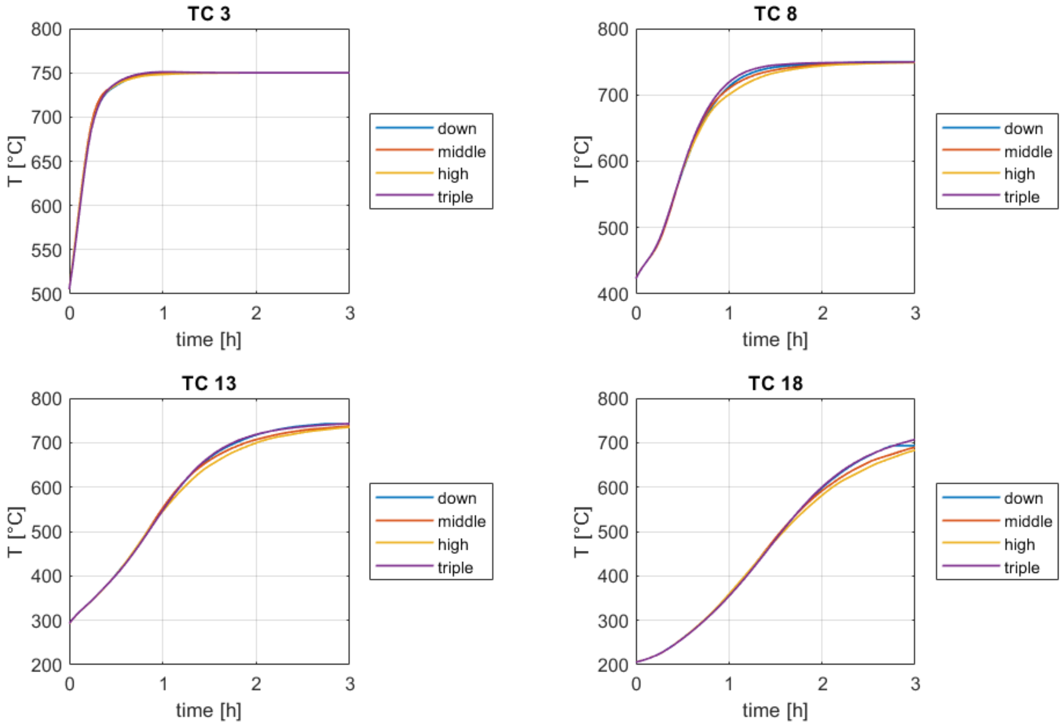

Figure 102 *Evaluation of temperature trend during charge phase.*

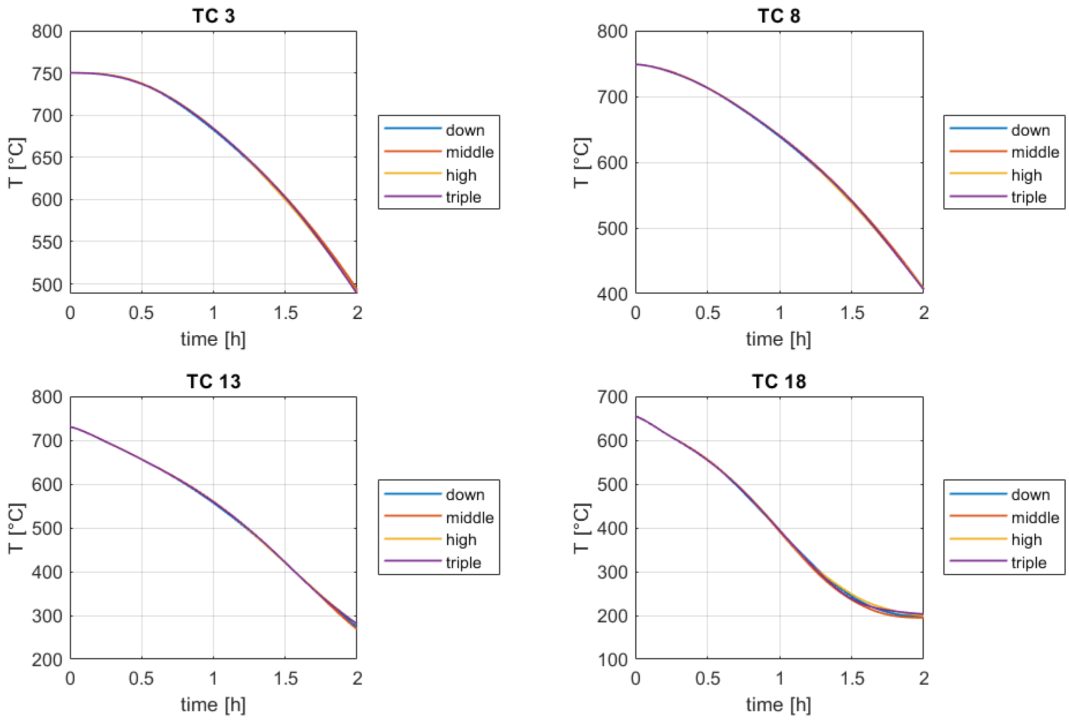

Figure 103 *Evaluation of temperature trend during discharge phase.*

As the temperature trend does not vary consistently, also the effect on thermocline is not so relevant. Figure 104 shows the effect of the different heights on the thermal front, by indicating the down, middle, up, triple external channel respectively with 1, 2, 3 and 4. From the contour plots it is possible to observe a little improvement for the "Z" and triple exit configuration, with the latter being the best solution. The triple and middle external channel seems to perform better during discharge.

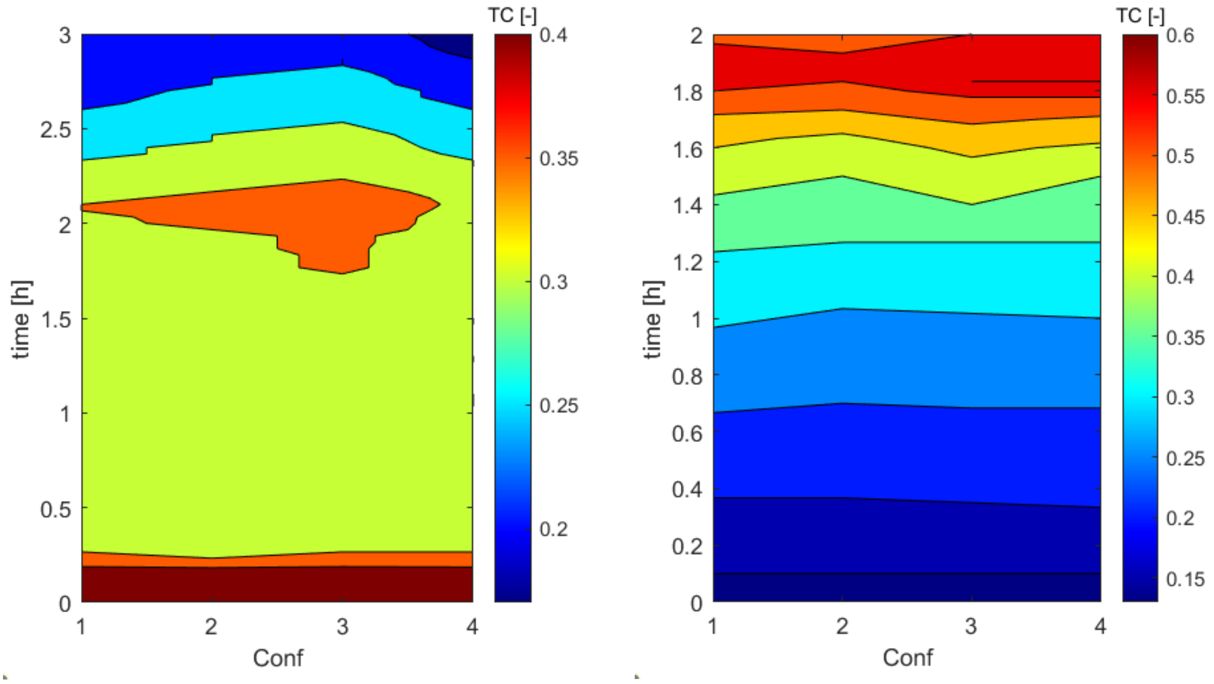

Figure 104 Evaluation of thermocline evolution during charge (left) and discharge (right) phases.

Looking at the hydrodynamic and thermal efficiencies, it is noticeable that the two are partially in contrast, although the temperature distribution is dependent on the fluid flow. Therefore, during the charge phase the "U" configuration shows the best thermal behavior along the axial direction, nonetheless the worse hydrodynamic efficiency. However, the benefits are not so relevant. No particular differences are registered during the discharge.

Hence, the triple exit configuration could be considered the most beneficial, as it slightly decreases the thermocline width.

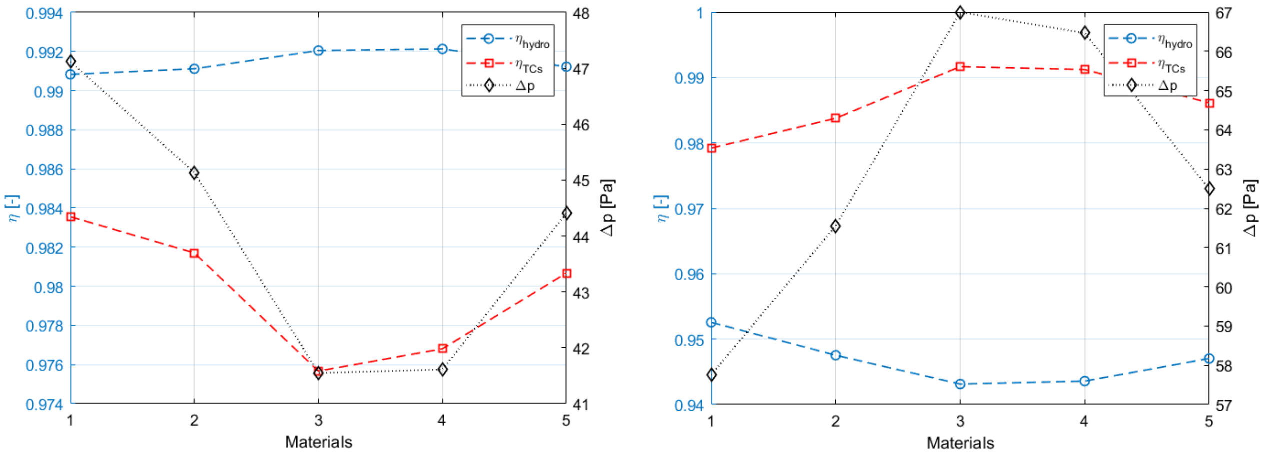

Figure 105 Summary of TES performance comparison during charge (left) and discharge (right) phases.

5.9 Different materials

5.9.1 Background

The packed region of the TES consists of ceramic spheres (denstone 2000), with low thermal conductivity, poured in a zone delimited by two wired meshes. In this section the effect of different materials with different thermal characteristics has been investigated. Therefore, 5 different materials have been compared: denstone 2000, aluminum, alumina, magnesia, silicon carbide. All of them are able to work at temperatures superior than 750 °C without altering its integrity and properties. The following figure shows all the properties of the material and its effect on the bed's properties, such as the effective thermal conductivity and diffusivity.

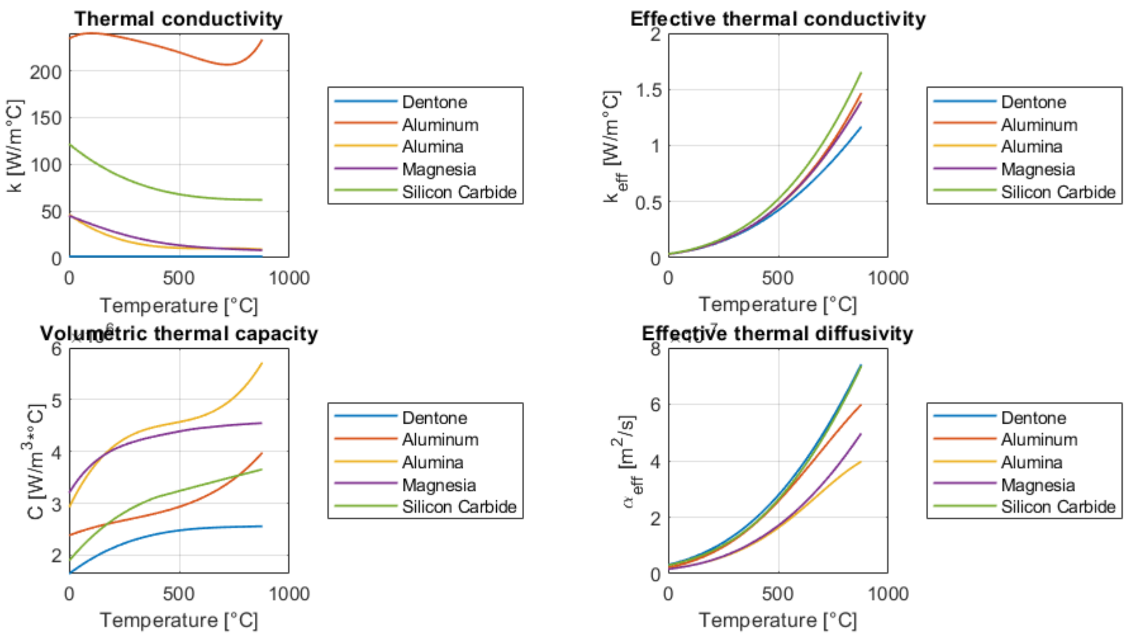

Figure 106 Properties of different materials and their effect on interesting parameters for the TES.

The first thing observable is that very different conductivities do not influence significantly the one of the bed, since it is calculated with Kunii and Smith formulation. Indeed, in that formulation the effect of thermal conductivity is relatively limited, while the effect of radiation is more relevant, especially at high temperature (as visible for silicon carbide, which has higher surface emissivity). Furthermore, the benefit of increased material's conductivity on the effective one is not noticeable for values higher than 30 W/m°C. The second visible aspect is the difference in volumetric thermal capacity, since alumina and magnesia it is doubled the one of denstone. With higher thermal capacity, the time of charge and discharge is longer and more energy can be stored.

5.9.2 Results

The shape of pressure drop and its distribution after 1 hour of working is dependent on temperature difference between the inner and the outer region. Therefore, materials with higher thermal capacity have lower pressure drop during charge and higher during discharge. However, this effect is caused by temperature difference, and thus by the different state of charge after 1 hour. Apart from this, the choice of material does not influence pressure drop distribution.

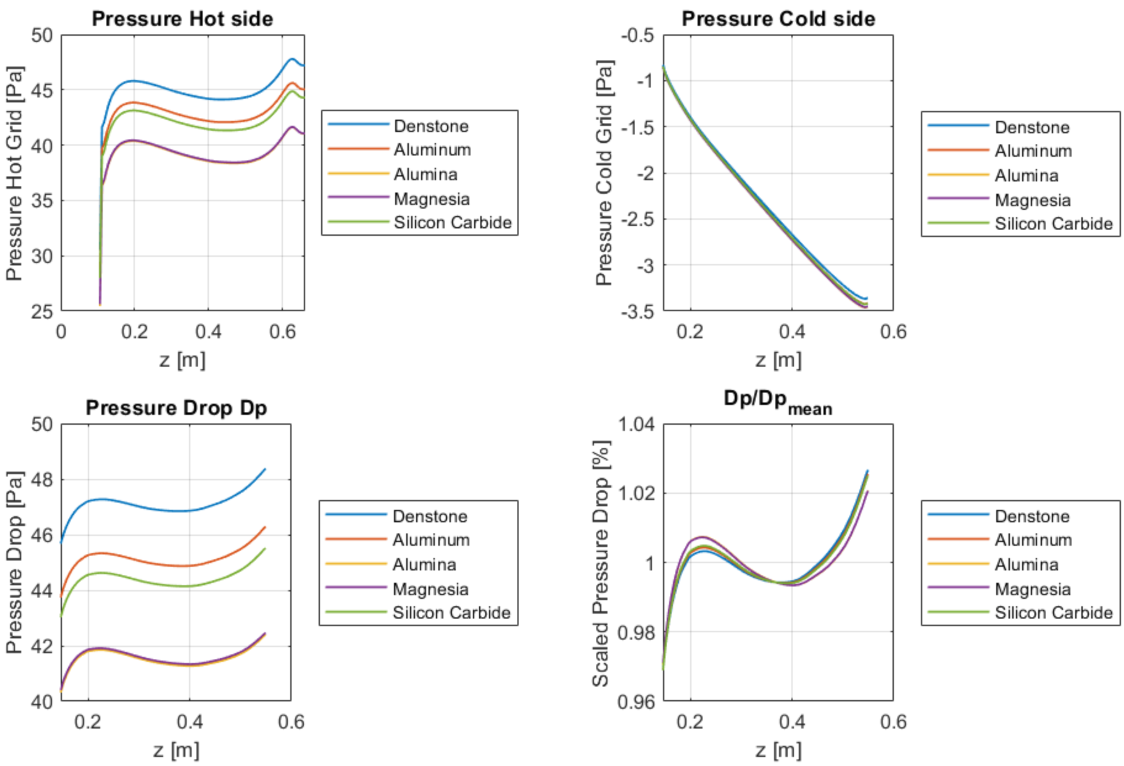

Figure 107 Evaluation of pressure drop during charge phase.

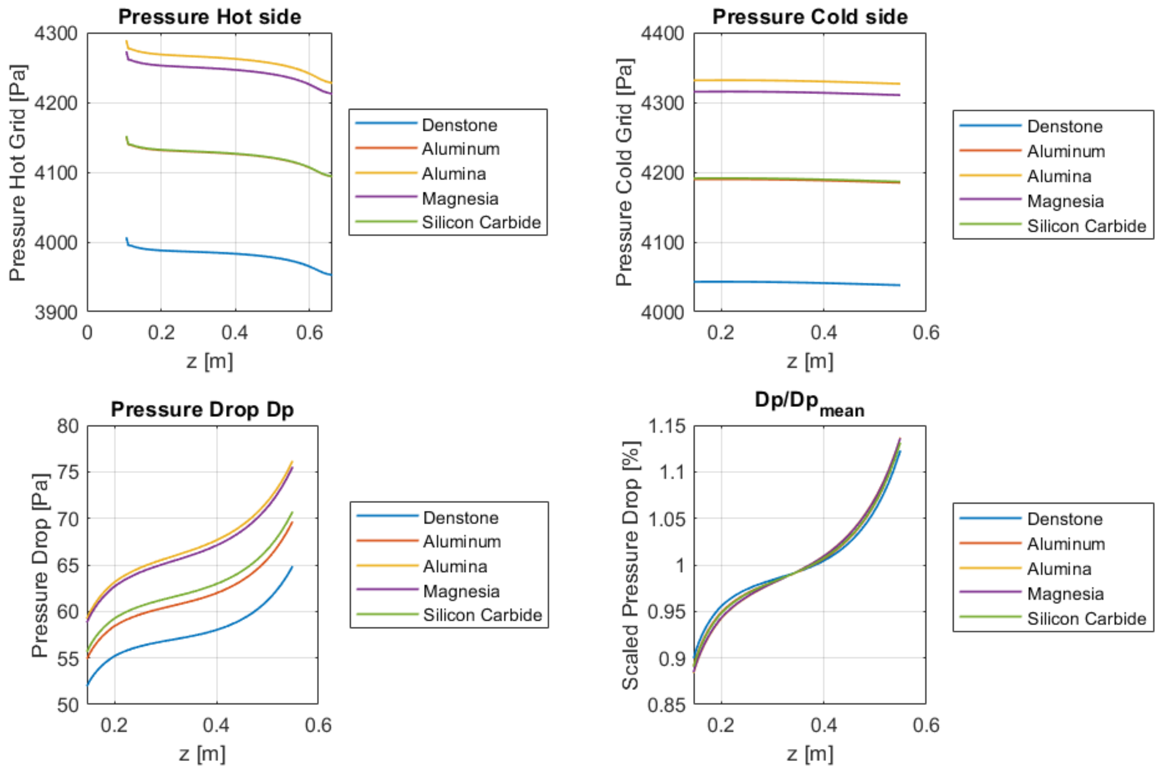

Figure 108 Evaluation of pressure drop during discharge phase.

As mentioned, the effect of varied thermal capacity is particularly important to understand the thermal behavior of the TES, while thermal conductivity and emissivity seems to be much less relevant if compared to it. As a result, all the transients are longer in for materials with high thermal capacity, regardless of conductivity.

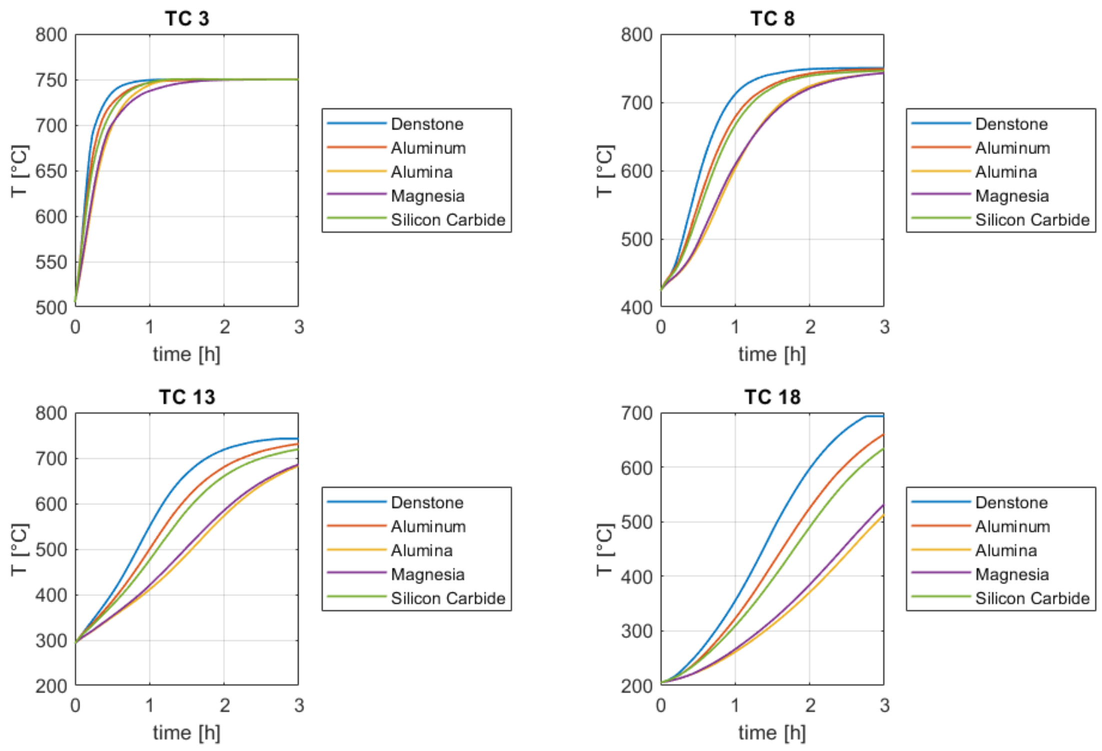

Figure 109 Evaluation of temperature trend during charge phase.

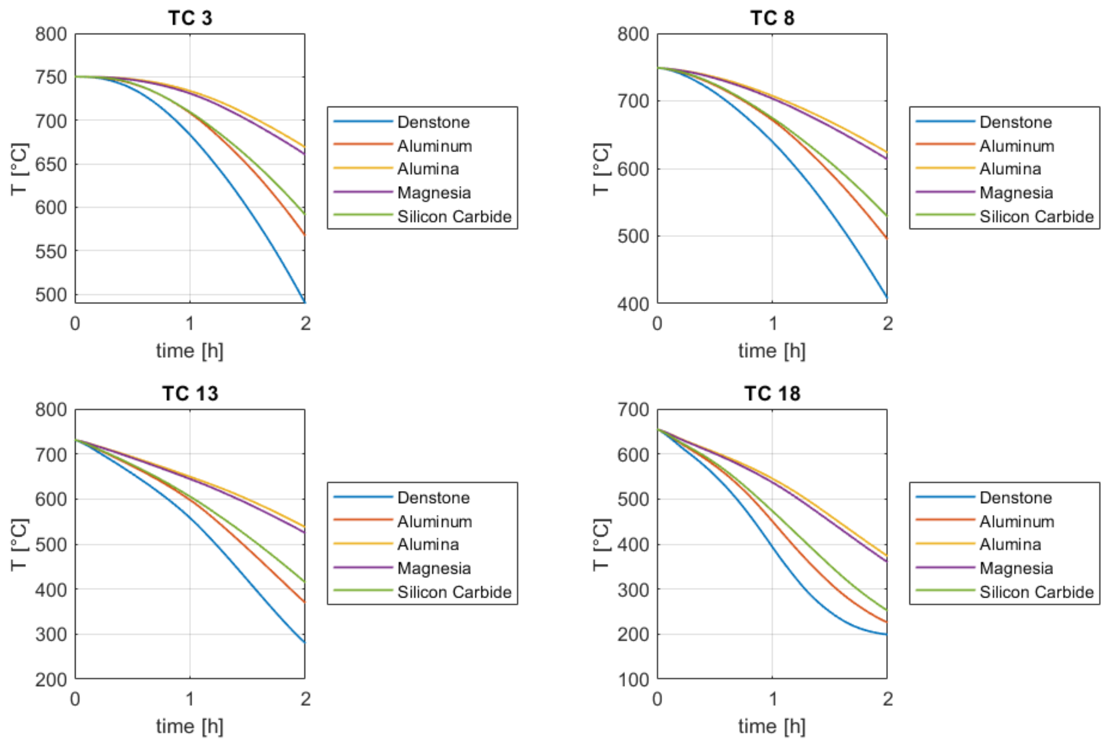

Figure 110 Evaluation of temperature trend during discharge phase.

The previously cited effect causes the difference in thermocline width. In materials with low thermal capacity, the thermal front tends to stabilize sooner during charge and to spread faster during the discharge phase. The thermocline spread is described in Figure 111, where in the x-axis is indicated the material: in particular, “1” represents denstone 2000, “2” is used for aluminum, “3” for alumina, “4” for magnesia and “5” for silicon carbide”.

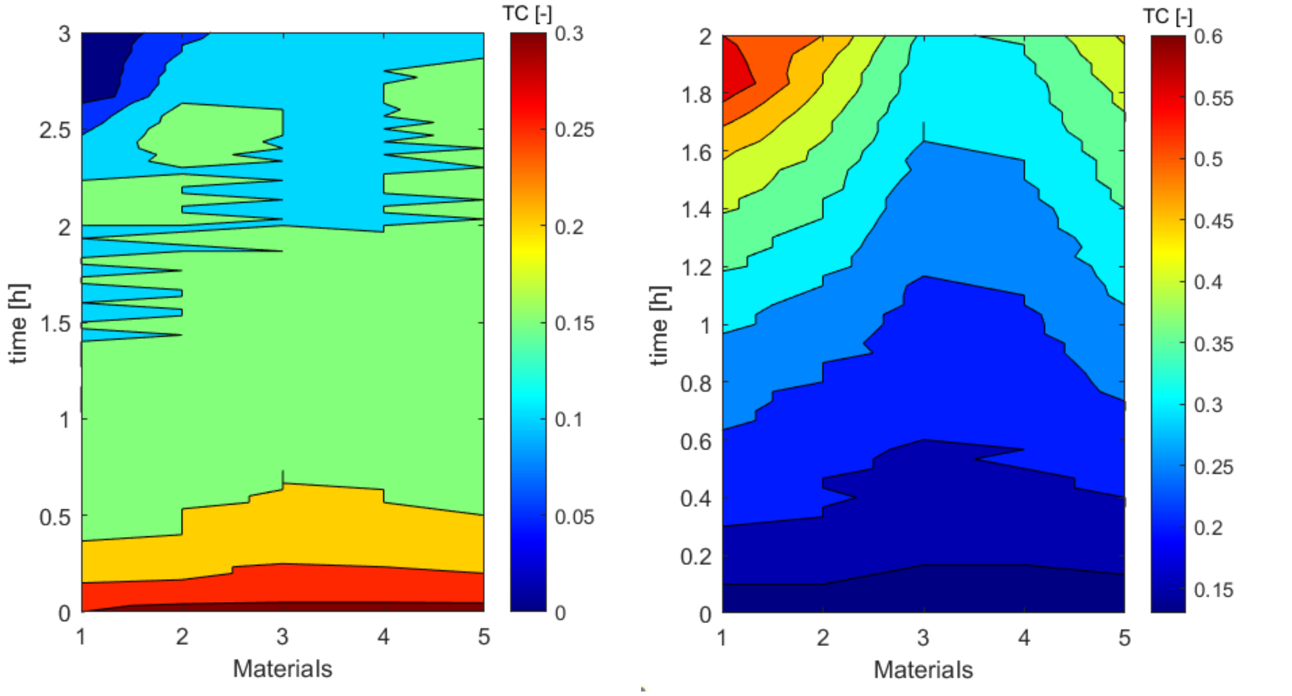

Figure 111 Evaluation of thermocline evolution during charge (left) and discharge (right) phases.

Looking at the thermal and hydrodynamic efficiency, they seem to not vary dramatically, and are influenced by the different thermal inertia of the materials.

The choice among different materials is not dependent only on thermal and mechanical properties, but also on cost, manufactory procedures and availability; however, this analysis allows to understand the general effect of materials with different conductivity, density and specific heat on packed bed TES. For a complete understanding of its effect, ulterior analysis and experimental investigations are needed.

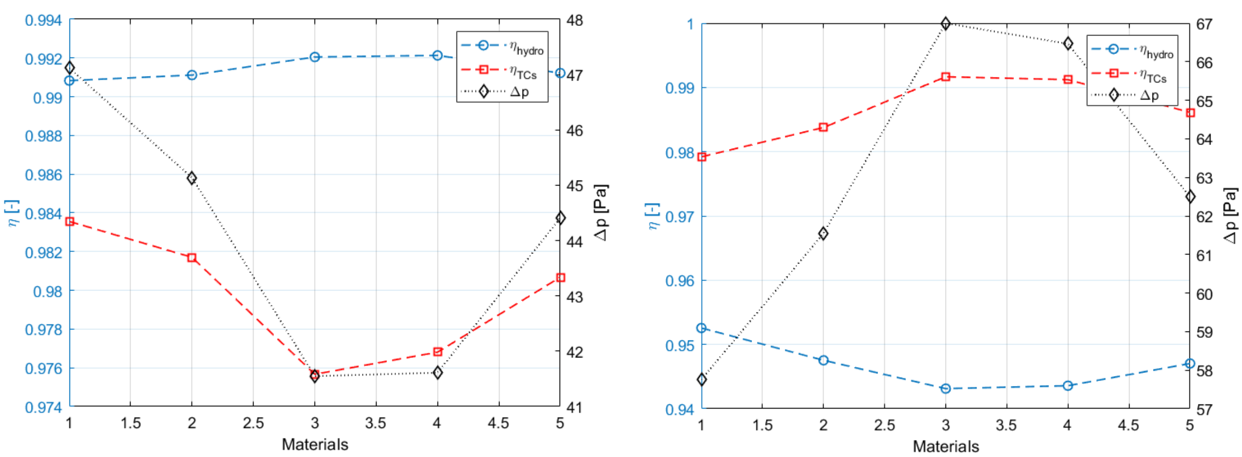

Figure 112 Summary of TES performance comparison during charge (left) and discharge (right) phases.

6 Conclusion

This thesis was focused on the modeling and development of a new TES concept to store energy coming from renewable sources and industrial processes and use it when needed for many applications, creating benefits in terms of energy savings, grid stability, continued production and backup supply.

The study has been divided in many sections, each one with a specific scope and outcome:

- Initially, different concepts about energy storage have been discussed. After a brief introduction to energy storage and TES, with a clear explanation of the benefit derived by the use of these devices in different applications. It was important to emphasize the characteristics of current state-of-art and the possible solutions proposed to overcome the principal TES challennges, as the aim of this study is to propose one of those alternatives.
- A review of packed bed thermal energy storage has been presented, including working principle, principal design concepts, advantages and disadvantages, influent parameters and future challenges.
- In section 2, the proposed prototype storage, built in the Solar Lab of KTH – Royal Institute of Technology, has been described, starting with its potential advantages. The most important is connected to the basic concept, which consists in a radial flow configuration. Due to this, the requirement for thermal insulation is reduced, as the hot region is in the inner zone of the storage, bringing to a potential reduction in costs. All the materials inside the TES have to respect the thermomechanical requirements and be able to withstand the maximum working temperature and the effect of many different charging and discharging cycles, without damaging and maintaining their properties and integrity.
- The review in section 3 was focused also on the physics of packed bed TES, including a description of the fluid flow and heat transfer mechanisms involved in the problem. The knowledge of these mechanism is foundamental in order to model this type of TES and to understand how to maximize its efficiency and overcome its weakness during the design and operation processes. Follows an analysis of all the possible solutions found in literature in order to model the lab-scale storage, and all the modeling procedures used for radial packed bed configurations.
- The model, proposed in section 4, consists in a CFD simulation coupled with a porous media approach, in such a way to model the packed bed as a homogeneous media identified by averaged properties and a certain porosity. The behavior of the TES has been investigated at different operative conditions, performing a simple charge and discharge, a cycle stability analysis, an evaluation of thermal dispersion when an insulation layer is considered.

- Once the model has been demonstrated to be representative of the problem, an improvement procedure (section 5) has been applied, in order to improve the performance of the storage. The procedure is based on fixed key performance indicators, which include the pressure drop distribution and its deviation from a uniform one, the temperature uniformity along the axial direction, and the thermocline spread, which is largely considered as one of the principal indicators of thermal behavior. In addition, thermal and hydrodynamic efficiency have been used as global indicators to evaluate the TES performance. Therefore, different measures have been proposed and evaluated, in order to know influence of some parameters on the TES performance and to propose improving solutions.

Following these procedures, from the initil research on energy storage typologies to the implementation and improvement of the proposed storage concept, a first assessment of the TES has been arranged, to evaluate its global performance and behavior. More in detail, the principal outcomes consist in:

- Substantial knowledge of energy storage solutions, their functions, benefits, classifications and applications, and limits. More detailed attention on thermal energy storage, including the state-of-art and possibilities to overcome its limitations using packed bed structures with solid filler.
- Individuation of the great potential of packed bed structures as thermocline TES. Understanding of advantages and challenges for a large scale development of the technology. Individuation of the principal parameters influencing its performance and innovative concepts. For a radial configuration, the principal issues are related to the uniformity of fluid flow in the axial direction and to the consequrnt shape of the thermocline.
- Understanding of the principal mechanism involved when a packed bed storage is employed to store energy. Among all, literature study on mathematic equations and numerical modeling to represent the fluid flow and heat transfer phenomena. Evaluation and representation of the key parameters to evaluate the thermal behavior in a structure of particles.
- Development of an appropriate methodology to model the proposed TES by using a combined CFD and porous media approach, resulting in an interesting compromise between accuracy and computationl cost. Thus, the method used by other autors is applicable also in this case, with some modifications associated to the specific case. A preliminary analysis shows a simple comparison of different turbulent models and allows to understand the uncertainties related to its choice. The storage shows a good responce in different conditions. As a matter of fact, the performance should be considered in relation to the size of the TES.

- First complete assessment of principal issues related to the radial configuration. Among them, the most relevant is the thermocline shape that must be accurately managed during different operations. An uniform fluid flow has been shown as a key figure for the correct development of the thermal front during stabilized cycles.
- Use and validation of some KPI useful to evaluate the storage performance during the improvement procedure. Among them, the thermal efficiency constitute an interesting parameter on the thermal behavior along the axial direction, but it is necessay to combine it with another physic quntity to detect the thermocline. The boolean function for the evaluation of the theral front thickness is a potential good index, but sometimes it could be not fully realistic and it depends highly on the way the thermocline ranges are chsen. The hydrodynamic efficiency is useful for a first assess on fluid pattern, but not a good indicator for the general behavior of the TES; moreover, it is highly dependent on the absolute value of the average pressure drop, which is more variable than the average temperature in the axial direction. The average pressure drop needs to be monitored, as it could constitute a relevant loss in packed bed structures, especially for small particles diameter.
- Individuation of principal parameters that can be modified for a better thermal management. Among them, the introduction of devices inside the storage, such as divider and cone structure seems to not improve significantly the performances, or to even decrease the fluid flow uniformity. On the other hand, operative conditions, such as inlet temperature and mass flow rate, or global parameters (particle diameter, materials, emissivity) represent the most influent ones and there are possibilities to obtain a better thermal behavior by choosing a suitable compromise. In particular, different materials influence consistently the storage capacity without changing the dimensions of the TES, while a slightly larger diameter of the particles could reduce dramatically the average pressure drop, maintaining an almost constant thermal behavior. The effect of a triple exit channel is interesting too, if technically feasible, as generates a more uniform fluid flow, especially in industrial scale storages.

As a recommendation for future works, an experimental validation of the model is necessary, to properly understand its accuracy with respect to the real storage. Furthermore, a more accurate model could be performed, including a most accurate methodology and/or the physical representation of the packed structure and the flow circulating inside. A better representation of the wired matrices in the inner and outer regions could also lead to a better understanding of the flow field before and after the packed region. Moreover, all the improvements and analyses should be performed in a 3D configuration. The effect of particle disposition could be a key factor, and needs to be considered in further assessments. The evaluation of the TES should be done also in other conditions, such as partial state of charge, partial and variable loads, and discharge after some hours of stand-by.

Thermal ratcheting is also a relevant issue in packed bed structure subjected to high temperature variation in time. This problem requires a specific investigation, involving the evaluation of thermomechanical stresses through all the packed bed. For this reason, it has not been included in this study and further investigations are required, to avoid excessive stresses on the external structure.

After solving some technical problems, the new TES should be integrated inside a system, such as an industrial process or a power cycle. One innovative possibility could be its integration in a CSP power plant with a supercritical CO_2 power block. With this analysis, the applicability of the storage inside a complex system is guaranteed. The following step consist in an economic assessment, to understand the cost of the TES and its impact on a system in terms of costs and LCOE, to be compared with the current state-of-art.

After a successful experimentation, the storage is ready to be designed and built at an industrial or facility scale. To do that, all the procedures, included the ones presented in this study, should be done again, and other considerations in the models, parameters and improvements will be necessarily done.

Bibliography

[1] "New Energy Outlook 2019 | Bloomberg New Energy Finance | Bloomberg Finance LP." https://about.bnef.com/new-energy-outlook/ (accessed Jul. 27, 2020).

[2] R. Guédez, "Integration of renewables and energy storage - technology overview and industrial perspectives," 2020, no. February.

[3] "Challenges of Electricity Storage Technologies." https://www.aps.org/policy/reports/popa-reports/electricity.cfm (accessed Jul. 27, 2020).

[4] I. Renewable Energy Agency, *ELECTRICITY STORAGE AND RENEWABLES: COSTS AND MARKETS TO 2030 ELECTRICITY STORAGE AND RENEWABLES: COSTS AND MARKETS TO 2030 About IRENA*. 2017.

[5] V. Dostal, M. J. Driscoll, and P. Hejzlar, "A Supercritical Carbon Dioxide Cycle for Next Generation Nuclear Reactors," 2004. Accessed: Jul. 27, 2020. [Online]. Available: http://web.mit.edu/canes/.

[6] G. Glatzmaier, "New Concepts and Materials for Thermal Energy Storage and Heat-Transfer Fluids," no. August 2011, 2011.

[7] I. Sarbu and C. Sebarchievici, "A Comprehensive Review of Thermal Energy Storage," *Sustainability*, vol. 10, no. 2, p. 191, Jan. 2018, doi: 10.3390/su10010191.

[8] A. Gil *et al.*, "State of the art on high temperature thermal energy storage for power generation. Part 1-Concepts, materials and modellization," doi: 10.1016/j.rser.2009.07.035.

[9] E. M. Shchukina, M. Graham, Z. Zheng, and D. G. Shchukin, "Nanoencapsulation of phase change materials for advanced thermal energy storage systems," *Chem. Soc. Rev.*, vol. 47, no. 11, pp. 4156–4175, 2018, doi: 10.1039/c8cs00099a.

[10] L. F. Cabeza, *Advances in Thermal Energy Storage Systems: Methods and Applications*. Elsevier Inc., 2014.

[11] P. K. N. AuYeung, "Solar Thermochemical Energy Storage | AIChE," 2017, Accessed: Jul. 27, 2020. [Online]. Available: https://www.aiche.org/resources/publications/cep/2017/july/solar-thermochemical-energy-storage.

[12] B. Wong, "Sulfur Based Thermochemical Heat Storage for Baseload Concentrated Solar Power Generation," *U.S. Dep. Energy*, no. November, p. 38, 2014.

[13] A. S. Lavine *et al.*, “Thermochemical energy storage with ammonia: Aiming for the sunshot cost target,” *AIP Conf. Proc.*, vol. 1734, 2016, doi: 10.1063/1.4949126.

[14] “IEA webstore. Technology Roadmap - Solar Thermal Electricity 2014.” https://webstore.iea.org/technology-roadmap-solar-thermal-electricity-2014 (accessed Jul. 27, 2020).

[15] IRENA, “RENEWABLE POWER GENERATION COSTS IN 2018,” Abu Dhabi, 2019.

[16] Z. Ma, G. C. Glatzmaier, and C. F. Kutscher, “Thermal Energy Storage and Its Potential Applications in Solar Thermal Power Plants and Electricity Storage,” 2011, doi: 10.1115/ES2011-54077.

[17] L. Miró, J. Gasia, and L. F. Cabeza, “Thermal energy storage (TES) for industrial waste heat (IWH) recovery: A review,” *Applied Energy*, vol. 179. Elsevier Ltd, pp. 284–301, Oct. 01, 2016, doi: 10.1016/j.apenergy.2016.06.147.

[18] M. Liu *et al.*, “Review on concentrating solar power plants and new developments in high temperature thermal energy storage technologies,” *Renew. Sustain. Energy Rev.*, vol. 53, pp. 1411–1432, 2016, doi: 10.1016/j.rser.2015.09.026.

[19] W. D. Steinmann, “Thermal energy storage systems for concentrating solar power (CSP) plants,” *Conc. Sol. Power Technol. Princ. Dev. Appl.*, pp. 362–394, 2012, doi: 10.1016/B978-1-84569-769-3.50011-X.

[20] H. Singh, R. P. Saini, and J. S. Saini, “A review on packed bed solar energy storage systems,” *Renew. Sustain. Energy Rev.*, vol. 14, no. 3, pp. 1059–1069, 2010, doi: 10.1016/j.rser.2009.10.022.

[21] I. Ortega-Fernández *et al.*, “Operation strategies guideline for packed bed thermal energy storage systems,” *Int. J. Energy Res.*, no. June, pp. 1–11, 2018, doi: 10.1002/er.4291.

[22] S. Trevisan, R. Guédez, H. Bouzekri, and B. Laumert, “Initial design of a radial-flow high temperature thermal energy storage concept for air-driven CSP systems,” *SOLARPACES 2018 Int. Conf. Conc. Sol. Power Chem. Energy Syst.*, vol. 2126, no. July, p. 200031, 2019, doi: 10.1063/1.5117746.

[23] J. D. McTigue, C. N. Markides, and A. J. White, “Performance response of packed-bed thermal storage to cycle duration perturbations,” *J. Energy Storage*, vol. 19, no. July, pp. 379–392, 2018, doi: 10.1016/j.est.2018.08.016.

[24] M. Y. Haller, C. A. Cruickshank, W. Streicher, S. J. Harrison, E. Andersen, and S. Furbo, “Methods to determine stratification efficiency of thermal energy storage processes - Review and theoretical comparison,” *Sol. Energy*, vol. 83, no. 10, pp. 1847–1860, Oct. 2009, doi: 10.1016/j.solener.2009.06.019.

[25] G. Zanganeh, A. Pedretti, A. Haselbacher, and A. Steinfeld, “Design of packed bed thermal energy storage systems for high-temperature industrial process heat,” *Appl. Energy*, vol. 137, pp. 812–822, 2015, doi: 10.1016/j.apenergy.2014.07.110.

[26] J. Marti, L. Geissbühler, V. Becattini, A. Haselbacher, and A. Steinfeld, “Constrained multi-objective optimization of thermocline packed-bed thermal-energy storage,” *Appl. Energy*, vol. 216, no. February, pp. 694–708, 2018, doi: 10.1016/j.apenergy.2017.12.072.

[27] I. González, C. David Pérez-Segarra, O. Lehmkuhl, S. Torras, and A. Oliva, “Thermo-mechanical parametric analysis of packed-bed thermocline energy storage tanks,” 2016. Accessed: Jul. 27, 2020. [Online]. Available: http://upcommons.upc.edu/e-prints.

[28] K. G. Allen, T. W. von Backström, and D. G. Kröger, “Packed bed pressure drop dependence on particle shape, size distribution, packing arrangement and roughness,” *Powder Technol.*, vol. 246, pp. 590–600, Sep. 2013, doi: 10.1016/j.powtec.2013.06.022.

[29] C. Xu, X. Li, Z. Wang, Y. He, and F. Bai, “Effects of solid particle properties on the thermal performance of a packed-bed molten-salt thermocline thermal storage system,” *Appl. Therm. Eng.*, vol. 57, no. 1–2, pp. 69–80, 2013, doi: 10.1016/j.applthermaleng.2013.03.052.

[30] A. De Klerk, “Voidage variation in packed beds at small column to particle diameter ratio,” *AIChE J.*, vol. 49, no. 8, pp. 2022–2029, Aug. 2003, doi: 10.1002/aic.690490812.

[31] “Mean porosity and pressure drop measurements in packed beds of monosized spheres: side wall effects.” https://www.researchgate.net/publication/303213122_Mean_porosity_and_pressure_drop_measurements_in_packed_beds_of_monosized_spheres_side_wall_effects (accessed Jul. 27, 2020).

[32] W. Van Antwerpen, C. G. Du Toit, and P. G. Rousseau, “A review of correlations to model the packing structure and effective thermal conductivity in packed beds of mono-sized spherical particles,” *Nuclear Engineering and Design*, vol. 240, no. 7. North-Holland, pp. 1803–1818, Jul. 01, 2010, doi: 10.1016/j.nucengdes.2010.03.009.

[33] “Principles of Heat Transfer in Porous Media - Maasoud Kaviany - Google Libri.”

https://books.google.it/books?hl=it&lr=&id=MI3bBwAAQBAJ&oi=fnd&pg=PR7&dq=Kavi any,+M.+Principles+of+heat+transfer+in+porous+media,+2nd+edition.+Springer&ots=GSv ht0ruxR&sig=Z7HSRIzGltCWepgLPS1SnPvrxxo#v=onepage&q=Kaviany%2C M. Principles of heat transfer in porous media%2C 2nd edition. Springer&f=false (accessed Jul. 28, 2020).

[34] M. Hänchen, S. Brückner, and A. Steinfeld, "High-temperature thermal storage using a packed bed of rocks - Heat transfer analysis and experimental validation," *Appl. Therm. Eng.*, vol. 31, no. 10, pp. 1798–1806, 2011, doi: 10.1016/j.applthermaleng.2010.10.034.

[35] T. Esence, A. Bruch, S. Molina, B. Stutz, and J. F. Fourmigué, "A review on experience feedback and numerical modeling of packed-bed thermal energy storage systems," *Sol. Energy*, vol. 153, pp. 628–654, 2017, doi: 10.1016/j.solener.2017.03.032.

[36] G. Zanganeh, A. Pedretti, S. A. Zavattoni, M. C. Barbato, A. Haselbacher, and A. Steinfeld, "Design of a 100 MWhth packed-bed thermal energy storage," *Energy Procedia*, vol. 49, pp. 1071–1077, 2014, doi: 10.1016/j.egypro.2014.03.116.

[37] K. Allen, T. Von Backström, E. Joubert, and P. Gauché, "Rock bed thermal storage: Concepts and costs," in *AIP Conference Proceedings*, May 2016, vol. 1734, no. 1, p. 050003, doi: 10.1063/1.4949101.

[38] H. F. Laubscher, T. W. Von Backström, and F. Dinter, "Developing a cost effective rock bed thermal energy storage system: Design and modelling," in *AIP Conference Proceedings*, Jun. 2017, vol. 1850, no. 1, p. 080015, doi: 10.1063/1.4984436.

[39] D. Schlipf, E. Faust, G. Schneider, and H. Maier, "First operational results of a high temperature energy storage with packed bed and integration potential in CSP plants," in *AIP Conference Proceedings*, Jun. 2017, vol. 1850, doi: 10.1063/1.4984445.

[40] S. Khare, M. Dell'amico, C. Knight, and S. Mcgarry, "Selection of materials for high temperature sensible energy storage," 2013, doi: 10.1016/j.solmat.2013.03.009.

[41] S.-G. NorPro, "Denstone® 2000 Support Balls Supreme Reliability and Survival from Denstone®," 2000.

[42] P. Klein, T. H. Roos, and T. J. Sheer, "Experimental investigation into a packed bed thermal storage solution for solar gas turbine systems," in *Energy Procedia*, Jan. 2014, vol. 49, pp. 840–849, doi: 10.1016/j.egypro.2014.03.091.

[43] A. Kushwaha, M. Poirier, R. E. Hayes, and H. Sapoundjiev, "Heat extraction from a flow reversal reactor in lean methane combustion," *Chem. Eng. Res. Des.*, vol. 83, no. 2 A, pp. 205–213, Feb. 2005, doi: 10.1205/cherd.04177.

[44] "(No Title)." https://www.specialmetals.com/assets/smc/documents/alloys/inconel/inconel-alloy-625.pdf (accessed Jul. 28, 2020).

[45] "(No Title)." https://www.unifrax.com/wp-content/uploads/2018/08/C-1421.pdf (accessed Jul. 28, 2020).

[46] "(No Title)." https://www.unifrax.com/wp-content/uploads/2018/09/Fiberfrax-Durablanket-S-IT.pdf (accessed Jul. 28, 2020).

[47] T. E. W. Schumann, "Heat transfer: A liquid flowing through a porous prism," *J. Franklin Inst.*, vol. 208, no. 3, pp. 405–416, Sep. 1929, doi: 10.1016/S0016-0032(29)91186-8.

[48] G. Weidenfeld, Y. Weiss, and H. Kalman, "A theoretical model for effective thermal conductivity (ETC) of particulate beds under compression," in *Granular Matter*, Oct. 2004, vol. 6, no. 2–3, pp. 121–129, doi: 10.1007/s10035-004-0170-1.

[49] E. V. Votyakov and A. M. Bonanos, "A perturbation model for stratified thermal energy storage tanks," *Int. J. Heat Mass Transf.*, vol. 75, pp. 218–223, Aug. 2014, doi: 10.1016/j.ijheatmasstransfer.2014.03.071.

[50] D. Handley and P. J. Heggs, "The effect of thermal conductivity of the packing material on transient heat transfer in a fixed bed," *Int. J. Heat Mass Transf.*, vol. 12, no. 5, pp. 549–570, May 1969, doi: 10.1016/0017-9310(69)90038-6.

[51] K. Perumal, J. Malang, P. Kumar, and A. Saptoro, "Computational Fluid Dynamics-Based Hydrodynamics Studies in Packed Bed Columns: Current Status and Future Directions," *Artic. Int. J. Chem. React. Eng.*, 2015, doi: 10.1515/ijcre-2014-0121.

[52] † Alfredo Guardo, ‡ Miguel Coussirat, † M. Angels Larrayoz, † and Francesc Recasens, and ‡ Eduard Egusquiza*, "CFD Flow and Heat Transfer in Nonregular Packings for Fixed Bed Equipment Design," 2004, doi: 10.1021/IE034229+.

[53] M. Coussirat, A. Guardo, B. Mateos, and E. Egusquiza, "Performance of stress-transport models in the prediction of particle-to-fluid heat transfer in packed beds," *Chem. Eng. Sci.*, vol. 62, no. 23, pp. 6897–6907, Dec. 2007, doi: 10.1016/j.ces.2007.08.071.

[54] A. Guardo, M. Coussirat, M. A. Larrayoz, F. Recasens, and E. Egusquiza, "Influence of the

turbulence model in CFD modeling of wall-to-fluid heat transfer in packed beds," *Chem. Eng. Sci.*, vol. 60, no. 6, pp. 1733–1742, Mar. 2005, doi: 10.1016/j.ces.2004.10.034.

[55] A. G. Dixon, M. Ertan Taskin, M. Nijemeisland, and H. H. Stitt, "Systematic mesh development for 3D CFD simulation of fixed beds: Single sphere study," *Comput. Chem. Eng.*, vol. 35, no. 7, pp. 1171–1185, Jul. 2011, doi: 10.1016/j.compchemeng.2010.12.006.

[56] J.-J. Lee, S.-J. Yoon, G.-C. Park, and W.-J. Lee, "Turbulence-induced Heat Transfer in PBMR Core Using LES and RANS," *J. Nucl. Sci. Technol.*, vol. 44, no. 7, pp. 985–996, 2007, doi: 10.1080/18811248.2007.9711338.

[57] A. G. Dixon, "COMSOL Multiphysics® Simulation of 3D Single-Phase Transport in a Random Packed Bed of Spheres." https://www.comsol.it/paper/comsol-multiphysics-simulation-of-3d-single-phase-transport-in-a-random-packed-b-18557 (accessed Jul. 28, 2020).

[58] A. Jafari, P. Zamankhan, S. M. Mousavi, and K. Pietarinen, "Modeling and CFD simulation of flow behavior and dispersivity through randomly packed bed reactors," *Chem. Eng. J.*, vol. 144, no. 3, pp. 476–482, Nov. 2008, doi: 10.1016/j.cej.2008.07.033.

[59] S. A. Zavattoni, G. Zanganeh, A. Pedretti, and M. C. Barbato, "Numerical analysis of the packed bed TES system integrated into the first parabolic trough CSP pilot-plant using air as heat transfer fluid," in *AIP Conference Proceedings*, Nov. 2018, vol. 2033, doi: 10.1063/1.5067121.

[60] S. Zavattoni *et al.*, "Effective thermal conductivity and axial porosity distribution of a rock-bed TES system: CFD modeling and experimental validation," 2012. Accessed: Jul. 28, 2020. [Online]. Available: https://www.researchgate.net/publication/250951688.

[61] S. Zavattoni, M. Brbato, Pedretti A., and Zanganeh G., "CFD simulations of a pebble bed thermal energy storage system accounting for porosity variations effects," 2011, Accessed: Jul. 28, 2020. [Online]. Available: https://www.researchgate.net/publication/250946250_CFD_simulations_of_a_pebble_bed_thermal_energy_storage_system_accounting_for_porosity_variations_effects.

[62] M. Cascetta, F. Serra, S. Arena, E. Casti, G. Cau, and P. Puddu, "Experimental and numerical research activity on a packed bed TES system," *Energies*, vol. 9, no. 10, 2016, doi: 10.3390/en9090758.

[63] P. J. Heggs, D. I. Ellis, and M. S. Ismail, "Prediction of flow distributions and pressure changes

in multi-layered annular packed beds," *Gas Sep. Purif.*, vol. 9, no. 4, pp. 243–252, Dec. 1995, doi: 10.1016/0950-4214(95)00006-W.

[64] P. J. Heggs, D. I. Ellis, and M. S. Ismail, "The modelling of fluid-flow distributions in annular packed beds," *Gas Sep. Purif.*, vol. 8, no. 4, pp. 257–264, Jan. 1994, doi: 10.1016/0950-4214(94)80006-5.

[65] R. Li and Z. Zhu, "Investigations on hydrodynamics of multilayer Π-type radial flow reactors," *Asia-Pacific J. Chem. Eng.*, vol. 7, no. 4, pp. 517–527, Jul. 2012, doi: 10.1002/apj.601.

[66] Z. Mu, J. Wang, T. Wang, and Y. Jin, "Optimum design of radial flow moving-bed reactors based on a mathematical hydrodynamic model," *Chem. Eng. Process. Process Intensif.*, vol. 42, no. 5, pp. 409–417, May 2003, doi: 10.1016/S0255-2701(02)00065-X.

[67] A. A. Kareeri, H. D. Zughbi, and H. H. Al-Ali, "Simulation of flow distribution in radial flow reactors," in *Industrial and Engineering Chemistry Research*, Apr. 2006, vol. 45, no. 8, pp. 2862–2874, doi: 10.1021/ie050027x.

[68] "Introduction to Heat Transfer - Theodore L. Bergman, Frank P. Incropera, Adrienne S. Lavine, David P. DeWitt - Google Libri." https://books.google.it/books?hl=it&lr=&id=YBaNaLurTD4C&oi=fnd&pg=PR21&dq=introduction+to+heat+transfer+incropera&ots=tPVD5kmJ8F&sig=KkTzqPnqgR2q0_pjc1VLYKxeGQ0#v=onepage&q=introduction to heat transfer incropera&f=false (accessed Jul. 28, 2020).

[69] H. K. Versteeg and W. Malalasekera, "An Introduction to Computational Fluid Dynamics Second Edition." Accessed: Jul. 28, 2020. [Online]. Available: www.pearsoned.co.uk/versteeg.

[70] "Which Turbulence Model Should I Choose for My CFD Application? | COMSOL Blog." https://www.comsol.com/blogs/which-turbulence-model-should-choose-cfd-application/ (accessed Jul. 28, 2020).

[71] C. john Bailey, K. Dhinsa, C. Bailey, and K. Pericleous, "Low Reynolds number turbulence models for accurate thermal simulations of electronic components Low Reynolds Number Turbulence Models for Accurate Thermal Simulations of Electronic Components turbulent dissipation length Ip Re Reynolds number, ueH/v," 2004, doi: 10.1109/ESIME.2004.1304081.

[72] "(No Title)." https://doc.comsol.com/5.4/doc/com.comsol.help.ssf/SubsurfaceFlowModuleUsersGuide.pdf

(accessed Jul. 28, 2020).

[73] "Which Porous Media and Subsurface Flow Interface Should I Use? | COMSOL Blog." https://www.comsol.com/blogs/which-porous-media-and-subsurface-flow-interface-should-i-use/ (accessed Jul. 28, 2020).

[74] D. Kunll and J. M. Smith, "Heat Transfer Characteristics of Porous Rocks."

[75] "Journal of Fluids Engineering Editorial Policy Statement on the Control of Numerical Accuracy."